OCS Study
BOEM 2013-01110

Meteorological and Wave Measurements for Improving Meteorological and Air Quality Modeling



U.S. Department of the Interior
Bureau of Ocean Energy Management
Gulf of Mexico OCS Region

BOEM
Bureau of Ocean Energy Management

OCS Study
BOEM 2013-01110

Meteorological and Wave Measurements for Improving Meteorological and Air Quality Modeling

Authors

Clinton P. MacDonald
Alison E. Ray
Paul T. Roberts
Charley A. Knoderer
Ludovic Bariteau
Chris W. Fairall
William J. Gibson
Jeffrey E. Hare

Prepared under BOEM Contract
M08PC20057
by
Sonoma Technology, Inc.
1455 N. McDowell Blvd., Suite D
Petaluma, CA 94954-6503

Published by

U.S. Department of the Interior
Bureau of Ocean Energy Management
Gulf of Mexico OCS Region

New Orleans, LA
July 2013

DISCLAIMER

This report was prepared under contract between the Bureau of Ocean Energy Management (BOEM) and Sonoma Technology, Inc. (STI). This report has been technically reviewed by the BOEM and has been approved for publication. Approval does not signify that the contents necessarily reflect the view and policies of the BOEM, nor does mention of trade names of commercial products constitute endorsement or recommendation for use. It is, however, exempt from review and in compliance with BOEM editorial standards.

REPORT AVAILABILITY

To download a PDF file of this Gulf of Mexico OCS Region report, please visit the U.S. Department of the Interior, Bureau of Ocean Energy Management, Environmental Studies Program Information System website and search on OCS Study BOEM 2013-01110.

This report can be viewed at select Federal Depository Libraries and obtained from the National Technical Information Service by using the contact information below.

U.S. Department of Commerce
National Technical Information Service
5301 Shawnee Road
Springfield, Virginia 22312
Phone: (703) 605-6000, 1-800-553-6847
Fax: (703) 605-6900
Email: orders@ntis.gov

CITATION

MacDonald C.P., Ray A.E., Roberts P.T., Knoderer C.A., Bariteau L., Fairall C.W., Gibson W.J., Hare J.E. **2013**. Meteorological and wave measurements for improving meteorological and air quality modeling. U.S. Dept. of the Interior, Bureau of Ocean Energy Management, Gulf of Mexico OCS Region, New Orleans, LA. OCS Study BOEM 2013-01110. 102 pp.

ACKNOWLEDGMENTS

The authors of this report thank several BOEM employees for their contributions to this project. In particular, C. H. Huang, the Contract Officer's Technical Representative and science advisor; Herma Banks, the Contract Officer; and Ron Lai and Dirk Herkoff (retired), senior technical advisors. The authors also thank LSU staff for their assistance with equipment installation and operations. In addition, the authors are extremely grateful to Chevron for providing use of its platform, ST-52, for hosting the equipment, and for its in-kind contributions of the transportation of project staff and equipment to and from the platform. Finally, the authors appreciate the support of Scientific Review Board members who helped design the measurement program: Allen White and Richard Crout from NOAA and Kristina Kasoros, also from NOAA (retired).

SUMMARY

A unique partnership of corporate, government, and university researchers collaborated to develop a marine environmental observation program on an offshore platform in the Gulf of Mexico. The primary goals of this project were to provide data to (1) improve our understanding of boundary layer processes and air-sea interaction over the Gulf of Mexico; (2) improve regional-scale meteorological and air quality modeling; and (3) provide a framework for advanced offshore measurements to support future needs, such as emergency response, exploration and lease decisions, wind energy research and development, and meteorological and air quality forecasting. In October 2010, meteorological and oceanographic sensors were deployed for an extended period (approximately 18 months) on a Chevron service platform (ST 52, 90.5W, 29N) to collect boundary layer and sea surface data sufficient to support these goals. This project is important because of the large industrial presence in the Gulf, the large regional population nearby, and the recognized need for precise and timely dispersion forecasts. Observations from this project consist of surface meteorology; marine boundary layer winds; vertical profiles of atmospheric temperature, relative humidity, and liquid water; cloud base heights; atmospheric boundary layer height; ocean temperature; ocean surface temperature; ocean wave height and frequency; downwelling (shortwave) solar and infrared (longwave) radiation; and lower atmospheric boundary layer momentum and heat fluxes. This project has collected an unprecedented set of measurements over the Gulf of Mexico that captures the range of meteorological and oceanographic interactions and processes that occur over all seasons.

TABLE OF CONTENTS

FIGURES vii

TABLES xi

1. Introduction 1

2. Project Objectives 3
   - 2.1 Data to Improve Predictions of Boundary Layer Parameters Using COARE 3
   - 2.2 Data to Improve Applicability of COARE through the Use of Routine Measurements 3
   - 2.3 Data to Further Improve Mixing Height Schemes Used By Models 4
   - 2.4 Data to Improve Regional-Scale Meteorological Model Predictions 4

3. Instruments and Their Deployment, Operations, and Maintenance 5
   - 3.1 Surface Meteorological Measurements 11
     - 3.1.1 Background 11
     - 3.1.2 Approach 11
   - 3.2 Oceanographic Measurements 14
     - 3.2.1 Background 14
     - 3.2.2 Approach 14
   - 3.3 Direct Flux Measurements 17
     - 3.3.1 Background 17
     - 3.3.2 Approach 17
   - 3.4 Vertical Profiles of Temperature, Wind, and Humidity Measurements 21
     - 3.4.1 Background 21
     - 3.4.2 Approach 21
   - 3.5 Mixing Height Measurements 24
     - 3.5.1 Background 24
     - 3.5.2 Approach 24
   - 3.6 Siting and Infrastructure 26
     - 3.6.1 Siting 26
     - 3.6.2 Communications and Data Collection 27
     - 3.6.3 Power 28
     - 3.6.4 Interference 28
     - 3.6.5 Hurricanes 28
   - 3.7 Instrument Preparation and Operations 29
     - 3.7.1 Pre-Deployment Interface and Testing 29
     - 3.7.2 Shipping 30
     - 3.7.3 In-Field Testing After the Initial Installation 31
     - 3.7.4 Onsite Maintenance and Operations 32

4. Data Availability 35

5. Data Processing and Quality Control 41

6. Data Formats 51

7. Preliminary Data Analyses 55
7.1 January 11, 2011, Case Study 55
7.2 Measured and Modeled Vertical Wind Profiles 59
7.3 Observed and COARE-Calculated Fluxes 61
7.3.1 Flux System Description 62
7.3.2 Method 64
7.3.3 Meteorological Data Evaluation 66
7.3.3.1 Air Temperature 67
7.3.3.2 Relative Humidity 68
7.3.3.3 Sea Temperature 68
7.3.3.4 Wind Speed and Direction 69
7.3.4 Data Quality Control and Filtering 71
7.3.5 Comparison of Direct Covariance Flux to COARE-Calculated Flux 74
7.3.5.1 Wind Stress 75
7.3.5.2 Sensible Heat Flux 76
7.3.5.3 Latent Heat Flux 76
7.3.5.4 Discussion 76
7.3.6 COARE Data Analysis Summary 81

8. Conclusions and Recommendations 83
8.1 Measurement-Related Recommendations 83
8.2 Data Analysis-Related Recommendations 84

Literature Cited 85

FIGURES

Figure 1. Location of Chevron Platform, ST-52 (SPLL1). 8

Figure 2. The ST-52 platform complex with approximate equipment locations. 8

Figure 3. Instruments mounted on the platform roof of ST-52B. 9

Figure 4. Locations of the IR skin temperature sensor on mid-deck and shortwave and longwave radiation sensors on upper deck roof of ST-52B. 9

Figure 5. Catwalks connecting the three platforms.. 10

Figure 6. Location of the underwater float temperature sensor.. 11

Figure 7. Shortwave and longwave radiation and surface meteorological tower on Chevron's ST-52B oil platform in the Gulf of Mexico. 13

Figure 8. Wind speed (WS), wind direction (WD), infrared (longwave) radiation (IR), downwelling (shortwave) radiation (DR), temperature (T), and relative humidity (RH) from March 2, 2012, through March 6, 2012. 14

Figure 9. Components of floating temperature sensor. 16

Figure 10. Float temperature on Chevron's ST-52B oil platform in the Gulf of Mexico. 16

Figure 11. Sea surface temperature, skin temperature, and float temperature from March 2, 2012, through March 6, 2012. 17

Figure 12. Flux package located under the AB Bridge. 19

Figure 13. Specific humidity, CO_2 concentration, and air temperature from the AB Bridge flux package on October 5, 2010. 20

Figure 14. Microwave radiometer mounted on the platform deck. 22

Figure 15. Temperature, relative humidity, and liquid water from the microwave radiometer from January 11, 2011. 22

Figure 16. ASC mini-sodar on Chevron's ST-52B oil platform in the Gulf of Mexico. 23

Figure 17. Mini-sodar wind profiles from January 11, 2011. 23

Figure 18. Vaisala CL31 ceilometer located on Chevron's ST-52B oil platform in the Gulf of Mexico. 25

Figure 19. Ceilometer backscatter, mixed layer height, and cloud height from January 11, 2011. 25

Figure 20. Wave data images posted to a website in real time. 28

Figure 21. Picture of Connex boxes on Chevron's ship..... 31

Figure 22. Major periods of missing, invalid, or suspect data. 40

Figure 23. Mini-sodar winds from February 10, 2012. Wind barbs are colored by vertical wind speed.. 43

Figure 24. Surface wind (top) and precipitation (bottom) data on February 10, 2012. 44

Figure 25. Microwave radiometer temperature sounding (blue), Lake Charles temperature sounding (red), and Slidell temperature sounding (green) for January 11, 2011, 1200 UTC (left) and January 12, 2011, 0000 UTC (right). 45

Figure 26. Microwave radiometer temperature sounding (blue), Lake Charles temperature sounding (red), and Slidell temperature sounding (green) for December 6, 2011, 1200 UTC (left) and December 7, 2011, 0000 UTC (right). 46

Figure 27. Visible satellite imagery over the northern Gulf of Mexico for January 11, 2011, at 1431 UTC. 47

Figure 28. Ceilometer backscatter with cloud bases, cloud tops, and mixing heights in meters above platform level (apl). 47

Figure 29. Surface meteorological data from the platform deck for June 23 through June 28, 2011, including (top to bottom) wind speed (WS) and wind direction (WD); infrared radiation (IR) and downwelling radiation (DR); relative humidity (RH) and pressure (P); and temperature (T) and rain (RAIN).. 48

Figure 30. Skin temperature from the infrared temperature sensor (red line) and fixed sea surface temperature from LSU for 11/15/2010 through 12/9/2010. 49

Figure 31. Wave heights and maximum wave heights for September 14 through September 18, 2011. 50

Figure 32. Illustration of unfiltered (blue) and filtered (red) specific humidity data from the AB Li-Cor 7500 sensor. 50

Figure 33. Mini-sodar wind data on January 11, 2011. 56

Figure 34. Microwave radiometer temperature, relative humidity, and liquid water data on January 11, 2011. Times are in UTC. 57

Figure 35. Visible satellite image taken at 1431 UTC on January 11, 2011..... 57

Figure 36. Ceilometer backscatter data, cloud base and top heights, and mixing heights on January 11, 2011. 58

Figure 37. COARE-calculated sensible heat flux (Hs) and air-sea temperature (T) difference (top), and COARE-calculated latent heat (Hl) and air-sea specific humidity (Q) difference (middle), and COARE-calculated streamwise stress and wind speed (bottom). 58

Figure 38. Seasonal averages of measured (sodar) versus model (NAM) winds. 60

Figure 39. Seasonal average diurnal profile of boundary layer winds as measured by the mini-Sodar. 61

Figure 40. Location of the AB and AC flux packages on the platform. 62

Figure 41. Close-up view of the AB flux package. 63

Figure 42. Meteorological conditions from the platform during 2011. 65

Figure 43. Meteorological conditions from the platform during 2012. 66

Figure 44. Time series of air temperatures for the two sonic anemometers (blue and red), and the temperature measurements from the roof of the B platform (magenta and black). 67

Figure 45. Relative humidity from STI (magenta) and LSU (black) instruments. 68

Figure 46. Time series of air and sea temperatures from STI (blue) and LSU (magenta) instruments. 69

Figure 47. Wind speed residuals as a function of STI wind direction (1 m/s bins). Horizontal dash lines indicate ±0.5 m/s. 70

Figure 48. Wind direction residuals as a function of STI wind direction (5-degree bins). Horizontal dash lines indicate ± 0.5 degrees. 71

Figure 49. A, B, and C platform orientation relative to true north. 72

Figure 50. U (blue) and W (red) spectra from the AB flux package at 0 and 6 UTC on August 9, 2011. 73

Figure 51. Illustration of unfiltered (blue) and filtered (red) specific humidity data from the AB Li-Cor 7500 sensor. 74

Figure 52. Top panel: BULK (calculated) stress (Taub) versus measured streamwise stress (Tauc) for the AB and AC bridges combined. Lower panel: Same flux, but bin-averaged and plotted as a function of 10-m neutral wind speed. 78

Figure 53. Top panel: BULK (calculated) sensible heat flux (Hsb) versus measured sensible heat flux (Hsc) for the AB and AC bridges. Lower panel: Same flux, but divided by wind speed and plotted as a function of sea-air temperature difference. 79

Figure 54. Top panel: BULK (calculated) latent heat flux (Hlb) versus measured latent heat flux (Hlc) for the AB and AC bridge. Lower panel: Same flux, but divided by wind speed and plotted as a function of sea-air specific humidity difference. 80

TABLES

Table 1. Measurements taken during the field study 6

Table 2. Platform description..... 27

Table 3. On-platform (internal) and off-platform (external) data sources used during data validation 33

Table 4. Data completeness statistics by instrument type 36

Table 5. Data capture statistics by instrument type 37

Table 6. Major downtimes of the instruments 38

Table 7. On-platform (internal) and off-platform (external) data sources used during data validation 42

Table 8. Data file names 52

Table 9. Fields located in data files 53

Table 10. Parameter names and descriptions..... 53

Table 11. Flux package sensor heights and sampling rates 63

1. INTRODUCTION

Researchers and technicians from Sonoma Technology Inc. (STI), University of Colorado at Boulder (CU), the National Oceanic and Atmospheric Administration (NOAA), and Louisiana State University (LSU), with scientific input from the Bureau of Ocean Energy Management (BOEM) and a Scientific Review Board,[1] developed an atmospheric boundary layer environmental observations program on an offshore platform in the Gulf of Mexico. Specifically, in October 2010, meteorological and oceanographic sensors were deployed for approximately 18 months on a Chevron service platform about 12.4 miles (20 km) south of Terrebonne Bay, Louisiana, to collect atmospheric boundary layer and sea surface data. The ocean depth at this location was 20.5 m. Observations from this project consist of surface meteorology; marine boundary layer winds; vertical profiles of atmospheric temperature, relative humidity, and liquid water; cloud base heights; atmospheric boundary layer height; ocean temperature; ocean surface temperature; ocean wave height and frequency; downwelling (shortwave) solar and infrared (longwave) radiation; and lower atmospheric boundary layer momentum and heat fluxes. The primary goals of this program were to collect and deliver data to support future work to (1) improve our understanding of boundary layer processes and air-sea interaction over the Gulf of Mexico; (2) improve small and regional-scale meteorological and air quality modeling; and (3) provide a framework for advanced offshore measurements to support future needs such as emergency response, exploration and lease decisions, wind energy research and development, and meteorological and air quality forecasting.

This project is important because of the large industrial presence in the Gulf, the sizeable regional population nearby, and the recognized need for precise and timely pollutant forecasts. It yielded an unprecedented set of boundary layer measurements over the Gulf of Mexico that captured a range of meteorological and oceanographic interactions and processes which occur over all seasons.

This report provides information on the

- Project objectives (Section 2)
- Instruments, and their deployment and operations (Section 3)
- Data availability (Section 4)
- Data processing and quality control (Section 5)
- Data formats (Section 6)
- Preliminary data analyses (Section 7)[2]
- Conclusions and recommendations (Section 8)

1 The Scientific Review Board consisted of three members: Allen White and Richard Crout from NOAA, and Kristina Kasoros from NOAA (retired).

2 While the primary objective of this program was to provide data for future analysis and modeling, preliminary data analyses were completed.

2. PROJECT OBJECTIVES

The overall objective of this study was to collect meteorological data that can be used to better characterize the atmospheric boundary layer over the Gulf of Mexico. This information will be used in future work to improve meteorological and air quality modeling along the Gulf Coast. A critical component of the study was to fill a data gap between surface (platform) measurements and observations at about 200 m msl as identified during the BOEM Atmospheric Boundary Layer (ABL) Study (MacDonald et al. 2004). As part of the ABL study, the project team and BOEM also identified other measurements and analyses needed to further improve modeling. This study addressed these measurement needs by providing the data necessary for subsequent research and analysis. Details on specific project objectives are described in the following paragraphs.

2.1 DATA TO IMPROVE PREDICTIONS OF BOUNDARY LAYER PARAMETERS USING COARE[3]

During the 1998–2001 BOEM field program (Vaisala Meteorological Systems and Sonoma Technology 2002), no direct flux measurements were made from which to verify the Coupled Ocean Atmosphere Response Experiment (COARE) output. In addition, a few parameters (wave height and frequency, downwelling shortwave and longwave solar radiation, and precipitation) required by COARE were calculated rather than measured. Therefore, the accuracy of the COARE algorithm was never verified against observations, and only limited improvements were made to COARE for application in the Gulf of Mexico. In this study, all parameters required by COARE were directly measured to reduce uncertainty in the COARE calculations. In addition, direct measurements of boundary layer parameters were made. Wind profiles were measured in the lowest few hundred meters; fluxes and turbulence measurements occurred at a fixed height. These direct measurements of boundary layer parameters can be compared to the calculated parameters and thus will lead to improvements to COARE. These measurements can also be used to develop and improve other boundary layer algorithms used in prognostic models.

2.2 DATA TO IMPROVE APPLICABILITY OF COARE THROUGH THE USE OF ROUTINE MEASUREMENTS

Not all meteorological parameters used by COARE are routinely measured at standard sites, thus these parameters must be calculated by COARE. For example, Coastal-Marine Automated Network (CMAN) stations do not measure sea surface skin temperature, shortwave downwelling radiation, and longwave downwelling radiation, or precipitation, resulting in uncertainty in the COARE output for these types of sites. To reduce this uncertainty, this study included measurements similar to those commonly available at routine sites (like CMAN sites) along with direct measurements of all required inputs and many of the outputs of COARE. Subsequent calculations of boundary layer parameters (fluxes, etc.) using the routinely available data can be

3 COARE is the acronym for the Coupled Ocean Atmosphere Response Experiment. However, based on current convention, its use throughout this report refers to the algorithm developed during that experiment, the COARE marine boundary layer algorithm (Fairall et al. 1996; Fairall et al. 2003). COARE uses routine oceanographic and meteorological measurements to calculate boundary layer parameters such as stress, heat, and momentum fluxes.

compared to the measurements made during this study. Future refinements to the COARE algorithm based on the findings can increase its applicability to data collected at other sites.

2.3 DATA TO FURTHER IMPROVE MIXING HEIGHT SCHEMES USED BY MODELS

Much work has been done to improve meteorological and air quality modeling in an offshore environment, such as the Gulf of Mexico's. For example, BOEM-sponsored work (Hanna et al. 2006) has been adopted in the widely used U.S. Environment Protection Agency (EPA) CALMET/CALPUFF modeling system. However, there are still issues with models' ability to properly represent the evolution of boundary layer heights, especially in coastal areas. The measurements that were collected in this study can be used to validate and improve schemes used by CALMET and other frequently used models to estimate mixing height.

2.4 DATA TO IMPROVE REGIONAL-SCALE METEOROLOGICAL MODEL PREDICTIONS

Past analyses have shown significant overwater aloft wind differences between weather forecast models and observed aloft winds over the Gulf of Mexico (Knoderer et al. 2004). During this study, we collected data that can be used to evaluate forecast models and set the stage for working with the National Center for Environmental Prediction (NCEP) to better understand and address any model biases. The results will also provide BOEM guidance for incorporating regional-scale model predictions in BOEM's modeling efforts.

3. INSTRUMENTS AND THEIR DEPLOYMENT, OPERATIONS, AND MAINTENANCE

To collect the data necessary to address the objectives presented in Section 2, a wide range of highly sophisticated instruments and supporting equipment were deployed on Chevron Oil Platform ST-52 about 12.4 miles (20 km) off the coast of Louisiana. The instruments, which are listed in Table 1, were operated from October 4, 2010, through April 1, 2012. A map showing the location of the platform is shown in Figure 1. Figure 2 shows the platform and the locations where the instruments were mounted. Figures 3 through 6 show the instruments on the platform complex. The microwave radiometer, minisodar, ceilometer, and surface meteorological tower were mounted on the main platform's (ST-52B) upper deck, which is at approximately 37 m msl. The sea skin temperature sensor was mounted on a rail of a mid-level deck on the southern corner of platform B at approximately 25 m msl. The deck extended over the water farther than the lower decks, yielding an unobstructed view of the water. Two sets of flux instruments were used; an instrument package was mounted vertically downward from each of the two catwalks that connect the platform complex. The first package was mounted under the bridge between the A and B platforms at approximately 11 m msl, and the other was mounted beneath the bridge that connects the A and C platforms at approximately 14 m msl. Depending on wind direction, this placement provided flux measurements that were often free of platform effects on the horizontal and vertical motion and were within the atmospheric surface layer. A floating temperature sensor was mounted on the platform's southeast leg; the sensor floated at about -0.2 m msl. Wave height and frequency measurements were taken adjacent to the southwest leg of platform B by LSU as part of a separate project (WAVCIS), but the data have been made available to this project.

Details of the measurements follow the figures and are organized by atmospheric or oceanographic feature measured.

Table 1.

Measurements taken during the field study

	Parameter	Instrument and Measurement Characteristics			
		Instrument Manufacturer	**Measurement Height(s) Above Mean Sea Level (m)**	**Vertical Resolution (m)**	**Frequency**
Upper-air	Wind Profiles	Mini-sodar Atmospheric Systems 4000	57–237	10	Sub-hourly
	Temperature Profiles	Microwave radiometer Radiometrics MP-3000A	87–10,000	50 below 500 m 100 between 500 m and 2000 m 250 above 2000 m	Sub-hourly and hourly
	Humidity Profiles	Microwave radiometer Radiometrics MP-3000A	87–10,000	50 below 500 m 100 between 500 m and 2000 m 250 above 2000 m	Sub-hourly
	Mixing Heights	Ceilometer Vaisala CL31	39–7,737 90–10,000	5 90–100	Sub-hourly and hourly
	Cloud Base Height	Ceilometer Vaisala CL31	39–7,737 90–10,000	5 90–100	Sub-hourly and hourly
Near Surface	Winds	Vane and propeller anemometer RM Young 5305	48	NA	Sub-hourly and hourly
	Temperature	Thermometer Vaisala HMP45AC	46 and 47	NA	Sub-hourly and hourly
	Precipitation	Texas Instruments TR525	38	NA	Sub-hourly and hourly
	LSU Temperature	Thermometer Vaisala HMP155	46 and 47	NA	Hourly
	Humidity	Hygrometer Vaisala HMP155	46 and 47	NA	Sub-hourly and hourly
	LSU Humidity	Hygrometer Vaisala HMP155	46 and 47	NA	Hourly
	LSU Pressure	Barometer Vaisala PTB101	14 but corrected to msl	NA	Hourly
	Downwelling Shortwave Radiation	Pyranometer Eppley PSP	39	NA	Sub-hourly and hourly
	Downwelling Longwave Radiation	Pyrgeometer Eppley PIR	39	NA	Sub-hourly and hourly
	LSU Visibility	Belfort C100	39	NA	Hourly

Table 1. Measurements taken during the field study (continued)

	Parameter	Instrument and Measurement Characteristics			
		Instrument Manufacturer	**Measurement Height(s) Above Mean Sea Level (m)**	**Vertical Resolution (m)**	**Frequency**
Flux	Flux (AB catwalk)	Sonic anemometer Gill WindMasterPro, Infrared hygrometer with gas analyzer Li-Cor LI-7500	10.2, 10.8[a]	NA	Sub-hourly
	Flux (AC catwalk)	Sonic anemometer Gill WindMasterPro, Infrared hygrometer with gas analyzer Li-Cor LI-7500	11.6, 12.6b	NA	Sub-hourly
Ocean	Wave measurements	Digiquartz Pressure Transducer Paroscientific 25A-158 ADCP Current Meter RD Instruments Workhorse Sentinel	Sea level but variable depending on tides and waves	NA	Sub-hourly
	Fixed-mount underwater temperature	Thermistor YSI	-0.60; but variable depending on tides and waves	NA	Sub-hourly and hourly
	Underwater temperature	Float sensor STI/LSU/NOAA-developed	-0.2	NA	Sub-hourly and hourly
	Sea skin temperature	I.R. Thermometer Everest Interscience, Inc. and Heitronics KT15.85-IIP IR sensorc	Sea level but mounted at ~25 m msl	NA	Sub-hourly and hourly

[a] Measurements taken at 2238 UTC August 5, 2012.
[b] Measurements taken at 2243 UTC August 5, 2012.
[c] Everest sensor was replaced with Heitronics on February 24, 2012.

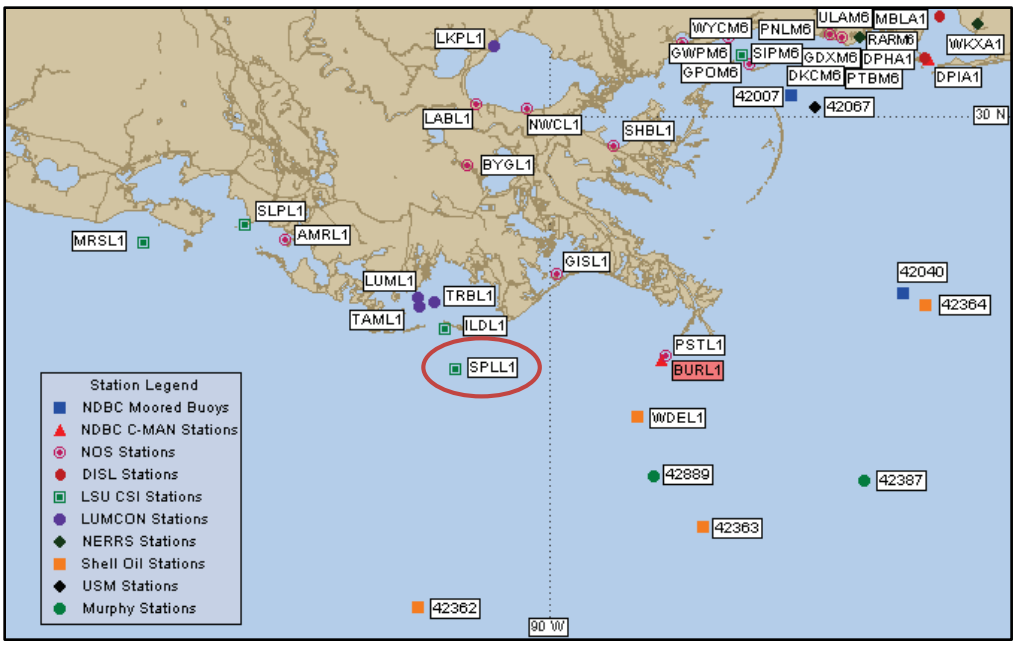


Figure 1. Location of Chevron Platform, ST-52 (SPLL1).

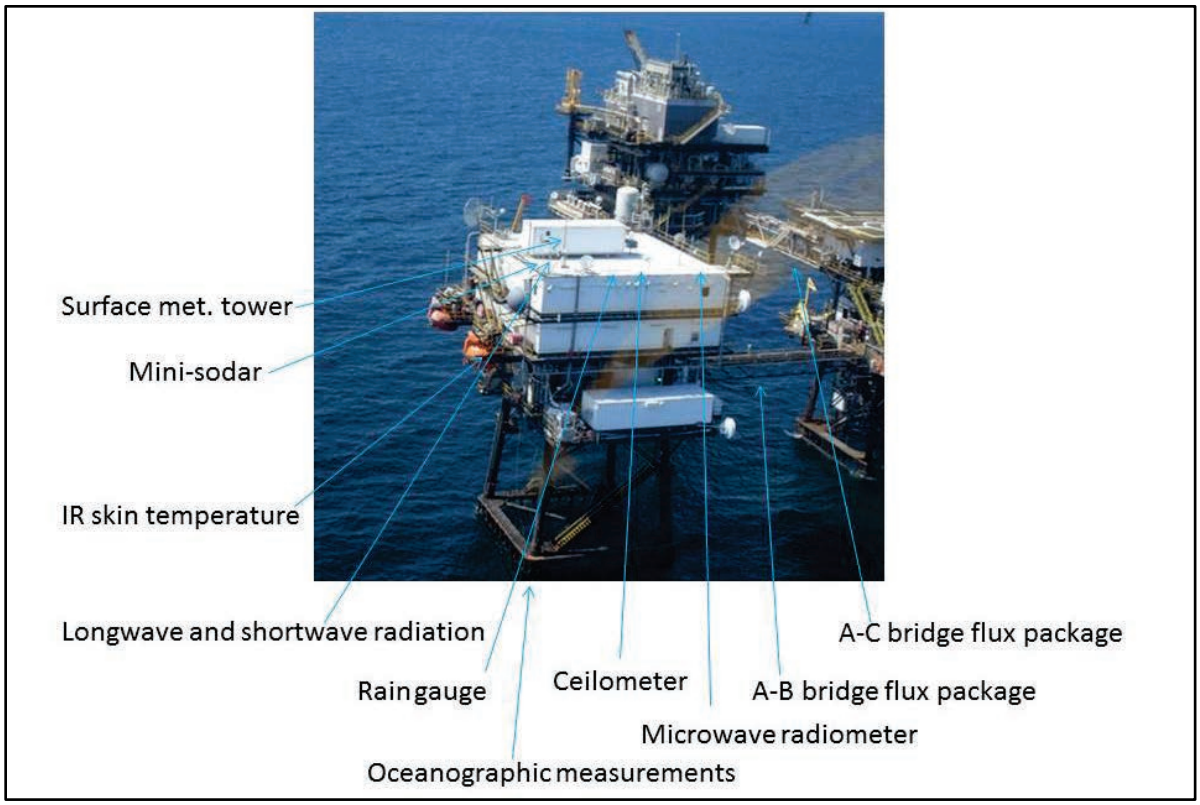


Figure 2. The ST-52 platform complex with approximate equipment locations. Most equipment is located on platform ST-52B in the foreground; ST-52A is on the right and ST-52C is in the background.

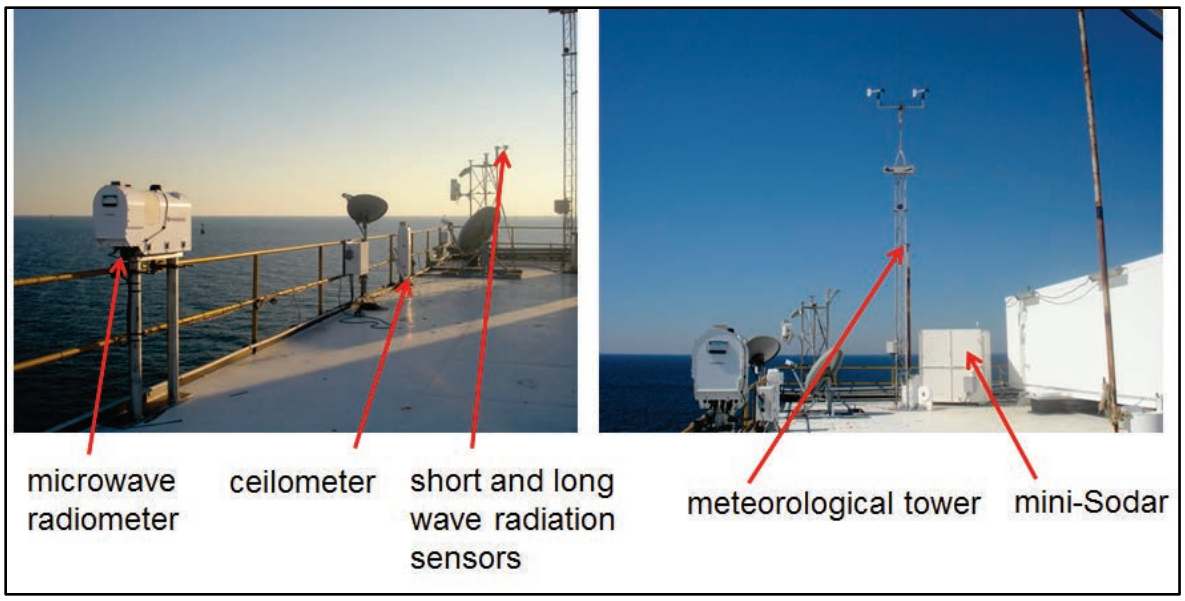


Figure 3. Instruments mounted on the platform roof of ST-52B.

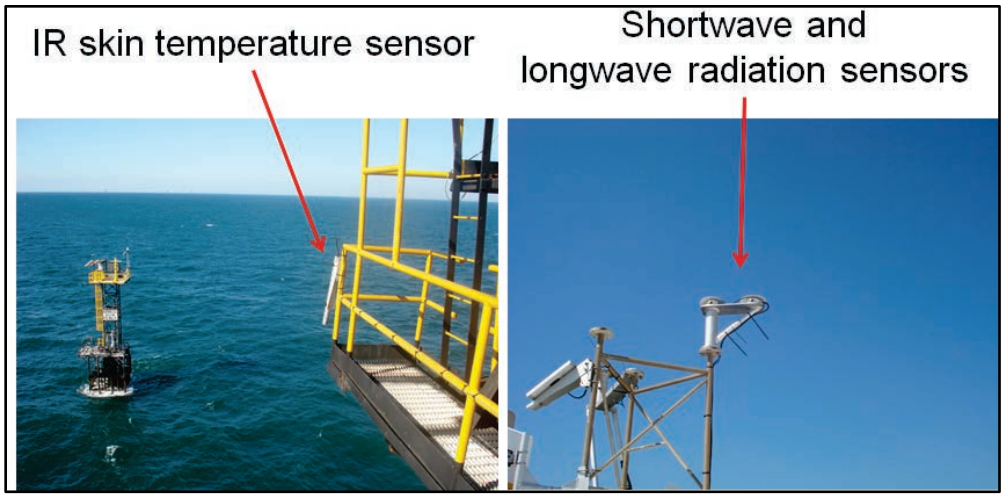


Figure 4. Locations of the IR skin temperature sensor on mid-deck and shortwave and longwave radiation sensors on upper deck roof of ST-52B.

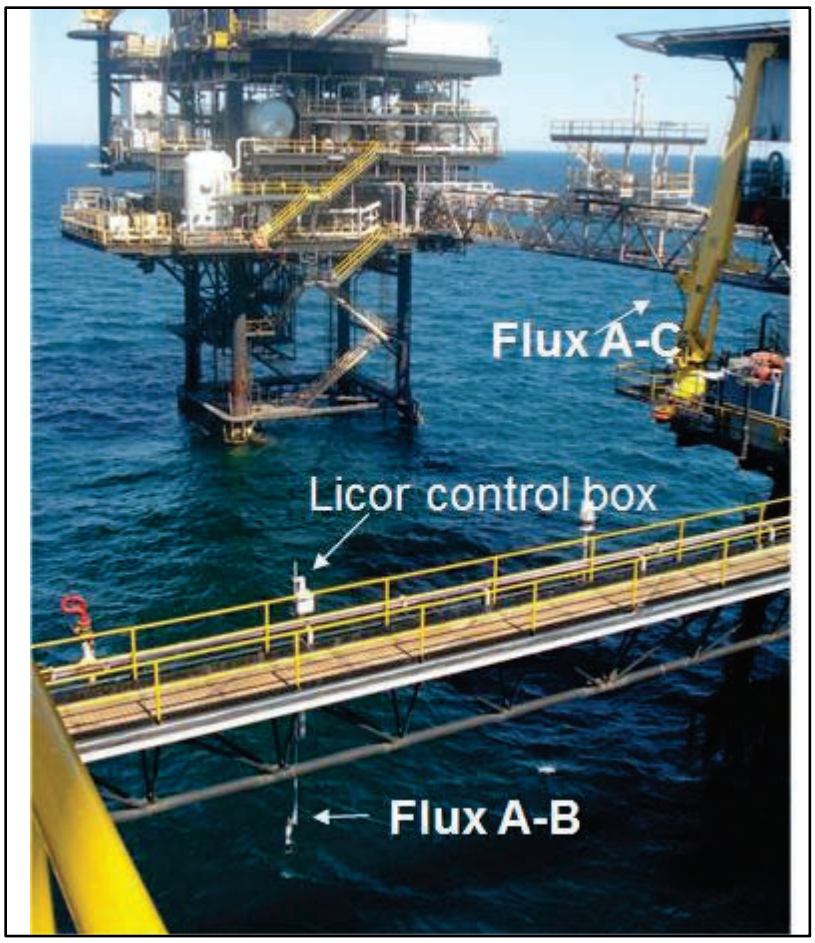


Figure 5. Catwalks connecting the three platforms. This photo was taken from a mid-level deck of platform ST-52B. Flux measurements were taken at about the middle of each catwalk.



Figure 6. Location of the underwater float temperature sensor. Only the top of the housing can be seen; the sensor is floating in a vertical pipe mounted on the leg of the platform. The LSU sea-state measurements are made in close proximity to this location.

3.1 SURFACE METEOROLOGICAL MEASUREMENTS

3.1.1 Background

An important element of this project is the collection of measurements for use in the COARE marine boundary layer algorithm (Fairall et al. 2003). The COARE algorithm can be used to calculate fundamental boundary layer scaling parameters such as the surface roughness length, the friction velocity, and the Monin-Obukhov length, in addition to the latent heat flux and the sensible heat flux. From these parameters, the mixing depth (h) and the vertical profiles of wind speed, temperature, and water vapor mixing ratio can be estimated for input to transport and dispersion models.

3.1.2 Approach

We collected an "ideal" set of measurements for use by COARE. Note that when COARE does not have the ideal set of measurements, it calculates them, leading to greater uncertainty in the results. Our measurement strategy was to enable comparisons of observed boundary layer measurements to COARE-calculated boundary layer data, using both the ideal and minimum sets of measurements required by COARE. These results can then be used to refine the COARE

algorithm for the Gulf of Mexico region and improve its output for future model applications that use data from sites with the minimum set measurements required by COARE (such as measurements collected by NWS buoys). Initial COARE evaluation and refinement work was performed in this study and results are presented in Section 7.

The COARE-required measurements that we collected consisted of

- wind speed,
- air temperature,
- relative humidity, and
- measurement heights for the surface meteorological measurement instruments.

The heights of the sensors are needed for input into the COARE. These parameters consist of measurement heights for wind, temperature, and relative humidity; and depth of the sea skin temperature sensor.

The additional measurements made to produce the ideal data set of additional measurements for COARE consisted of

- downwelling shortwave and longwave solar radiation,
- precipitation,
- sea skin temperature, and
- wave height and frequency.

A tipping bucket rain gauge was installed on the platform deck. It measured rainfall as total rainfall per minute so that an hourly rainfall rate could be determined. An Eppley Precision Spectral Pyranometer (PSP) First Class Radiometer was installed on a mounting bracket atop a short (3 m) tower on the platform deck to measure shortwave downwelling radiation (see Figure 7). Next to it an Eppley Precision Infrared Radiometer (PIR) Pyrgeometer was installed to measure longwave radiation. In addition, as part of a separate project, LSU measured wave height, wave frequency, and water current and took duplicate meteorological measurements on the platform deck. The LSU meteorological measurements consisted of wind speed, wind gusts, wind direction, air temperature, sea level barometric surface pressure, and visibility. Note that the LSU meteorological data use the NWS system of measurement convention of taking measurements for 2 minutes at the top of the hour and reporting the measurement as an hourly value, while the primary meteorological data were collected as continuous (once per 10 second) one-minute averages and accumulated into hourly averages. The data from the LSU measurements are included in the data delivery. Figure 7 shows the surface meteorological tower containing the anemometers and the temperature, relative humidity, downwelling shortwave and infrared (longwave) radiation, and skin temperature sensors. Figure 8 shows a sample of the surface meteorological data.

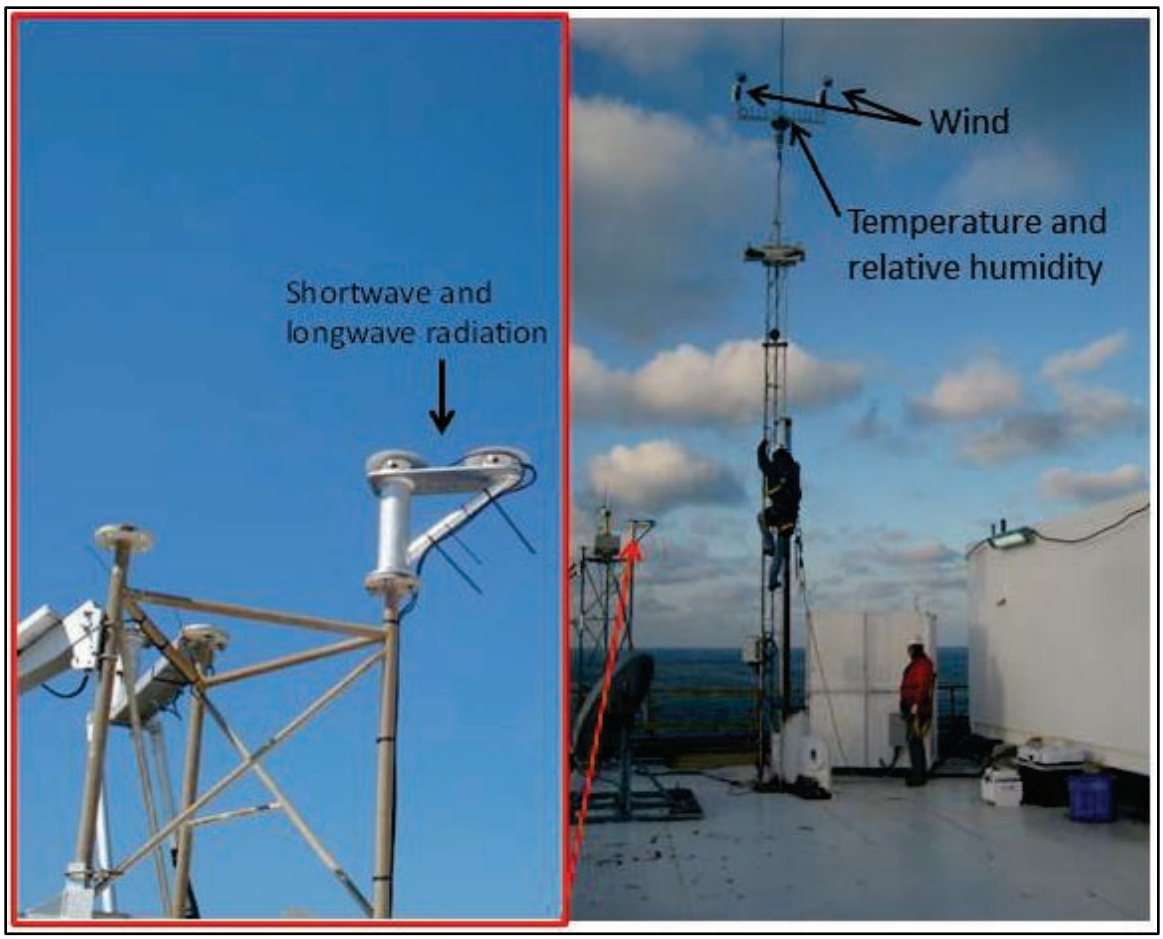


Figure 7. Shortwave and longwave radiation and surface meteorological tower on Chevron's ST-52B oil platform in the Gulf of Mexico.

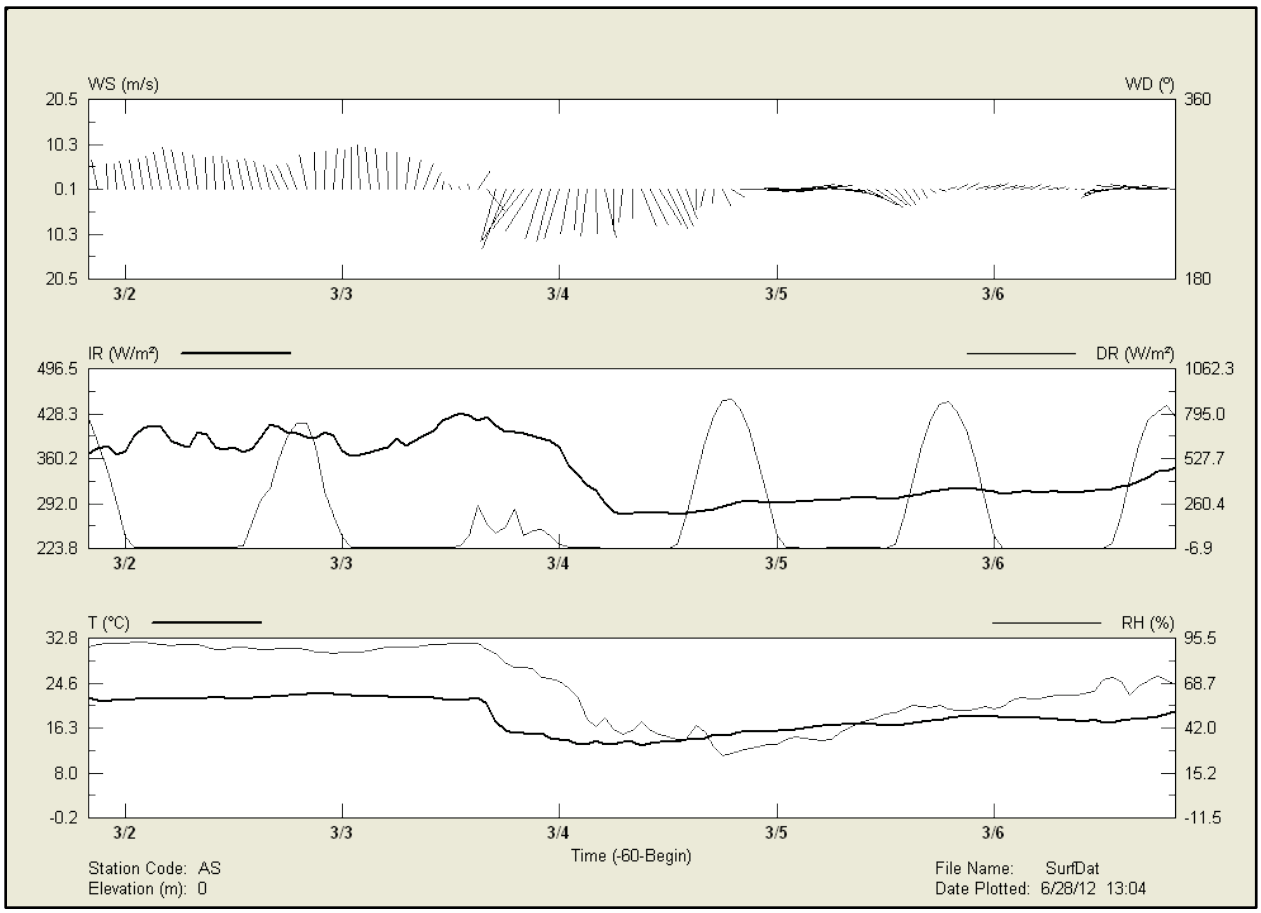


Figure 8. Wind speed (WS), wind direction (WD), infrared (longwave) radiation (IR), downwelling (shortwave) radiation (DR), temperature (T), and relative humidity (RH) from March 2, 2012, through March 6, 2012.

3.2 OCEANOGRAPHIC MEASUREMENTS

3.2.1 Background

As described in the project objectives, there is a need to improve the applicability of COARE when using only routine measurements as inputs, especially measurements collected at standard buoys. To that end, measurements collected by standard buoys, such as wave height and period and underwater temperature, were collected along with other oceanographic measurements.

3.2.2 Approach

We obtained measurements of wave spectra, wave height, wave period, and near-surface water temperature that were being collected as part of a separate study (WAVCIS) being conducted by LSU. LSU made these measurements available for this study. The oceanographic sensors are as follows: a Digiquartz pressure transducer (Paroscientific model 245A-158), an ADCP current meter (RD Instruments model Workhorse Sentinel, 600 KHz transducer with a 50 m pressure sensor), and an electronic thermometer (locally made with a YSI Thermistor bead). The pressure

sensor and the ADCP sensors provided for the measurements of directional waves, near-bottom to near-surface water column current speed and current direction (in 1-m bins), and the two water level measurements. The near-surface water temperature and pressure sensors were positioned approximately 4.5 m below mean water level. This depth minimized the depth-attenuation of the high-frequency wave signals during relatively calm conditions but was deep enough to measure most of the large wave conditions that typically occurred during frontal passages. The ADCP sensor was mounted about 2.1 m off the bottom of the platform (under water) and projected about 1.5 m out from the rig leg, so that the beams from the ADCP cleared the sides of the platform.

A custom floating thermometer was fabricated to measure near-surface water temperature (see Figure 9). A 20-ft (6.1 m) length of 4-in (0.1 m) PVC pipe was capped at both ends, perforated with a series of slots that ran the length of the pipe, sheathed with anti-foul copper foil, and mounted on a leg of the platform perpendicular to the surface of the sea. One end of a coiled (1/4-in; 0.635 cm) air hose, with a 2-conductor 24 gauge wire inserted through it, was connected to the top of the pipe. The other end was attached to a copper float consisting of a sealed 20-cm-long copper tube that has a thermistor potted inside of it. The float allows the sensor to remain suspended approximately 20 cm below the surface. The perforations in the pipe are made of fairly narrow vertical slots throughout the pipe applied to dampen the wave action, resulting in a somewhat smaller change in the water level while still allowing for a flushing action to occur within the pipe. The air coil was sealed at both ends so that it too provided some floatation while facilitating the movement of the float up and down the length of the pipe. The mounted float sensor is shown in Figure 10; sample data are shown in Figure 11.

An IR thermometer was installed to measure the surface of the sea using a non-intrusive measurement method. An Everest Interscience, Inc., 4000L Sea-Therm Infrared Temperature sensor fitted with an insulated baffle was initially installed. It proved not to be waterproof despite being redesigned and replaced twice by the manufacturer. The data from this sensor are suspect because the sensor frequently displayed significant temperature excursions. The sensor was sent back to the manufacturer for a third modification, but the engineer was unable to complete the work. Ultimately, a Heitronics KT15.85-IIP IR sensor was purchased and installed on the platform. This sensor operated very well. In addition, as part of the oceanographic sensors, a thermistor mounted on the tower leg at a fixed position of approximately -1 m msl provided a secondary near-surface sea temperature measurement.

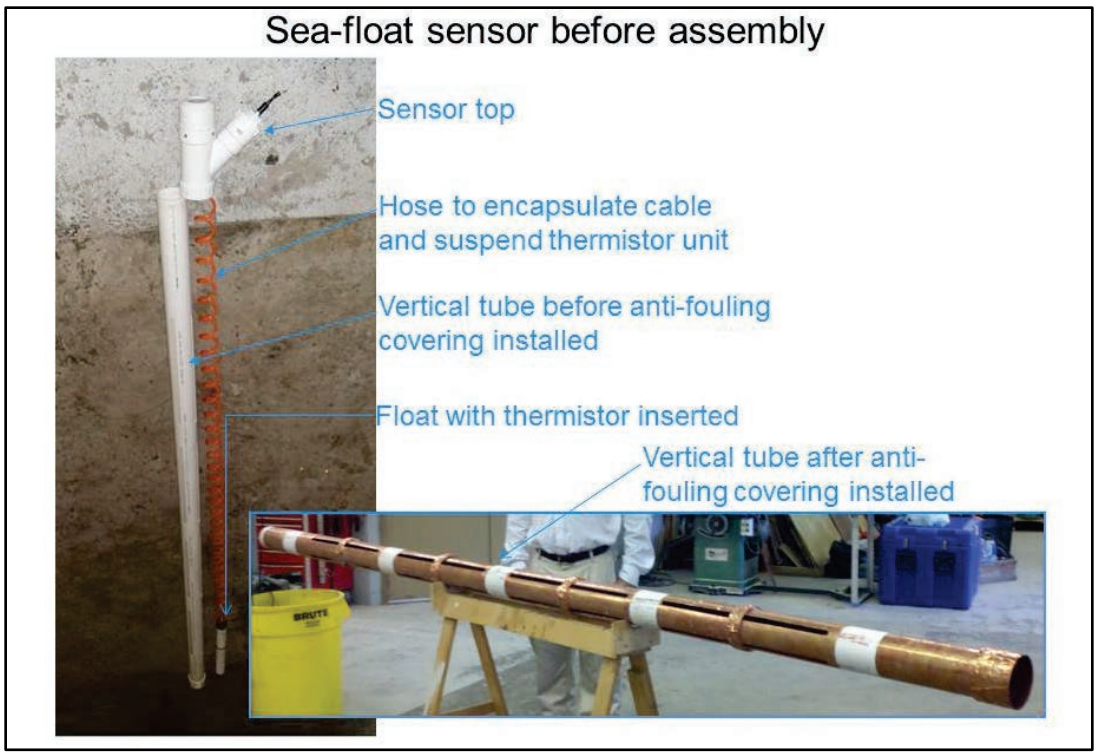


Figure 9. Components of floating temperature sensor.

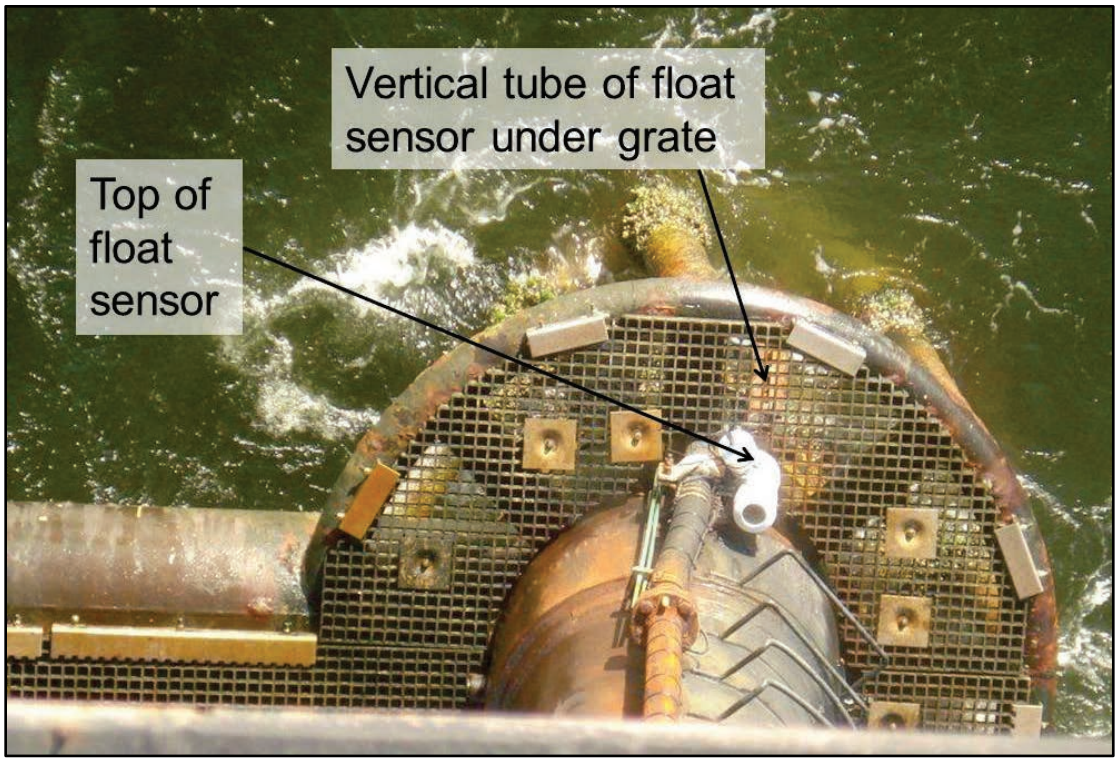


Figure 10. Float temperature on Chevron's ST-52B oil platform in the Gulf of Mexico.

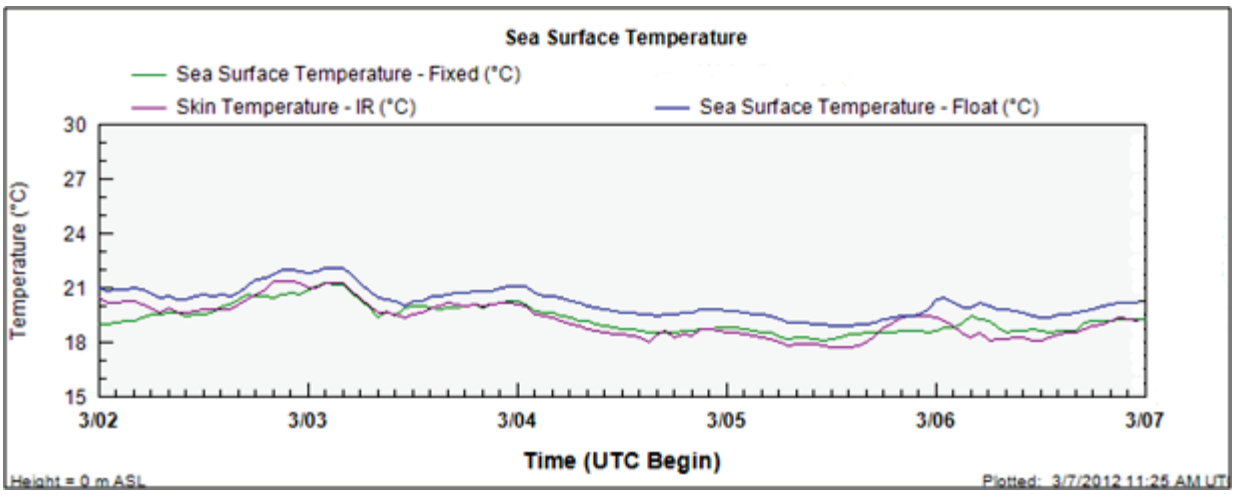


Figure 11. Sea surface temperature, skin temperature, and float temperature from March 2, 2012, through March 6, 2012.

3.3 DIRECT FLUX MEASUREMENTS

3.3.1 Background

The transfer of momentum, heat, and mass between the atmosphere and ocean surface is accomplished by turbulent processes. Atmospheric mixing processes in the lower marine boundary layer (that portion of the atmosphere closest to the sea surface) are driven by mechanical and thermal forcing, and these turbulent eddies extend from the surface up to the height of the boundary layer (typically between 500 m and 2000 m). The energy contained within these eddies cascades down to smaller and smaller time and spatial scales; it is within this large breadth of scales that the turbulence is able to make energy transfers to and from the surface of the water. These fundamental transfer processes determine the boundary conditions at the sea surface, and any effort to model atmospheric dispersion requires determination of the source strength (or sink strength) of heat and momentum at the sea surface. Direct measurement of turbulence statistics and fluxes required the use of specialized instrumentation and analysis techniques, which are briefly outlined below.

3.3.2 Approach

Turbulent flux measurements were taken with an ultrasonic anemometer/thermometer (sonic anemometer). The operating principle of this instrument exploits the fact that a sound wave is carried with a moving fluid (the wind), and the small-scale wind fluctuations along three axes can be computed from the time-of-flight of an ultrasonic pulse. The frequency of wind velocity measurement was 10 times per second (Hz), and this response rate enabled measurement of the turbulence and turbulent fluxes on time and spatial scales sufficient to calculate the statistics with a high degree of accuracy. The sonic anemometer also enabled a measurement of small-scale temperature fluctuations (the speed of sound is proportional to the temperature of the medium), and we computed turbulent air temperature statistics from the time-flight estimates. By computing the covariance of the various measured combinations of vertical velocity, horizontal

velocity, and temperature, we made direct measurements of the fluxes of momentum (which have two components—streamwise and cross-stream) and sensible heat. The sonic anemometer also served to provide an additional measurement of the mean wind speed and direction.

Latent heat flux measurements were taken by using a fast-response infrared hygrometer and gas analyzer on time and spatial scales coincident with those of the sonic anemometer. This instrument was deployed as close to the sonic anemometer as possible without disturbing the flow of air through the sampling volume. This device operates on the principle that water vapor absorbs infrared radiation at a well-defined frequency. By simultaneously measuring the absorption of radiation at an adjacent non-absorbing reference frequency, the instrument is able to determine small-scale (10-Hz) fluctuations in absolute humidity. Latent heat flux was calculated by computing the covariance of the vertical velocity fluctuations from the sonic anemometer and the absolute humidity measurements from the hygrometer.

The same principle of the attenuation of a selected frequency of infrared light was used for the measurement of small-scale fluctuations of carbon dioxide (CO_2) in the near-surface atmosphere. The gas analyzer thus enabled estimates of the turbulent fluxes of moisture and CO_2. Although not requested by BOEM, CO_2 measurements were part of the flux measurement package and were included. These measurements may be helpful for other potential applications related to climate change. Figure 12 shows the flux package installed under the AB Bridge. A second flux package was installed under the AC Bridge. Figure 13 provides a sample of the data collected.

The direct covariance or eddy-correlation flux measurement technique was used to calculate fluxes. In essence, turbulent fluctuations of vertical velocity were computed with streamwise horizontal velocity fluctuations (to obtain wind stress or momentum flux), with the temperature fluctuations (to obtain the sensible heat flux), and with the small-scale fluctuations of H_2O and CO_2 (to obtain the latent heat flux and CO_2 flux, respectively). By averaging over a time scale sufficient to capture statistics on length scales as large as the marine boundary layer, while carefully avoiding averaging through potential complicating factors such as mesoscale atmospheric disturbances, we computed the turbulent fluxes and other statistics. Details on the fluxes are provided in Section 7.

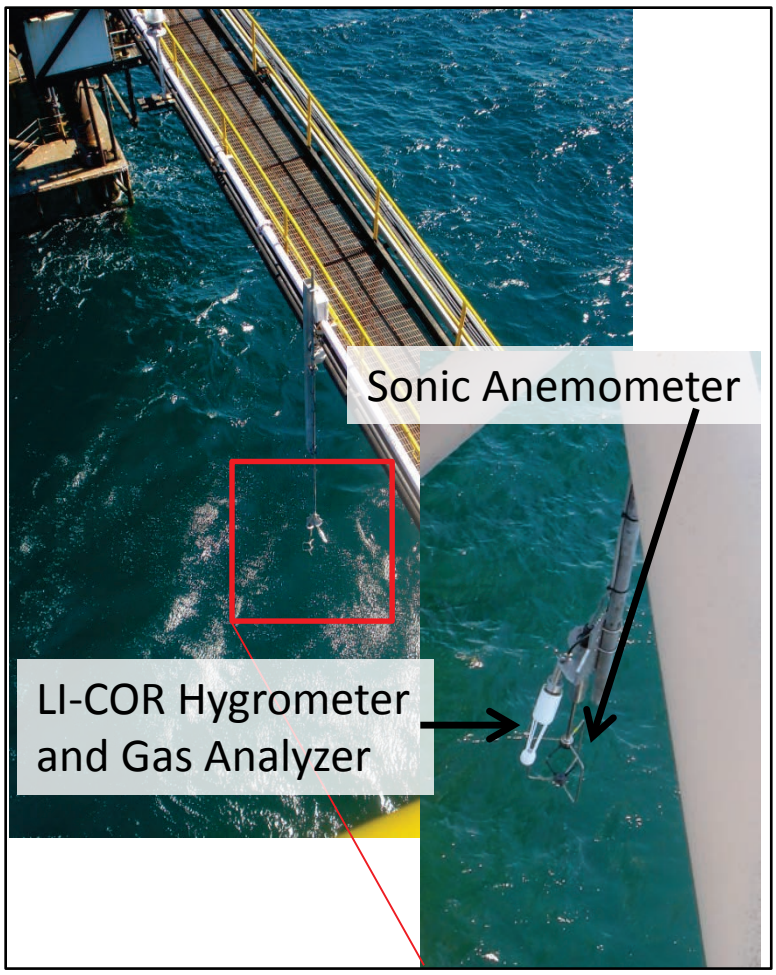


Figure 12. Flux package located under the AB Bridge. The flux package includes a Gill sonic anemometer and a Li-Cor hygrometer and CO_2 gas analyzer.

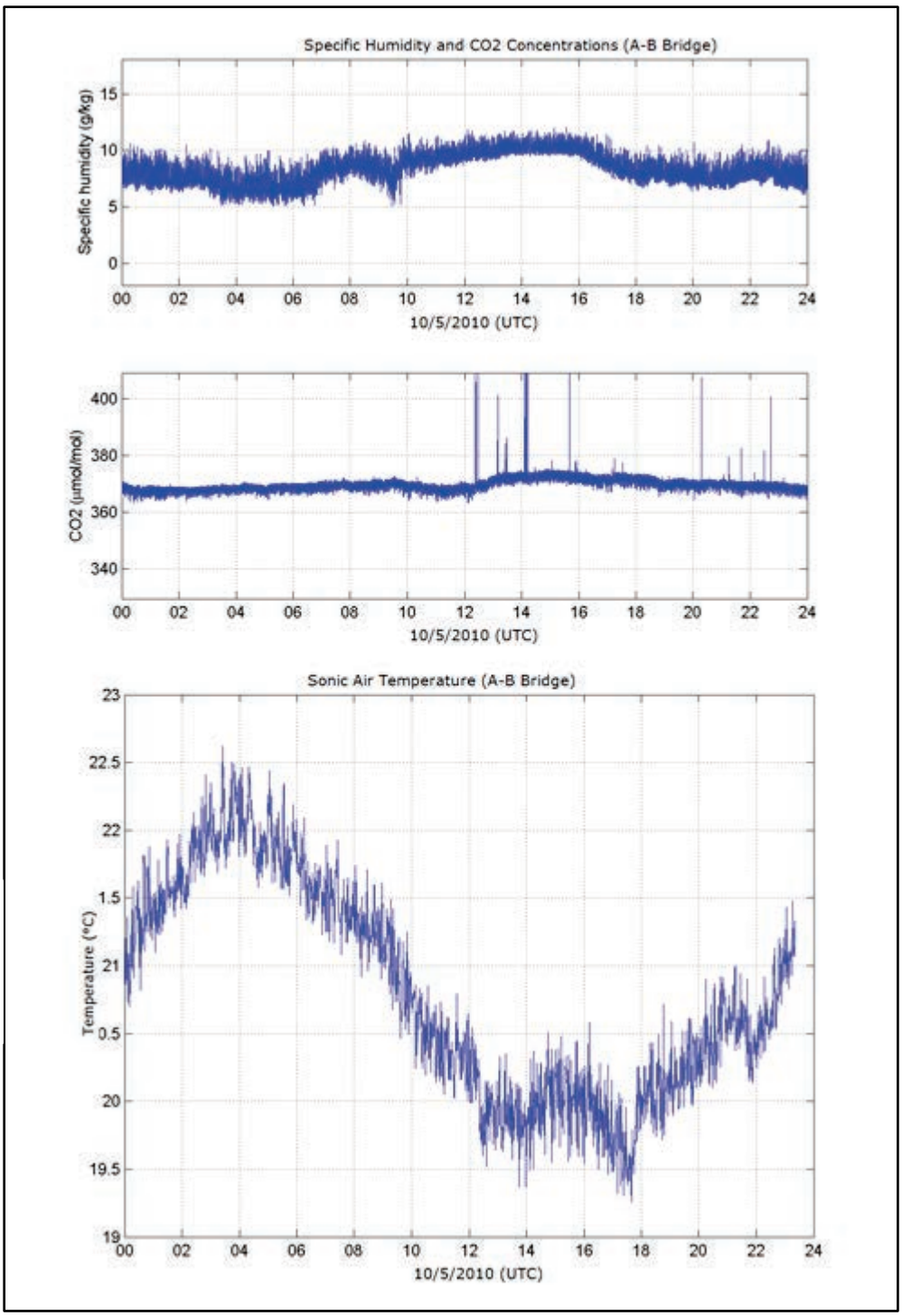


Figure 13. Specific humidity, CO_2 concentration, and air temperature from the AB Bridge flux package on October 5, 2010.

3.4 VERTICAL PROFILES OF TEMPERATURE, WIND, AND HUMIDITY MEASUREMENTS

3.4.1 Background

Vertical profiles of temperature, wind, and humidity are needed for understanding and characterizing boundary layer processes and for model evaluation, validation, initialization, and nudging. The profiles can be used to quantify the time variability and evolutionary processes of atmospheric stability and buoyancy generated by variations in both temperature and moisture; boundary layer depth; vertical wind shear; and transport and dispersion processes throughout the depth of the boundary layer.

3.4.2 Approach

We used a Radiometrics microwave profiler (radiometer) to measure vertical profiles of temperature and humidity and used an Atmospheric Systems Corporation (ASC) mini-sodar to measure wind profiles.

The microwave profiler is a hyperspectral microwave receiver (radiometer). This instrument observes microwave energy emitted by the atmosphere, and Planck's law allows conversion of the microwave energy to brightness temperatures. Algorithms convert radiometer observations to temperature, humidity, and liquid water profiles. The profiles were measured from about 50 to 10,000 m apl. The vertical resolution of the data from the microwave radiometer is about 50 m below 500 m apl, 100 m between 500 and 2000 m apl, and 250 m above 2000 m apl. The radiometer mounted to the platform deck is shown in Figure 14, and a sample of the data collected is shown in Figure 15.

The mini-sodar consists of a single phased-array antenna that uses acoustic pulses (i.e., chirps or beeps) to measure the profile of the three-dimensional wind vector in the lower atmospheric boundary layer (Crescenti 1997). The phased-array mini-sodar antenna consists of a phased array of emitters (speakers), which acts to steer the acoustic pulses so that the individual components of the wind (two horizontal and one vertical; or u, v, and w) can be resolved. After each pulse, the mini-sodar "listens" for the backscattered sound and determines the wind speed from the Doppler shift in the acoustic frequency.

Background noise measurements taken on the selected platform, ST-52B, indicated the need to provide additional soundproofing for the instrument to prevent "clutter" or interference by ambient noise. Atmospheric Systems Corporation (ASC) designed a soundproof enclosure in which to encase the sodar. The mini-sodar (and its attendant soundproofing material) mounted to the platform deck is shown in Figure 16, and a sample of the data is shown in Figure 17.

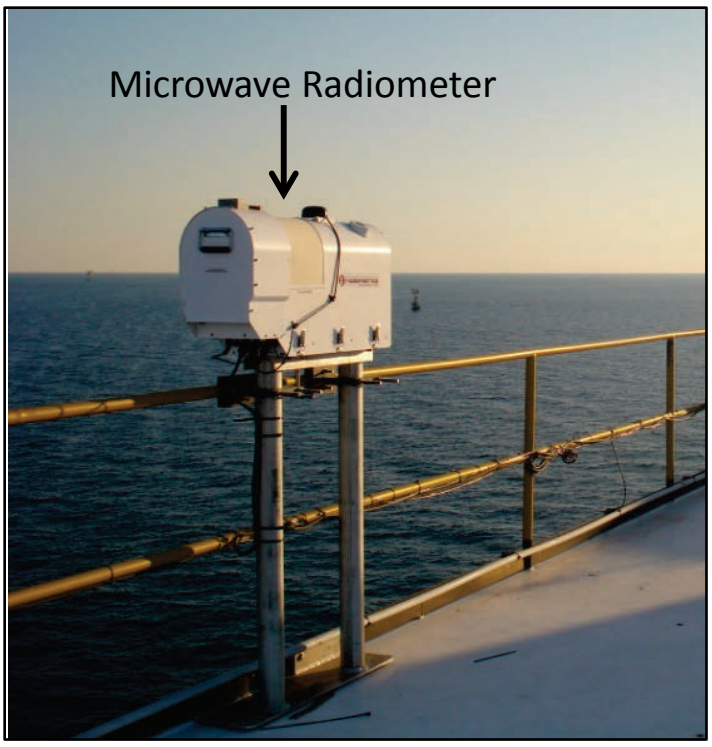


Figure 14. Microwave radiometer mounted on the platform deck.

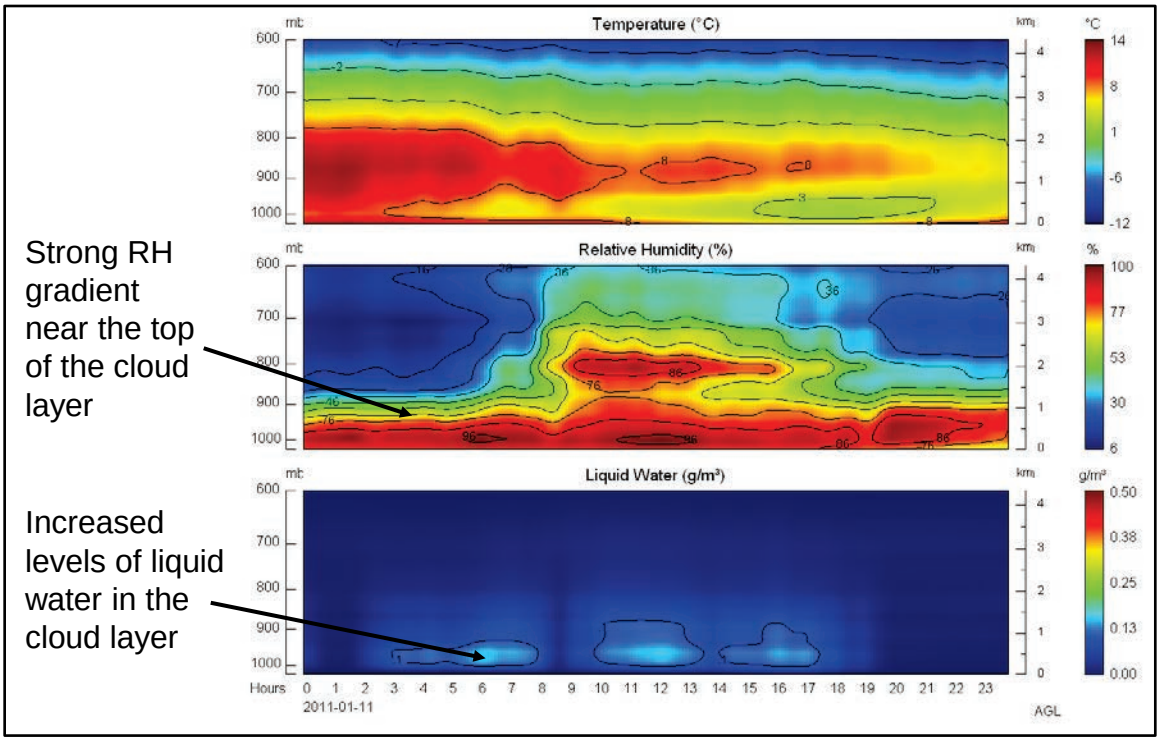


Figure 15. Temperature, relative humidity, and liquid water from the microwave radiometer from January 11, 2011.

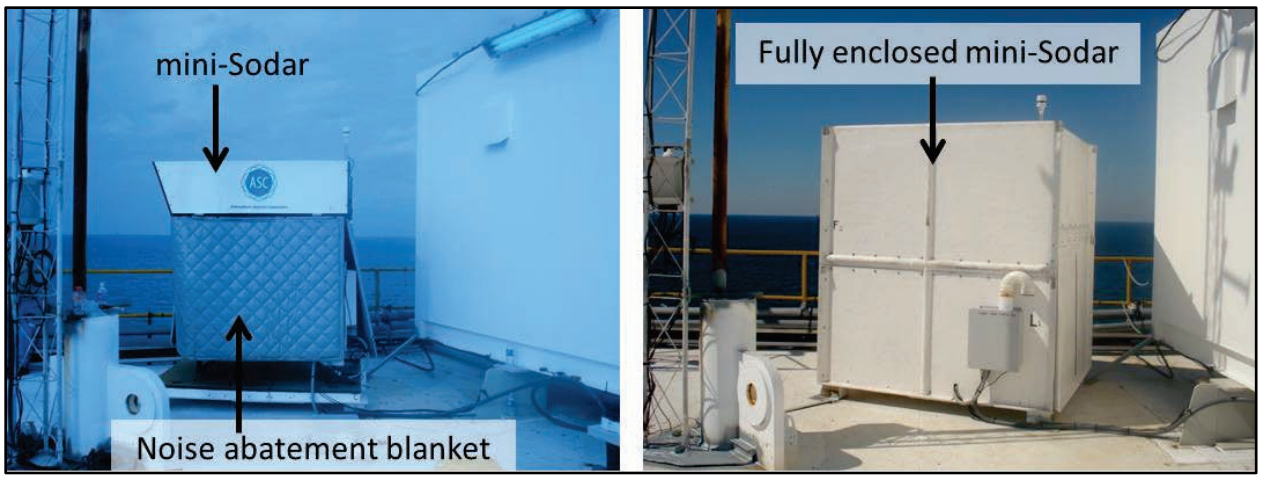


Figure 16. ASC mini-sodar on Chevron's ST-52B oil platform in the Gulf of Mexico.

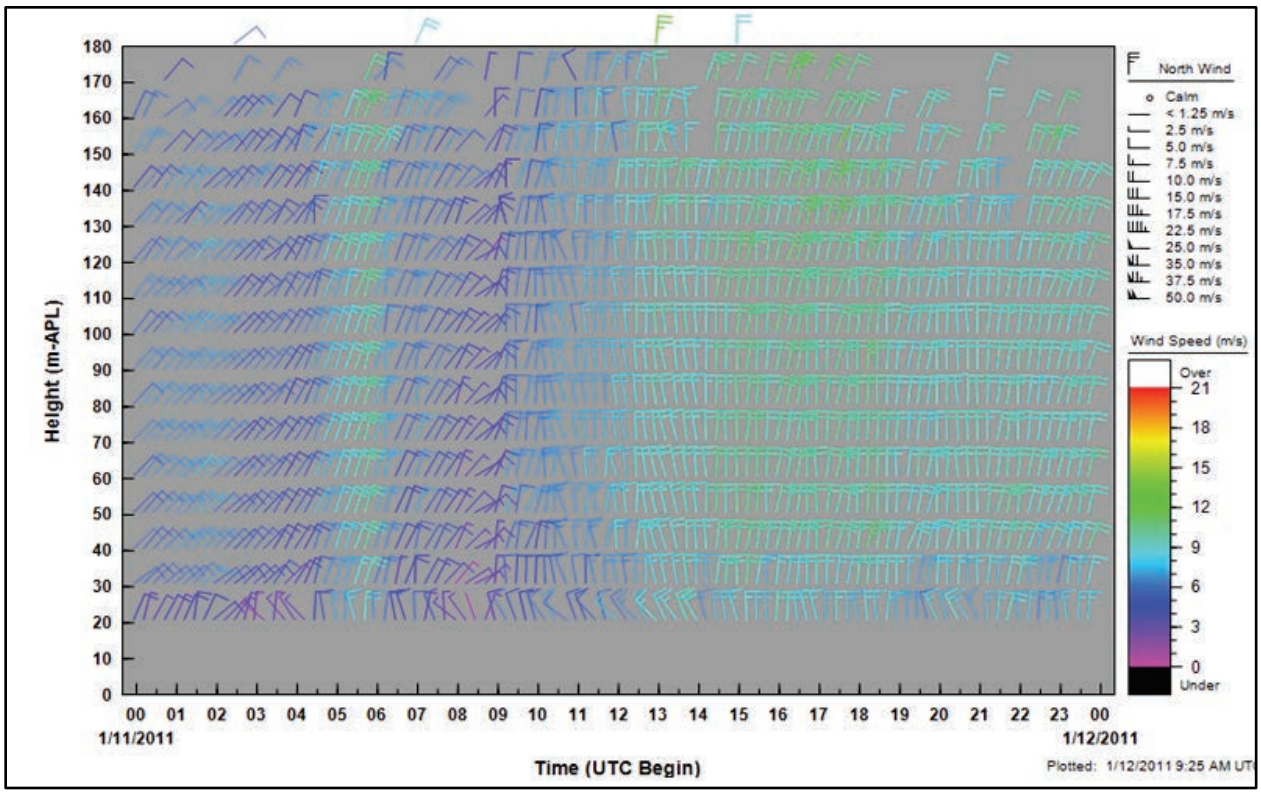


Figure 17. Mini-sodar wind profiles from January 11, 2011.

3.5 MIXING HEIGHT MEASUREMENTS

3.5.1 Background

The surface-based mixed layer (mixing height) is the portion of the planetary boundary layer above the surface through which vigorous vertical mixing of heat, moisture, momentum, and pollutants occurs (Holzworth 1972). Mixing heights are important to air quality because they control the vertical dispersion of pollutants, which directly influences their concentrations. Air quality data analysis and modeling benefit greatly from temporally and spatially resolved observations of boundary layer depth, especially over the Gulf of Mexico, where meteorological models tend not to accurately represent mixing heights (MacDonald et al. 2003).

Historically, mixing depths have been estimated from hourly surface temperature observations, twice daily National Weather Service rawinsonde data (Holzworth 1972), and observational models that use rawinsonde data (Berman et al. 1997). However, in the offshore environment, rawinsondes are too expensive to use over an extended period of time and do not provide the continuous data needed for improving air quality and meteorological modeling. Other viable alternatives include radar wind profilers and ceilometers.

3.5.2 Approach

A Vaisala CL31 ceilometer was deployed to collect data from which subhourly mixing heights were estimated. Figure 18 shows the ceilometer on the platform. The selection of this ceilometer for inclusion in this study was based upon its performance in a previous near-shore study in which it showed its ability to detect mixing heights in a marine environment (Gilroy 2008), and because it had algorithms to automatically detect mixing heights. It had the added advantage of providing cloud-height data. The CL31 works by vertically emitting an eye-safe laser beam and detecting the reflection of the beam by particles with a receiver. The continuous reflectivity (or backscatter) data were available from about 2 to 7700 m apl; for boundary layer characterization, the sensitivity was adequate up to 3000 m apl. Subhourly boundary layer heights with a vertical resolution of 5 m were derived from the backscatter data using the algorithm in the manufacturer's software. Sample data from the ceilometer used in the current study are shown in Figure 19.

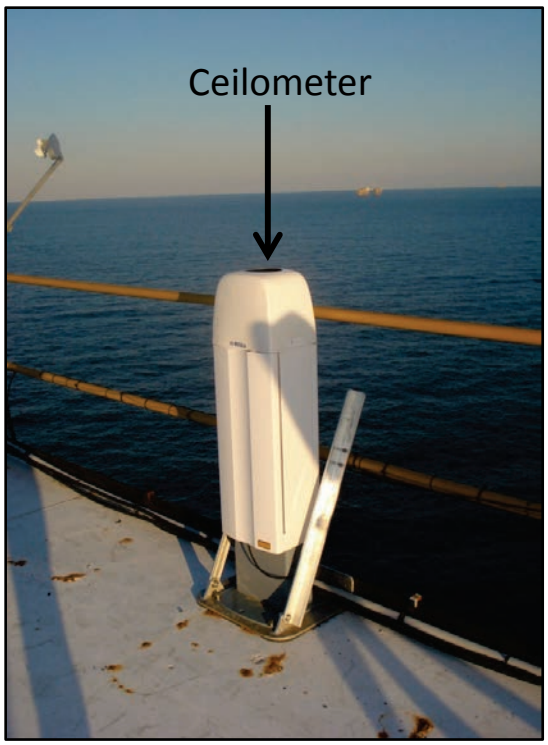


Figure 18. Vaisala CL31 ceilometer located on Chevron's ST-52B oil platform in the Gulf of Mexico.

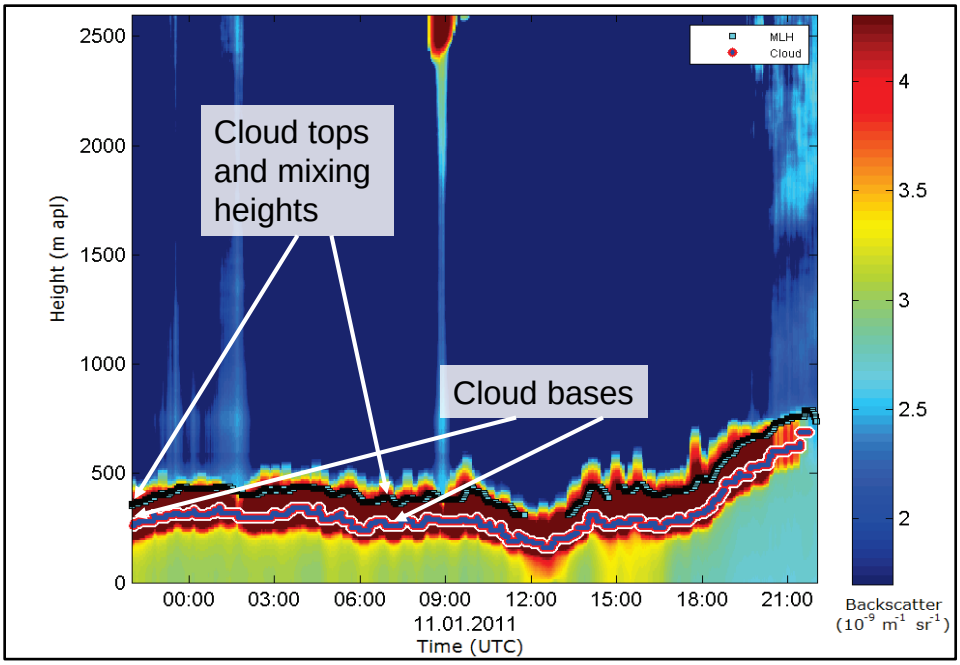


Figure 19. Ceilometer backscatter, mixed layer height, and cloud height from January 11, 2011.

3.6 SITING AND INFRASTRUCTURE

This section describes how our team conducted this study in a safe manner; obtained the use of a platform suitable for project objectives; developed the infrastructure needed to support operation of the instruments; and delivered, installed, and operated the instruments.

3.6.1 Siting

We selected a platform by identifying numerous potential sites that could meet the scientific objectives of the project. Once potential sites were identified, we were able to work with platform operators to determine which platforms could accommodate the equipment for up to two years. With a refined list of potential platforms, we determined which platforms were best suited for the project considering logistical and scientific issues. In particular, based on experience, we sought to find a platform with the following attributes:

- Space for the equipment.
- A platform deck lower than 50 m msl. This criterion was critical to achieving the science objectives, including measurements of fluxes, and to satisfy COARE requirements for measurements below 50 m to calculate boundary layer parameters.
- Readily available power.
- Platform operators on site. Platform operators were very helpful in providing support for small maintenance items, such as rebooting computers. This helped increase data recovery while conserving resources.
- Little or no ambient noise to interfere with the mini-sodar. There was some noise identified, so we mitigated it using sound-insulating methods.
- No large structures (building, cranes, etc.) in locations that could have interfered with measurements.
- Ability to mount equipment to the deck.
- No active wells or space for the equipment at a distance from wells that required little or no equipment modifications to meet explosion-proofing requirements.
- Space to house staff during installation, maintenance, and deinstallation visits. This feature limited time spent traveling to and from the platform during multi-day trips.

After narrowing the list of site candidates by the criteria listed above, we visited a platform (see Table 2) and subsequently obtained approval from the Scientific Review Board and BOEM to proceed with conducting measurements on the platform.

Table 2.

Platform description

Platform name	Chevron Platform, ST-52B, South of Terrebonne Bay, Louisiana
WAVCIS name	CSI-06. LSU operates wave measurement and surface meteorological instruments on this platform.
National Data Buoy Center (NDBC) name	Station SPLL1
Coordinates	28º52',-90º29' (see Figure 1)
Platform deck (roof) height	37 m msl
Catwalk height	~15 m msl. Note: we mounted the flux instruments on booms below the catwalks to help mitigate flow distortion issues and to obtain atmospheric surface-layer measurements (see Figure 12).
Water depth	20.5 m
Power available?	Yes, but we augmented existing power with solar power.
Wave measurements already available?	Yes.
Water temperature?	Yes, but the data were collected at ~2 m below the sea surface; we added skin temperature and near-surface temperature.
Existing surface meteorology?	Yes, but at about 42 m msl; we added flux measurements below the catwalk at ~10 to 12 m msl.
Active wells?	Although active wells are in the complex, this platform was for crew quarters, eliminating the need for explosion-proofing the equipment.
Available for at least 12 months?	Yes.
Internet communications available?	Yes, but we had to add bandwidth to accommodate the additional data.
Routine access available?	Yes.

3.6.2 Communications and Data Collection

Reliable communications with the equipment on the platform were required to ensure high data recovery rates and minimize costly trips to the platform. Two-way Internet allowed equipment to be remotely monitored using a Virtual Network Computing (VNC) connection. It was frequently possible to debug and solve instrument problems remotely and to determine what equipment should be brought to the platform to effect repairs.

Using an Internet connection, we automatically pushed most of the data daily from the oil platform to file transfer protocol (FTP) servers. When the data were uploaded, an automatic process took the data in their raw form and stored them in a Microsoft® SQL Server® database, effectively combining all data into a single data set. Another automatic process generated images of the data and uploaded them to a website. These processes provided us with an efficient way to check data and catch problems that occurred. An example of the website used is shown in Figure 20.

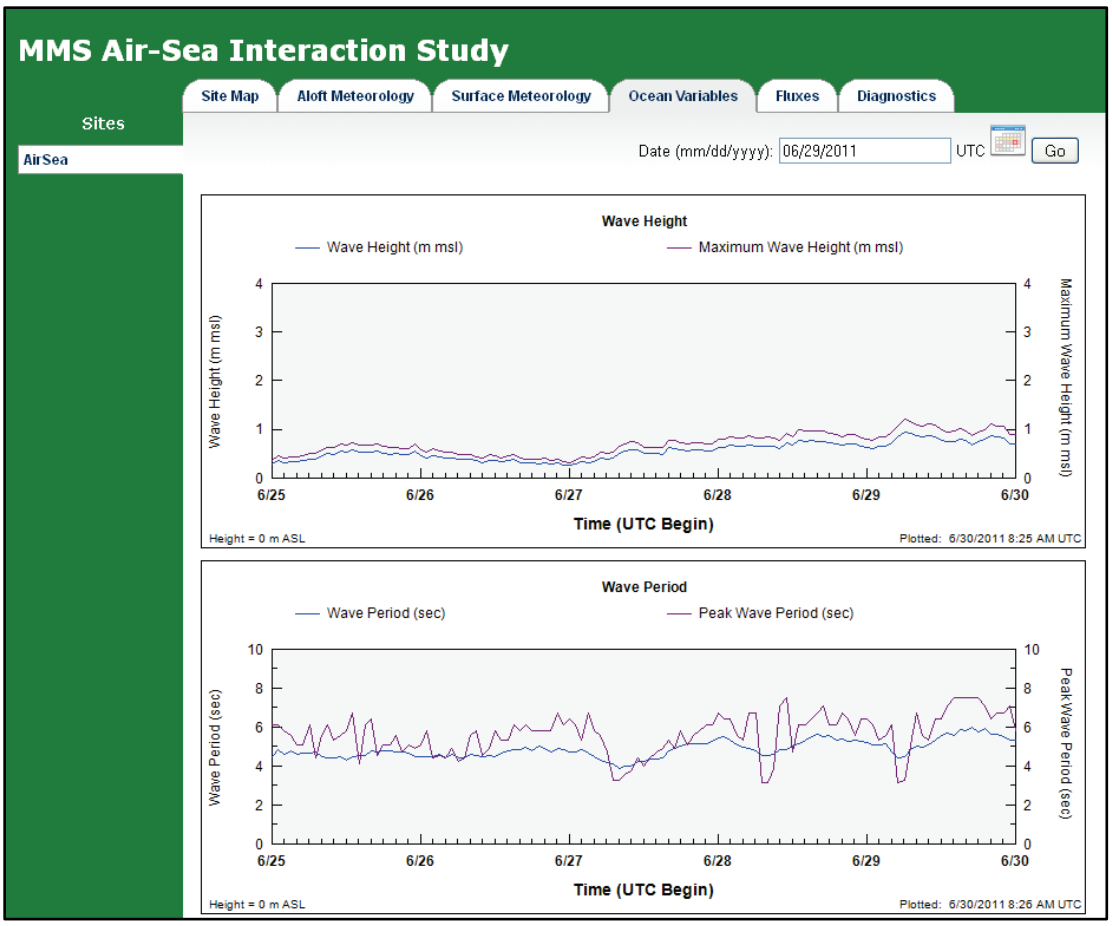


Figure 20. Wave data images posted to a website in real time.

3.6.3 Power

Optimally, we would have operated the equipment on a platform that already had power available. However, the power on the selected platform was limited, so we used a battery system. Solar panels were used to charge the batteries for surface meteorology and flux packages. The microwave radiometer and ceilometer operated on platform power, as did the chargers for the batteries for the rest of the instrument systems.

3.6.4 Interference

Audible noise can interfere with the proper operation of the mini-sodar. To help mitigate this problem, we encased the mini-sodar in an additional sound-dampening enclosure.

3.6.5 Hurricanes

Hurricanes were a real concern in the Gulf of Mexico. Mitigating the negative effects of hurricanes during this measurement program included the following:

- The equipment was able to withstand hurricane-force winds. For example, we secured the equipment to the decks with welded steel grids rated to withstand hurricane-force winds and used special mounting brackets for all instruments.
- We purchased the required special equipment insurance for offshore areas and for hurricanes.
- We conducted in-depth meteorological forecasting before any platform visits.

3.7 INSTRUMENT PREPARATION AND OPERATIONS

The objectives of routine instrument operations were to ensure high-quality data and high data recovery rates. Operations were divided into two main elements for this project: (1) pre-deployment instrument interface and testing, and (2) routine operations.

3.7.1 Pre-Deployment Interface and Testing

All instruments were shipped to LSU. At LSU's facilities, STI, LSU, and CU personnel assembled the complete, integrated measurement system, including all power sources, computers, data management systems, and communications. In addition, special mounting brackets were fabricated for each instrument. The instruments were tested as a complete system over several weeks to ensure that they met manufacturer specifications and that all systems, from data collection to data delivery and archiving, worked together properly. During this testing phase, several issues were resolved. For example:

- The microwave radiometer computer had to be replaced with a Cappuccino DC computer to accommodate platform power.
- A replacement flux system was purchased because one Li-Cor Li-7500 and one sonic anemometer supplied in-kind by NOAA did not work, and NOAA did not have another set available for loan.
- The microwave radiometer, ceilometer, and mini-sodar had resource conflicts on the computer; these problems were resolved.
- The IR skin sensor was not waterproof.
- The modems supplied in-kind by NOAA did not work because they did not transfer data fast enough to handle flux measurements. NOAA mistakenly stated that they had been used for this purpose before, so considerable effort was spent trying to get them to work beyond their specifications. New modems were purchased.
- The new modems were damaged by a power surge and had to be replaced.
- The program supplied by NOAA for the solar radiation sensor had to be rewritten because it didn't work with the current version of the Campbell data logger.

- Only beta versions of programs for the microwave radiometer and ceilometer were available for remote processing of the data, and no documentation was available; procedures were developed.
- The new mini-sodar had pauses in its pinging, unexplained reboots, and speaker failures. The problems turned out to be subparts from a new supplier that the manufacturer was using; the parts were replaced.
- The sound-dampening enclosure for the mini-sodar was not delivered on schedule by the manufacturer; when it arrived, the sections could not be broken down as specified to allow it to be moved to the platform roof. The enclosure was modified so that it could be taken apart into small sections. In addition, the enclosure did not dampen the sound enough, so a secondary sound-dampening blanket had to be purchased and delivered and the enclosure modified so that the blanket could be installed.
- Chevron updated its rules on shipping containers, and new crates had to be fabricated to house the equipment inside of Connex boxes.

3.7.2 Shipping

The equipment for this project was transported to the oil platform by a small ship (see Figure 21). For this project, considerable planning and coordination was needed to ensure that the equipment arrived on schedule and in good condition. Before shipping, all equipment was placed in crates in Connex boxes. The most fragile equipment was individually crated.



Figure 21. Picture of Connex boxes on Chevron's ship.

3.7.3 In-Field Testing After the Initial Installation

After installation of the integrated measurement system on the platform, the system was tested to ensure that all equipment, including power sources, computers, data management systems, and communications, worked properly. In particular, installation staff completed the following in-field testing for each instrument:

- Leveled the instruments and determined their orientation, when appropriate
- Anchored all instruments to the platform deck or meteorological tower
- Tested data loggers to verify programming, time synchronization, sensor input configuration, and data storage function
- Verified data file creation for all instruments
- Verified data collected against internal and external data sources, including the LSU meteorological sensors and surface meteorological data from nearby Houma, Louisiana

- Synchronized clocks on all instruments based on The Official U.S. Time website (NIST and USNO 2013)
- Verified data transfers to the host computer on oil platform
- Verified proper operation, data storage, data retrieval, and communications to and from STI servers

3.7.4 Onsite Maintenance and Operations

Maintenance of the instruments was critical to successful operations. For this reason, STI's team conducted maintenance and made emergency site visits as needed. During platform visits, staff performed the following maintenance:

- Visually inspected all instruments and cabling
- Verified that all instruments were collecting reasonable data for the current weather conditions
- Inspected all instrument bases to ensure that they remained bolted to the platform deck
- Verified all instrument orientations and levels
- Backed up data files
- Verified disk space on all instruments/data loggers
- Verified that the mini-sodar speakers were operating
- Cleaned the window/lens on the ceilometer
- Cleaned the domes on the solar radiation sensors
- Cleaned the radome, temperature/relative humidity screen, superblower filter, rain sensor board, and infrared thermometer (IRT) window on the microwave radiometer
- Cleaned the temperature/relative humidity radiation shield on the surface meteorological tower
- Cleaned the infrared hygrometer/CO_2 gas analyzer lenses. Midway through the project, an automatic wash system was installed to clean these lenses.
- Visually inspected the wave measurement, underwater temperature, infrared temperature (skin temperature), and sea float temperature sensors
- Repairs were made on an as-needed basis and included such items as replacing defective temperature sensors, replacing wind speed bearings, or repairing connections.

In addition, data quality checks were performed to ensure that the data collected were complete and reasonable. Each day, a meteorologist at STI's Weather Operations Center compared the surface and upper-air data from the site with external data sources as a quality control measure,

allowing for the identification of any operational or equipment problems. Table 3 shows the data and instrument checks that were performed. In addition, a meteorologist compared data collected at the site and checked for data reasonableness.

Table 3.

On-platform (internal) and off-platform (external) data sources used during data validation

Instrument	Parameter	Internal Data Checks	External Data Checks
Mini-sodar	Winds	Check for consistency with surface wind data	Check for consistency with wind data from nearby buoys, rawinsondes, and numerical models (North American Mesoscale Model [NAM], Global Forecast System [GFS], etc.)
Microwave radiometer	Temperature profiles and humidity profiles	Check for consistency with surface temperature and relative humidity data	Check for consistency with temperature and relative humidity data from nearby buoy, rawinsondes, and numerical models (NAM, GFS, etc.)
Ceilometer	Mixing heights and cloud heights	Check for consistency with microwave radiometer temperature data	Check for consistency with cloud data, satellites, and rawinsondes
Wind vane and cup anemometer	Winds	Check for consistency with mini-sodar winds Check for consistency with LSU winds	Check for consistency with wind data from nearby buoys, coastal surface meteorological stations, and numerical models (NAM, GFS, etc.)
Thermistor and hygrometer	Temperature and relative humidity	Check for consistency with LSU temperature and relative humidity	Check for consistency with wind data from nearby buoys, coastal surface meteorological stations, and numerical models (NAM, GFS, etc.)
Barometer	Pressure	None	Check for consistency with pressure data from nearby buoys, coastal surface meteorological stations, and numerical models (NAM, GFS, etc.)
Pyranometer	Downwelling shortwave radiation	Check for consistency with cloud data obtained from the ceilometer	Check for consistency with cloud data, satellites, and rawinsondes
Pyrgeometer	Downwelling longwave radiation	Check for consistency with cloud data	Check for consistency with cloud data, satellites, and rawinsondes
Sonic anemometer	Winds and temperature	Check for consistency with surface wind and temperature data Check for consistency between AB and AC sonic winds and temperatures	Check for consistency with wind and temperature data from nearby buoys

Table 3. On-platform (internal) and off-platform (external) data sources used during data validation (continued)

Instrument	Parameter	Internal Data Checks	External Data Checks
Infrared hygrometer and gas analyzer	Specific humidity and CO_2 concentration	Check for consistency between AB and AC bridge-specific humidities and CO_2 concentrations	Check for consistency with relative humidity data from nearby buoys and CO_2 levels from other stations
Wave measurements	Wave height, wave period, and water depth	Check for consistency with surface wind data	Check for consistency with wave data from nearby buoys
Fixed sea surface thermometer	Sea surface temperature	Check for consistency with the sea float temperature and the skin temperature	Check for consistency with sea surface temperature data from nearby buoys
Sea float thermometer	Sea float temperature	Check for consistency with the sea surface temperature and the skin temperature	Check for consistency with sea surface temperature data from nearby buoys
Infrared thermometer	Skin temperature	Check for consistency with the sea surface temperature and the sea float temperature	Check for consistency with sea surface temperature data from nearby buoys

4. DATA AVAILABILITY

The data collection began on October 1, 2010, and was completed on April 1, 2012. The instruments were operated with great success and provided very robust offshore data that met the project objectives. Tables 4 and 5 summarize key data recovery statistics for data completeness and data capture.

The most stringent metric for data recovery statistics is data completeness, which is the percentage of valid data points after rigorous data quality control divided by the total number of records possible determined using the instrument installation date, frequency of measurement, and operations end date. For example, an instrument that produces hourly averaged data would have a denominator of 720 observations per 30-day month. A data completeness of 50% would mean that 360 observations that were collected are valid and ready for use in data analysis. The installation date for all instruments was October 4, 2010, except for the sea float temperature sensor, which was installed on June 24, 2011. The end date was April 1, 2012. Therefore, for instruments that reported hourly values, the total number of possible records was 548 days * 24 hours = 13,174. For instruments that report more than one value per hour, such as the sodar, the total number of possible records was calculated as appropriate. As summarized in Table 4, the data completeness rates are mostly above about 83% and some are as high as 100%. The notable exception is the skin temperature sensor, which had a data completeness of 44%. In addition, data completeness for the flux sensors on each bridge was 39% for the AB bridge and 20% for the AC bridge due primarily to flow distortions created by the oil platforms; when flow distortions occurred data were made invalid. When the fluxes from the two bridges are combined, the data completeness improved to 55%.

Table 4.

Data completeness statistics by instrument type

Instrument	Number of Valid Data Points	Number of Data Points Received	Data Accumulation Frequency	Data Completeness (%)
Mini-Sodar Winds	379,042	430,730	15 minutes, multiple heights	88
Microwave Radiometer Temperature and Humidity	267,672	316,176	2.5 minutes, multiple heights	85
Ceilometer Mixing Heights	34,846	52,696	15 minutes	66
Ceilometer Cloud Heights	46,908	52,696	15 minutes	89
Winds	10,954	13,174	60 minutes	83
LSU Winds[a]	10,971	13,174	60 minutes	83
Ambient Temperature	10,923	13,174	60 minutes	83
LSU Ambient Temperature[a]	10,902	13,174	60 minutes	83
Relative Humidity	12,519	13,174	60 minutes	95
Pressure	12,519	13,174	60 minutes	95
Downwelling (shortwave) Radiation	12,549	13,174	60 minutes	95
Infrared (longwave) Radiation	12,373	13,174	60 minutes	94
Precipitation	12,519	13,174	60 minutes	95
Skin Temperature	5,815	13,174	60 minutes	44
Sea Float Temperature	5,653	5,901	60 minutes	96
LSU Sea Temperature	13,128	13,174	60 minutes	100
Wave Data (Including Wave Height, Wave Period, and Water Depth)	13,128	13,174	60 minutes	100
AC Bridge Flux Sensors	15,154	74,742	10 minutes	20
AB Bridge Flux Sensors	28,992	74,742	10 minutes	39
Combined Flux Sensors	41,062	74,742	10 minutes	55

[a] LSU operates a separate set of surface meteorology instruments.

A less stringent metric for the data recovery statistics is data capture, which is the percentage of total data points collected (regardless of validity) divided by the total number of records possible determined using the instrument installation date, frequency of measurement, and operations end date. As summarized in Table 5, the data capture rates are mostly above about 85%, and some are as high as 100%. The notable exception is the AC bridge flux data, which had a data rate capture of 74%. Also, before December 3, 2010, because of problems with the lenses being covered in salt and instrument failures, the flux data were not considered in the data capture calculations.

Table 5.

Data capture statistics by instrument type

Instrument	Number of Data Points Collected	Number of Data Points Possible	Data Accumulation Frequency	Data Capture (%)
Mini-Sodar Winds[a]	50,325	52,696	15 minutes	95
Microwave Radiometer Temperature and Humidity	267,672	316,176	2.5 minutes, multiple heights	85
Ceilometer Mixing Heights	34,846	52,696	15 minutes	66
Ceilometer Cloud Heights	46,908	52,696	15 minutes	89
Winds	12,519	13,174	60 minutes	95
LSU Winds	11,417	13,174	60 minutes	87
Ambient Temperature	12,519	13,174	60 minutes	95
LSU Ambient Temperature	11,417	13,174	60 minutes	87
Relative Humidity	12,519	13,174	60 minutes	95
Pressure	12,519	13,174	60 minutes	95
Downwelling (shortwave) Radiation	12,549	13,174	60 minutes	95
Infrared (longwave) Radiation	12,549	13,174	60 minutes	95
Precipitation	12,532	13,174	60 minutes	95
Skin Temperature	12,529	13,174	60 minutes	95
Sea Float Temperature[b]	5,901	6,791	60 minutes	87
LSU Sea Temperature	13,128	13,174	60 minutes	100
Wave Data (Including Wave Height, Wave Period, and Water Depth)	13,128	13,174	60 minutes	100
AC Bridge Flux Sensors	55,169	74,742	10 minutes	73
AB Bridge Flux Sensors	65,652	74,742	10 minutes	87

[a] For this instrument and data capture statistic, the number of points possible equals ~548 days x 24 hours x 4, for which the 4 accounts for 15-minute data frequency.

[b] The sea float sensor was installed on June 24, 2011.

Major instrument downtimes and major periods of suspect or invalid data and the reasons for the missing data are presented in Table 6 and are summarized in graphical form in Figure 22. Missing data periods in the table are cross-referenced with the information in Figure 22. Text on missing data periods that require additional information follows the table.

Table 6.

Major downtimes of the instruments

Case	Downtime	Instrument(s) Affected	Problem
1	11/01/2010 to 12/04/2010	AC flux instruments	Radio modem failure
2	12/19/2010 to 01/12/2011	AC flux instruments	Radio modem failure
3	03/25/2011 to 04/30/2011	AC flux instruments	Radio modem failure
4	05/02/2011 to 06/16/2011	Microwave radiometer	Power surge/ V-band receiver failure
5	05/03/2011 to 05/17/2011	Ceilometer	Power surge turned instrument off
6	05/03/2011 to 05/18/2011	All flux instruments	Power surge turned instruments off
7	05/18/2011 to 05/24/2011	Mini-sodar	Battery failure
8	05/27/2011 to 05/30/2011	Ceilometer, computer, surface meteorology, skin temperature, and all flux instruments	Power surge turned instrument off
9	06/09/2011 to 06/12/2011	Mini-sodar	Battery failure
10	06/09/2011 to 06/14/2012	Surface meteorology instruments	Battery failure
11	06/28/2011 to 07/25/2011	Sea float temperature sensor	Sensor failure
12	09/03/2011 to 09/05/2011	Surface meteorology and skin temperature	Power shut off for Tropical Storm Lee
13	09/03/2011 to 09/09/2011	Mini-sodar, ceilometer, microwave radiometer, and flux instruments	Power shut off for Tropical Storm Lee
14	09/05/2011 to 09/05/2011	Wave data	Power shut off for Tropical Storm Lee
15	12/23/2011 to 01/03/2012	Surface meteorology and flux instruments	Power surge turned instruments off
16	12/23/2011 to 01/20/2012	Microwave radiometer and ceilometer	Power surge turned instruments off
17	02/26/2012 to 03/04/2012	Mini-sodar	Battery failure
18	02/26/2012 to 04/01/2012	Ceilometer	Blower failure

Note that the flux instruments required a wash system to be installed when data quality issues were observed after several weeks of operations. The wash system was installed on December 3, 2010. Data before this time period were deemed invalid. Additional downtimes were encountered with the AC bridge flux instruments, due primarily to radio modem failures.

An Everest IR sensor was used to measure skin temperature initially because of its purported ability to correct for black body radiation from the sky; however, this sensor was not suitably weatherproof as promised by the manufacturer. As a result, the data from this sensor were labeled as suspect even when the data appear to be oceanographically reasonable. In addition, the majority of the time, the data values were reading either extremely low (~-40°C) or high (~100°C) and were invalidated. After replacing the Everest sensor twice, on February 24, 2012, a Heitronics KT15.85-IIP IR sensor was installed to measure skin temperature. Data completeness from this replacement instrument was 100%. The Heitronics KT15.85-IIP IR skin

temperature data were corrected to account for black body radiation from the sky that was reflected off the ocean surface. The sky black body radiation was measured by an upward-looking KT15.85-IIP IR sensor mounted inside the microwave radiometer.

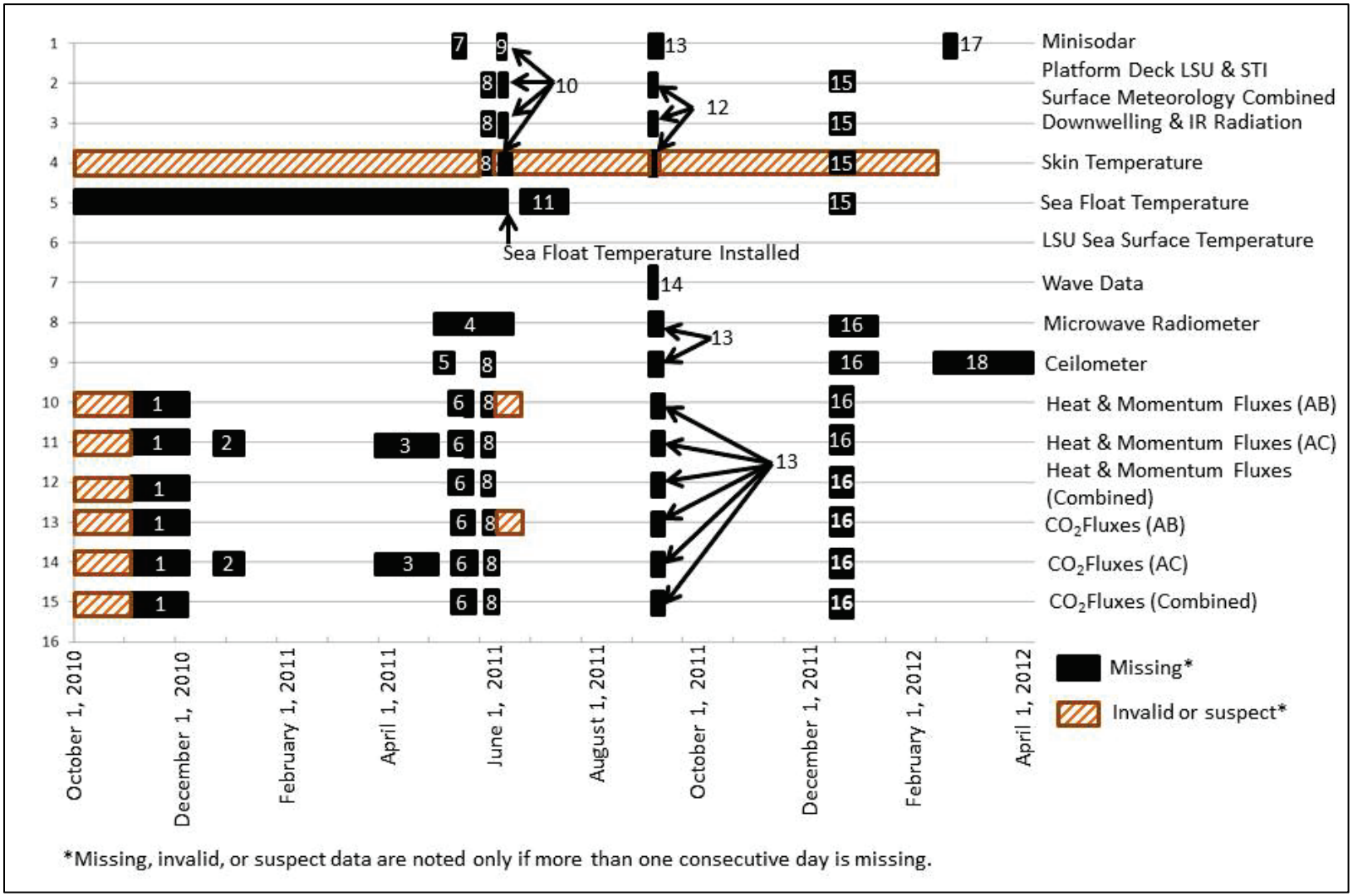


Figure 22. Major periods of missing, invalid, or suspect data. Numbers refer to the case numbers in Table 6.

5. DATA PROCESSING AND QUALITY CONTROL

Data quality assurance and control is a key component of producing a data set ready for use by data analysts and modelers. STI meteorologists who understand the data collected as well as the instruments used to collect the data quality-assured and validated the data using STI's in-house data quality control programs (SurfDat and GraphXM). During the data validation process, the meteorologists identified inconsistent observations (outliers) and assigned quality control (QC) codes to each data point to indicate its validity. Several stages, or "Levels," in the data validation process were used:

- *Level 0.0* Raw, non-quality-controlled data.
- *Level 0.5* Data that were subjected to automatic QC screening by software.
- *Level 1.0* Data that were subjected to quantitative and qualitative reviews for accuracy, completeness, and internal consistency.
- *Level 2.0* Data that were subjected to quantitative and qualitative reviews for external consistency.

The following steps were used to bring data to Level 2.0 validation. The Level 0.0 data were obtained from the platform daily via the Internet. Backup copies of the Level 0.0 data were automatically made and archived. In addition, backup data were obtained via a portable hard drive during each site visit, and any missing data were added to the database.

Data were manually reviewed by experienced meteorologists. The reviewers carefully examined plots of the data, looking for outliers, and evaluated the reasonableness of the data. The reviewers flagged the resulting data as "valid," "suspect," "invalid," or "missing," using the appropriate QC codes:

- 0 = Valid
- 7 = Suspect
- 8 = Invalid with a data value of -980
- 9 = Missing with a data value of -999

Reviewers used internal and external sources of data to help them determine the validity of the observations. Internal data sources included other parameters that were measured by the same instrument, collocated data sources, and other manually-generated data (e.g., instrument performance logs and site operator logs). Table 7 lists internal and external data sources and gives a brief explanation of how we use them to QC the data. Examples of external data include the NOAA buoy data, National Weather Service (NWS) upper-air and surface weather charts, and satellite images. An example of external data use is the comparison of NOAA buoy winds to platform winds as a reasonableness check.

Table 7.

On-platform (internal) and off-platform (external) data sources used during data validation

Instrument	Parameter	Internal Data Checks	External Data Checks
Mini-sodar	Winds	Compared with surface wind data	Compared with wind data from nearby buoys, rawinsondes, and numerical models (NAM, GFS, etc.)
Microwave radiometer	Temperature profiles and humidity profiles	Compared with surface temperature and relative humidity data	Compared with temperature and relative humidity data from nearby buoy, rawinsondes, and numerical models (NAM, GFS, etc.)
Ceilometer	Mixing heights and cloud heights	Compared with microwave radiometer temperature data	Compared with cloud data, satellites, and rawinsondes
Wind vane and cup anemometer	Winds	Compared with mini-sodar winds Compared with LSU winds	Compared with wind data from nearby buoys, coastal surface meteorological stations, and numerical models (NAM, GFS, etc.)
Thermistor and hygrometer	Temperature and relative humidity	Compared with LSU temperature and relative humidity	Compared with wind data from nearby buoys, coastal surface meteorological stations, and numerical models (NAM, GFS, etc.)
Barometer	Pressure	None	Compared with pressure data from nearby buoys, coastal surface meteorological stations, and numerical models (NAM, GFS, etc.)
Pyranometer	Downwelling shortwave radiation	Compared with cloud data obtained from the ceilometer	Compared with cloud data, satellites, and rawinsondes
Pyrgeometer	Downwelling longwave radiation	Compared with cloud data	Compared with cloud data, satellites, and rawinsondes
Sonic anemometer	Winds and temperature	Compared with surface wind and temperature data Compared between AB and AC sonic winds and temperatures	Compared with wind and temperature data from nearby buoys
Infrared hygrometer and gas analyzer	Specific humidity and CO_2 concentration	Compared between AB and AC bridge-specific humidities and CO_2 concentrations	Compared with relative humidity data from nearby buoys and CO_2 levels from other stations
Wave measurements	Wave height, wave period, and water depth	Compared with surface wind data	Compared with wave data from nearby buoys
Fixed sea surface thermometer	Sea surface temperature	Compared with the sea float temperature and the skin temperature	Compared with sea surface temperature data from nearby buoys

Table 7. On-platform (internal) and off-platform (external) data sources used during data validation (continued)

Instrument	Parameter	Internal Data Checks	External Data Checks
Sea float thermometer	Sea float temperature	Compared with the sea surface temperature and the skin temperature	Compared with sea surface temperature data from nearby buoys
Infrared thermometer	Skin temperature[a]	Compared with the sea surface temperature and the sea float temperature	Compared with sea surface temperature data from nearby buoys

[a] The skin temperature data were corrected to account for black-body radiation from the sky.

The quality-controlled data were then stored on DVDs in the data file formats agreed upon by BOEM and STI on March 9, 2011. Examples of the quality control performed for each instrument follow.

Figure 23 shows an example of sodar wind data that were invalidated due to precipitation interference. This figure shows the mini-sodar wind data colored by vertical wind speed. The vertical wind speeds of about 5.8 m/s (as indicated by blue color on wind barbs) in Figure 23 show the fall speed of the rain drops. In addition, the wind speeds and directions for precipitation events were inconsistent with the surface wind observations shown in Figure 24. Therefore, these winds were invalidated.

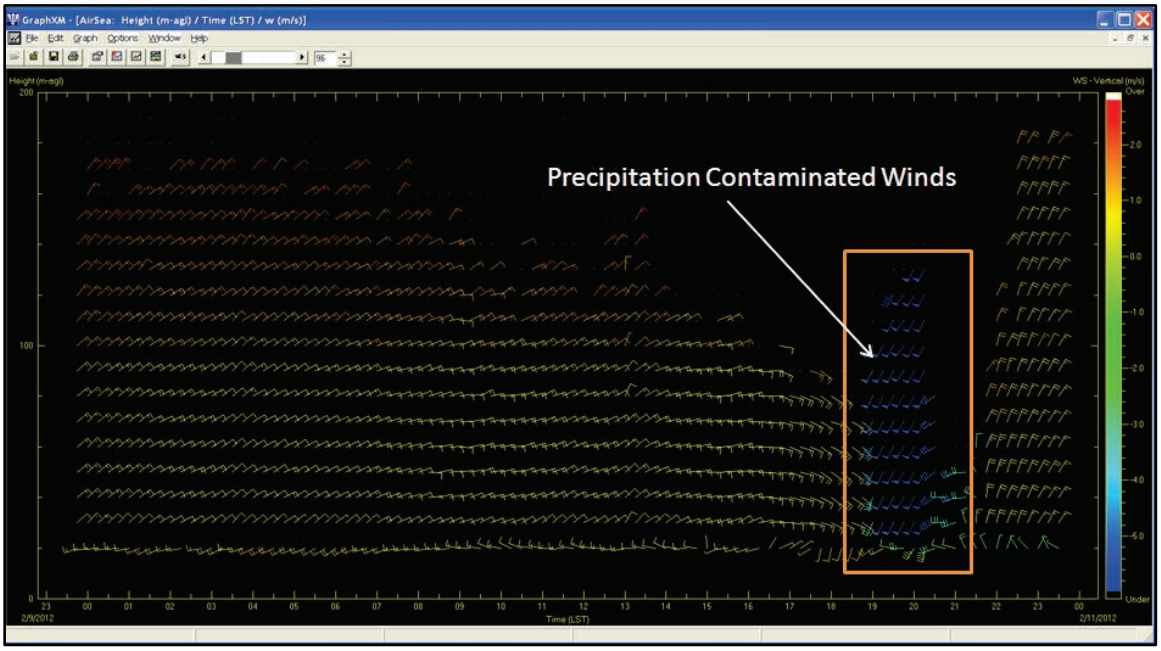


Figure 23. Mini-sodar winds from February 10, 2012. Wind barbs are colored by vertical wind speed. Times are in UTC.

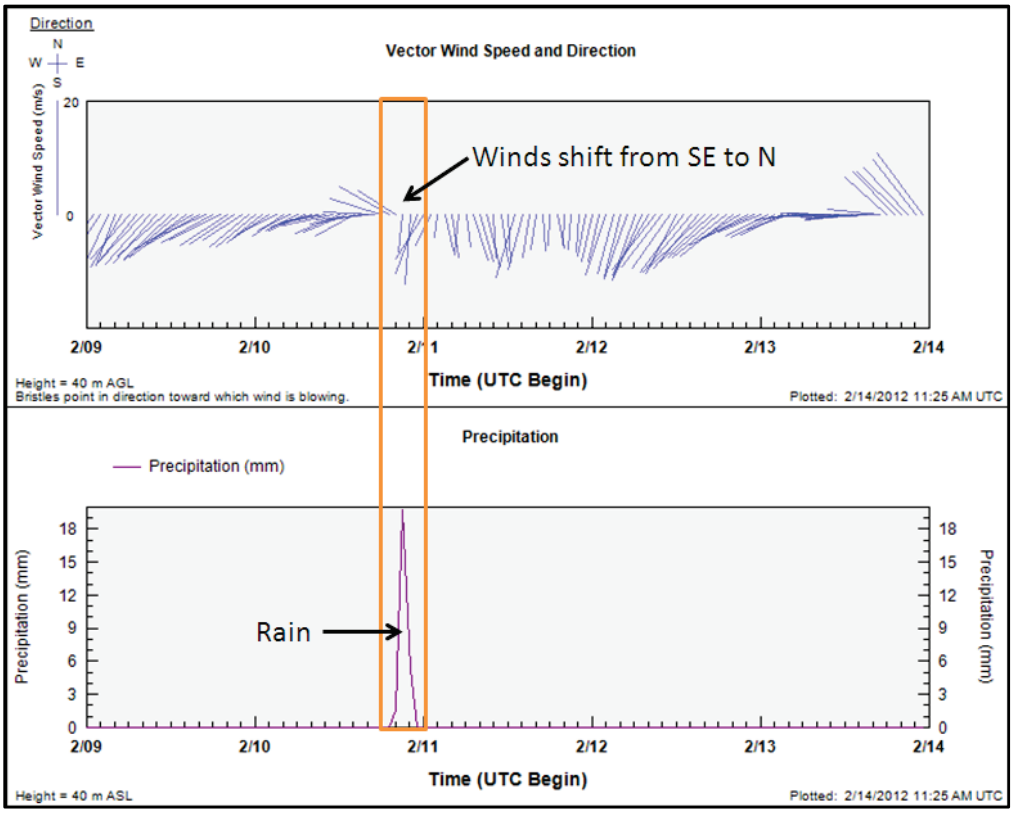


Figure 24. Surface wind (top) and precipitation (bottom) data on February 10, 2012. Bristles point in the direction toward which the wind is blowing.

The microwave radiometer data were reviewed every day by an experienced meteorologist. In addition, at the end of the study, selected soundings were compared to soundings taken at Lake Charles, Louisiana, and Slidell, Louisiana. Figures 25 and 26 show four comparisons for January 11, 2011, at 1200 UTC; January 12, 2011, at 0000 UTC; December 6, 2011, at 1200 UTC; and December 7, 2011, at 0000 UTC. In general, the soundings show good agreement. Because the microwave radiometer was over water and the rawinsondes were over land, inversions over the water were typically weaker, as shown in Figure 26.

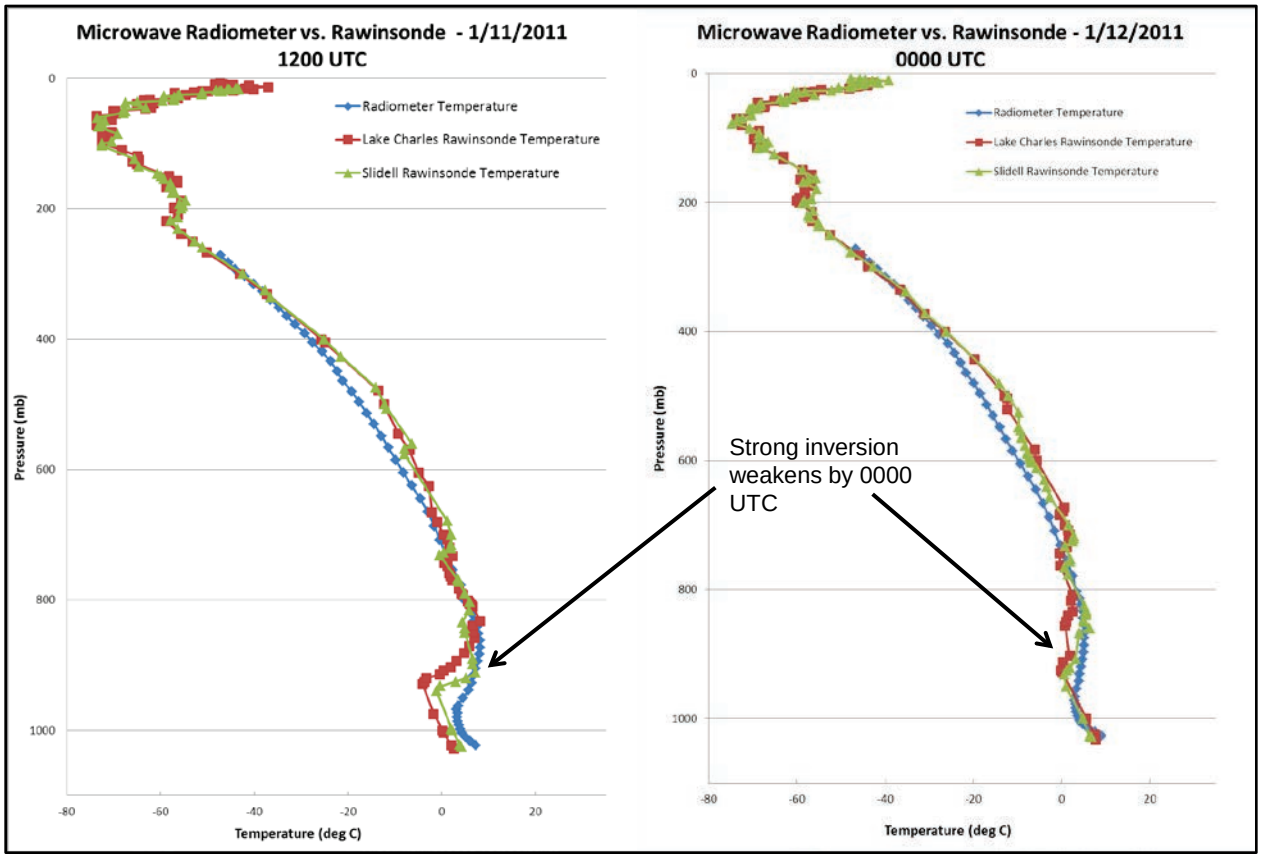


Figure 25. Microwave radiometer temperature sounding (blue), Lake Charles temperature sounding (red), and Slidell temperature sounding (green) for January 11, 2011, 1200 UTC (left) and January 12, 2011, 0000 UTC (right).

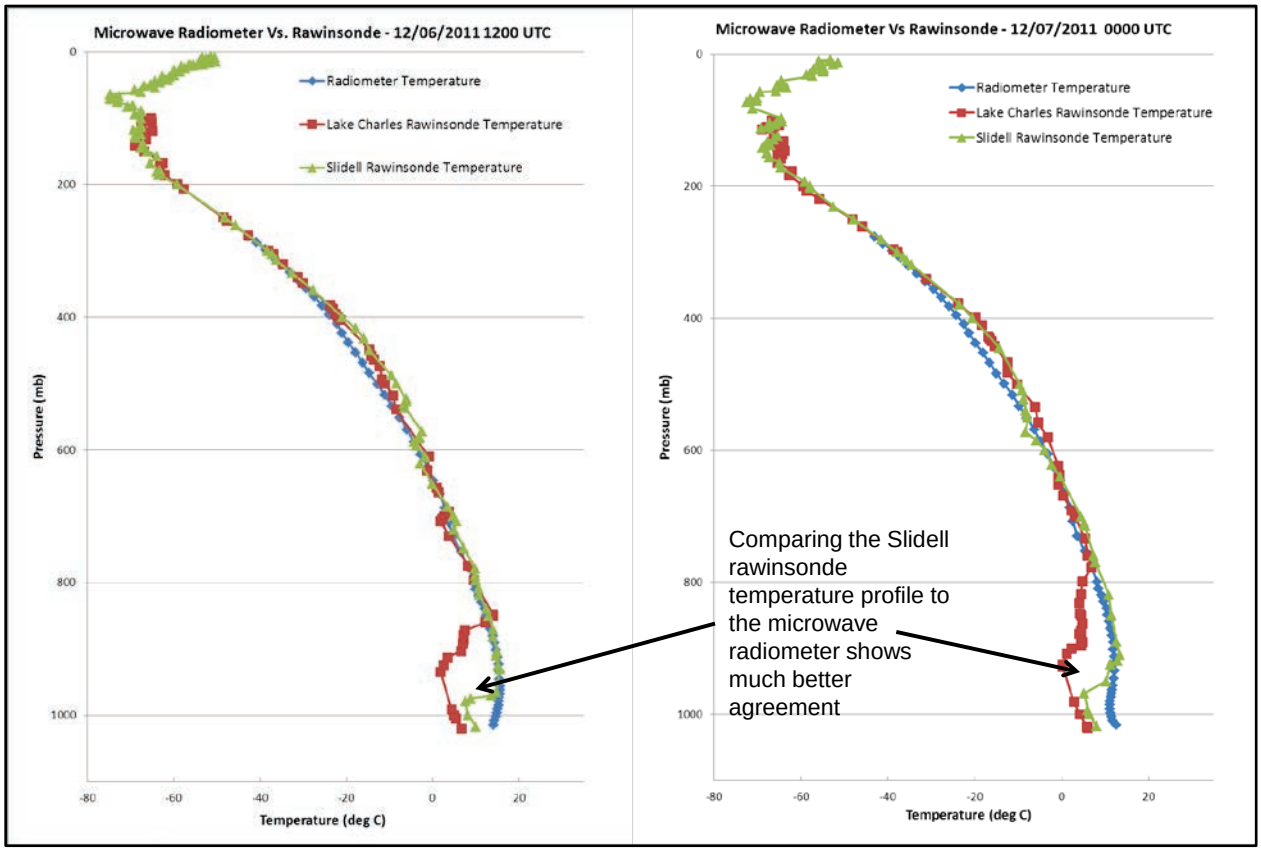


Figure 26. Microwave radiometer temperature sounding (blue), Lake Charles temperature sounding (red), and Slidell temperature sounding (green) for December 6, 2011, 1200 UTC (left) and December 7, 2011, 0000 UTC (right).

The ceilometer mixing heights and cloud heights were generated by applying an automated algorithm developed by Vaisala to the raw data. In addition, the cloud heights were compared to satellite data to determine reasonableness. Figure 27 shows a satellite image for January 11, 2011, at 1431 UTC, revealing a broad area of low clouds over the Gulf of Mexico. Figure 28 shows the ceilometer backscatter data collected on that day with the cloud heights and mixing heights overlaid. The cloud bases and tops observed in the ceilometer are consistent with the low clouds present in the visible satellite imagery.

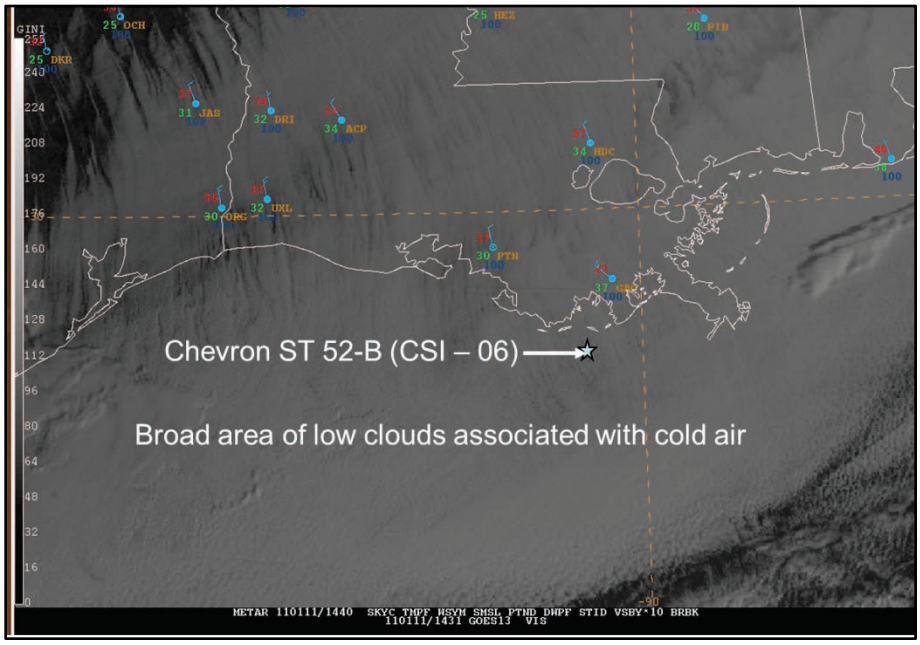


Figure 27. Visible satellite imagery over the northern Gulf of Mexico for January 11, 2011, at 1431 UTC.

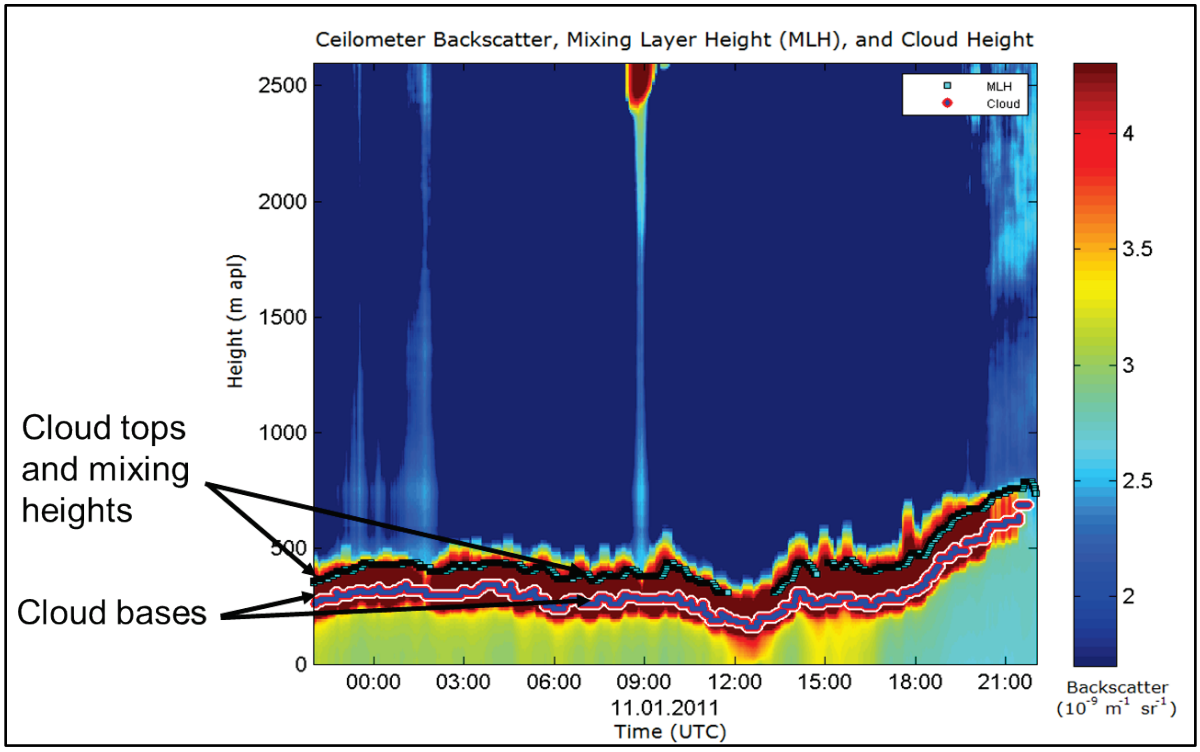


Figure 28. Ceilometer backscatter with cloud bases, cloud tops, and mixing heights in meters above platform level (apl).

Figure 29 shows an example of the surface meteorological data for the period from June 23, 2011, through June 28, 2011, located on ST-52B. This is an example of using collocated data sources to validate data. The rainfall is consistent with the wind direction shift and the decreasing downwelling radiation.

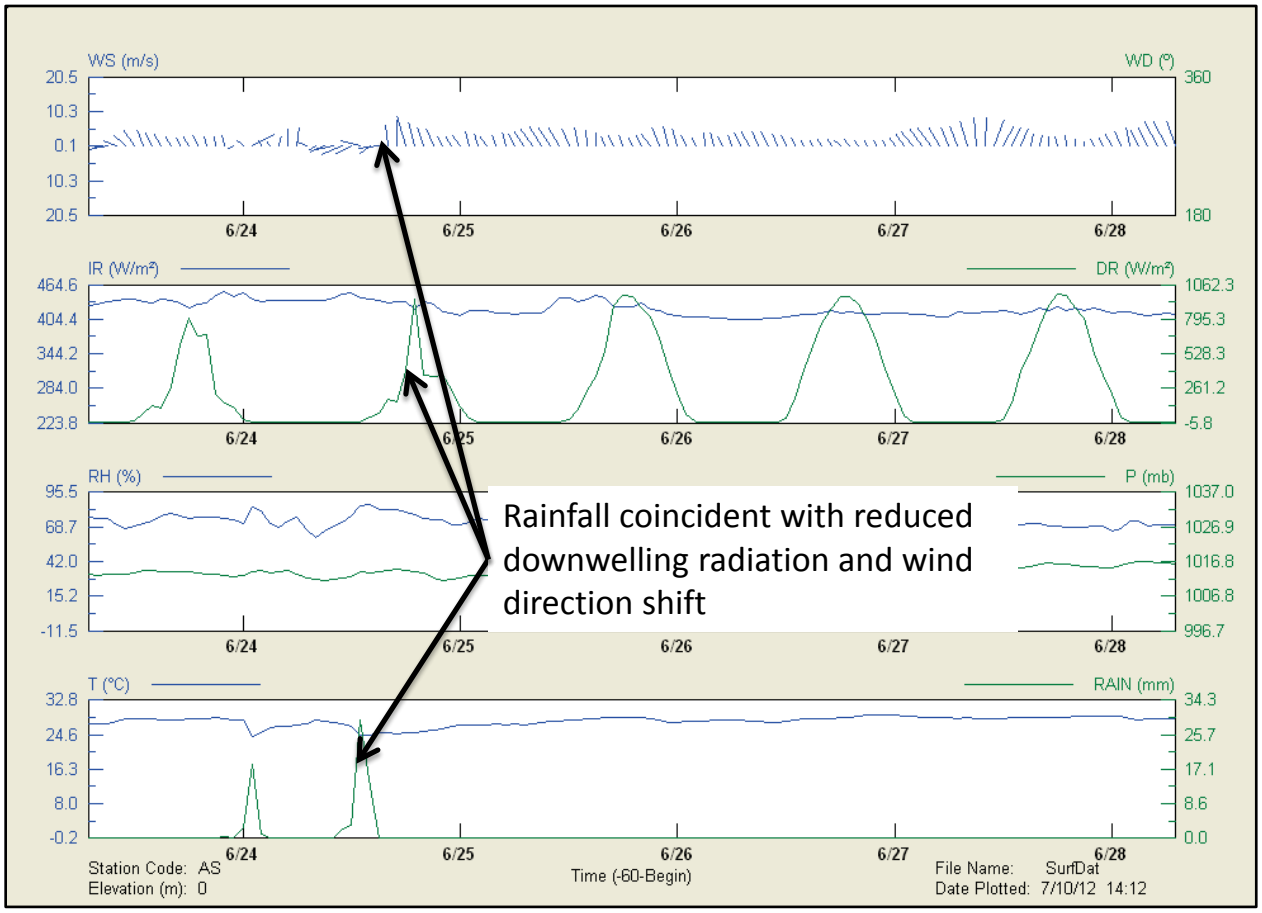


Figure 29. Surface meteorological data from the platform deck for June 23 through June 28, 2011, including (top to bottom) wind speed (WS) and wind direction (WD); infrared radiation (IR) and downwelling radiation (DR); relative humidity (RH) and pressure (P); and temperature (T) and rain (RAIN). Times are in UTC.

Figure 30 shows an example of the skin temperature and sea surface temperature data. The skin temperature was invalidated at these times because there were periods where the measured skin temperature values would drop from roughly 28°C to -26°C. These variations were caused by water in the sensor's electronics.

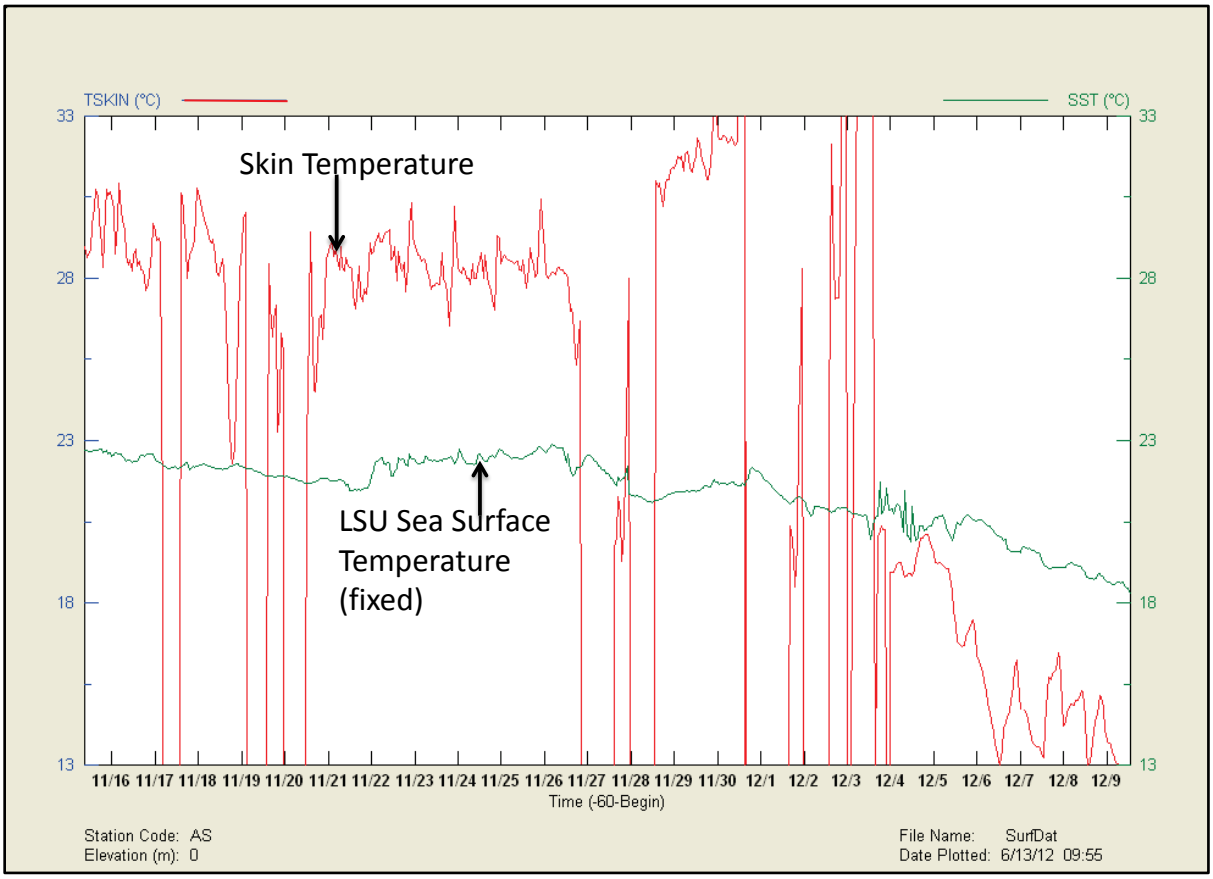


Figure 30. Skin temperature from the infrared temperature sensor (red line) and fixed sea surface temperature from LSU for 11/15/2010 through 12/9/2010. Times are in UTC.

Figure 31 shows an example of the wave height and maximum wave heights for September 14 through September 18, 2011. Comparisons of the wave height and peak wave height were done to check the internal consistency of the data.

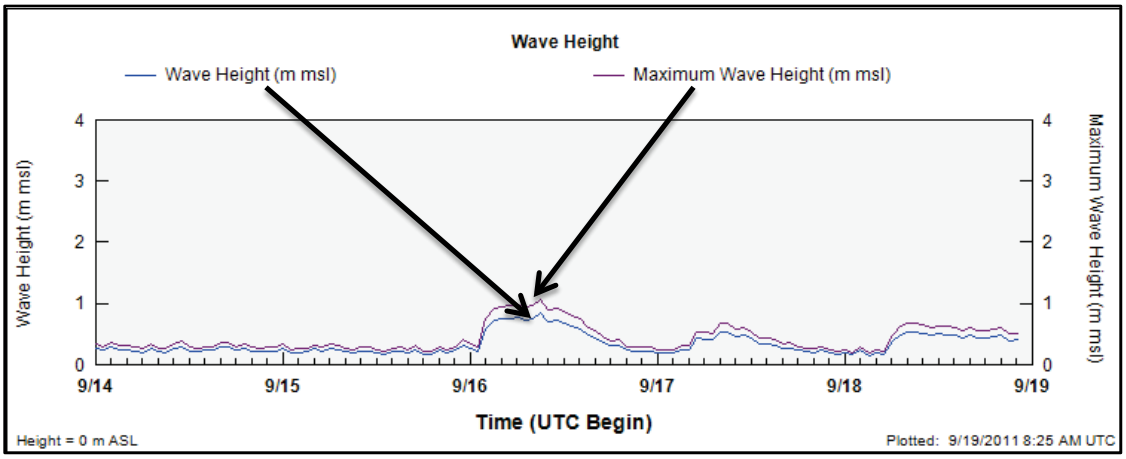


Figure 31. Wave heights and maximum wave heights for September 14 through September 18, 2011.

Figure 32 shows an example of quality control that was completed on the specific humidity data. The Automatic Gain Control (AGC) of the Li-Cor 7500 was used in complement with other data filters to remove bad specific humidity data. In this case, the low humidity values were caused by the wash system that was developed to keep the lenses of the Li-Cor 7500 clean. These data points were made invalid.

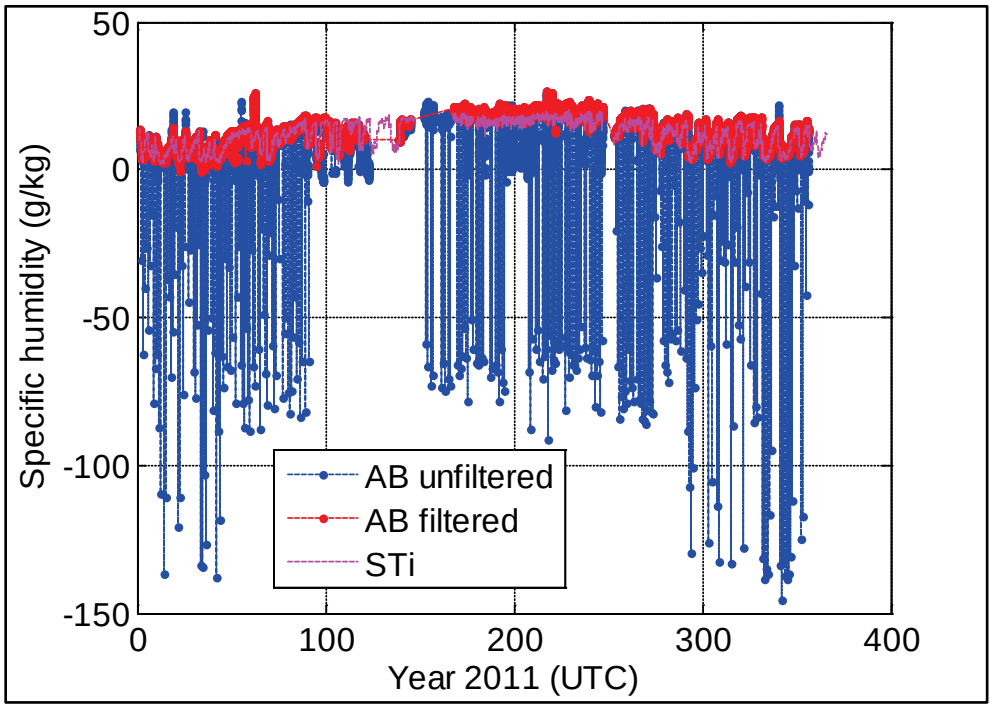


Figure 32. Illustration of unfiltered (blue) and filtered (red) specific humidity data from the AB Li-Cor 7500 sensor.

Section 7 provides additional information on the flux data processing and quality control.

6. DATA FORMATS

The accompanying DVD contains the quality-controlled data collected during this study in comma-separated format (CSV), except for the ceilometer backscatter data, which is in its native format. The time standard for the data is Coordinated Universal Time (UTC). This section describes the file naming convention and the file formats.

Table 8 lists the data file names, where

- <YYYY> = four-digit year
- <Y> = one-digit year
- <MM> = two-digit month
- <DD> = two-digit day
- <HH> = two-digit hour
- <MM> = two-digit minute
- <SS> = two-digit second
- <x> = level number (for radiometer)

Table 9 lists the fields in the data files (except for the radiometer, ceilometer, and flux data files).

A description of the microwave radiometer file formats can be found in Sections 6.3.5, 6.3.6, and 6.3.7 (pages 65 through 66) of the Radiometrics Profiler Operator's Manual[4]. Note, the radiometer data are stored in three files: Level 0 files (raw sensor data in volts), Level 1 files (brightness temperatures), and Level 2 files (profile retrievals).

The flux data formats are provided in Section 7.

The ceilometer file format can be found in Chapter 5 (page 58) of the Vaisala CL31 Users Guide (Vaisala 2004).

4 Please contact Radiometrics at (303) 449-9192 for the operator's manual.

Table 8.

Data file names

Parameter	Instrument	File Name	All Data in File or Individual Files	Data Accumulation Frequency
Wind speed and direction	Mini-sodar	Mini-sodar.csv	All	15 minutes, multiple heights
Profiles of temperature, relative humidity, and liquid water and additional meta data associated with these measurements	Microwave Radiometer	<YYYY>-<MM>-<DD>_<HH>-<MM>-<SS>_lv<x>.CSV Example: 2010-11-10_235900_lv2.CSV	Individual Files	2.5 minutes, multiple heights
Backscatter data	Ceilometer	A<Y><MM><DD><HH>.dat Example: A0111023.dat	Individual Files	16 seconds, multiple heights
Mixing and cloud height	Ceilometer	CeilometerMHCH.csv	All	15 minutes
Wind speed and direction Temperature LSU wind speed and direction LSU temperature Relative humidity LSU pressure Downwelling (shortwave) radiation Infrared (longwave) radiation Precipitation	Surface Meteorology	SurfaceMeteorology.csv	All	60 minutes
Wave height Wave period Water depth	Pressure Transducer and ADCP Current Meter	Wave.csv	All	60 minutes
AB and AC bridge sonic winds AB and AC bridge sonic temperature AB and AC bridge specific humidity AB and AC bridge CO_2 concentrations AB and AC bridge heat flux and stress (covariance streamwise (u^1w^1), covariance cross-streamwise (v^1w^1), and combine AB and AC bridge covariance streamwise)	Sonics and Licors	ST52_10minflux_2010.r1 ST52_10minflux_2011.r1 ST52_10minflux_2012.r1	All	10 minutes

Table 9.

Fields located in data files

Field	Description
Site Name	Site identifier
Data Type	Instrument
Parameter Name	Parameter description
DateTime(UTC)	Date and time in UTC
Height	Height in meters above ground level (m apl)
Value	Data value
Units	Parameter measured (units for parameter measured)
QC Code	QC code for parameter
QC Level	QC level for parameter

Table 10 lists the parameter names and descriptions. See Section 7 for a description of the flux data files.

Table 10.

Parameter names and descriptions

Parameter	Description
Temperature	Air temperature (°C)
LSU-Temperature	LSU air temperature (°C)
Wind Speed	Scalar-averaged wind speed (m/s)
Wind Direction	Vector-averaged wind direction (°)
LSU Wind Speed	Scalar-averaged wind speed (m/s)
LSU Wind Direction	Vector-averaged wind direction (°)
Sigma Theta	Wind direction standard deviation (°)
Downwelling Radiation	Downwelling radiation (W/m^2)
Infrared Radiation	Infrared radiation (W/m^2)
Pressure	Atmospheric pressure (mb)
Relative Humidity	Relative humidity (%)
Rain	Precipitation (mm)
Wave Height	Wave height (m)
Maximum Wave Height	Maximum wave height (m)
Wave Period	Wave period (sec)
Peak Wave Period	Peak wave period (sec)
Water Depth	Water depth (m)
Sea Skin Temperature	Infrared skin temperature (°C)
Sea Surface Temperature – Fixed	Fixed sea surface temperature (°C)
Sea Surface Temperature – Float	Floating sea surface temperature (°C)
Mixing Height	Mixing height (m apl)
Cloud Height	Cloud height (m apl)

An electronic copy of this report and the validated data collected during this reporting period are provided on a DVD that accompanies this report. The DVD is labeled as follows:

Format: Microsoft® Office 2010, ASCII text, Vaisala Ceilometer format.

Meteorological and Wave Measurements
[October 1, 2010 through April 1, 2012]
BOEM Contract #M08PC20057
STI-908059-5458
Prepared for the
Bureau of Ocean Energy Management
September 2012

7. PRELIMINARY DATA ANALYSES

The goal of this project was to collect meteorological data to better characterize the atmospheric boundary layer over the Gulf of Mexico. However, to demonstrate data use and set the stage for future analyses, preliminary data analyses were completed as part of this project. In particular, we

1. Performed a preliminary case study analysis to investigate the relationship between large-scale meteorology and boundary layer conditions at the platform.
2. Investigated how well the NAM (North American Mesoscale Model) predictions compare to the measured vertical wind profiles collected by the mini-Sodar.
3. Investigated how well COARE-calculated fluxes compare to the measured heat and momentum fluxes.

These preliminary analyses are presented below.

7.1 JANUARY 11, 2011, CASE STUDY

This case study illustrates how data collected from this study could be used to better understand the relationships among the large-scale weather patterns, vertical temperature and relative humidity structures, mixing heights, boundary-layer winds, and energy fluxes.

On January 11, 2011, a cold front moved south over the Gulf of Mexico. The front brought cold air over the Chevron platform. The northerly winds associated with this cold front ranged from about 6 to 10 m/sec. As measured by the mini-sodar (see Figure 33), the winds were homogeneous in direction and speed through at least the lowest 200 m of the boundary layer. This cold air boundary began to arrive at the platform at about 0300 UTC, at which time the layer of cold air was measured to be confined to the lowest ~400 m of the boundary layer (see the temperature data from the microwave radiometer in Figure 34). As the day went on, the layer of cold air deepened, reaching about 1 km by 1700 UTC according to the radiometer temperature data. Nearly saturated air (i.e., air with relative humidity near 100%) was observed within the boundary layer (see the relative humidity data from the microwave radiometer in Figure 34). Above the boundary layer, the air was dry (i.e., RH ~30%). The saturated air within the boundary layer resulted in thin stratus clouds over the Gulf as captured by the visible satellite image taken at 1431 UTC (see Figure 35). As measured by the ceilometer, the bases of these clouds were about 300 m msl in the morning and then elevated to about 500 m msl in the late afternoon (see Figure 36). In addition, the ceilometer indicates that these clouds were quite thin (~100 m). The tops of the clouds were also the top of the mixed layer as measured by the ceilometer (see Figure 36). There was good correlation amongst the mixing and cloud heights and temperature structure throughout the day; as the cold layer deepened in the afternoon, the cloud and mixing heights increased accordingly.

During this period, COARE-calculated[5] sensible heat flux was moderate to strong upward and ranged from about 70 w/m^2 in the early morning to about 150 w/m^2 in the middle of the day (see Figure 37). The strong sensible heat flux was driven by large air-sea temperature differences,

5 Measured fluxes were not available on this day.

which increased throughout the morning until midday as the cold air moved over the warm Gulf waters. Late in the day, as the ocean warmed the air above, the air-sea temperature difference decreased, as did the sensible heat flux. The spikes in sensible heat flux observed at 500 and 1330 UTC were driven by increases in wind speeds at those times. The COARE-calculated latent heat flux was relatively weak upward and ranged from about 175 w/m^2 in the morning to about 200 w/m^2 in the middle of the day (see Figure 37). The relatively small latent heat flux was because of a moist boundary layer that caused relatively small vertical gradients in specific humidity.

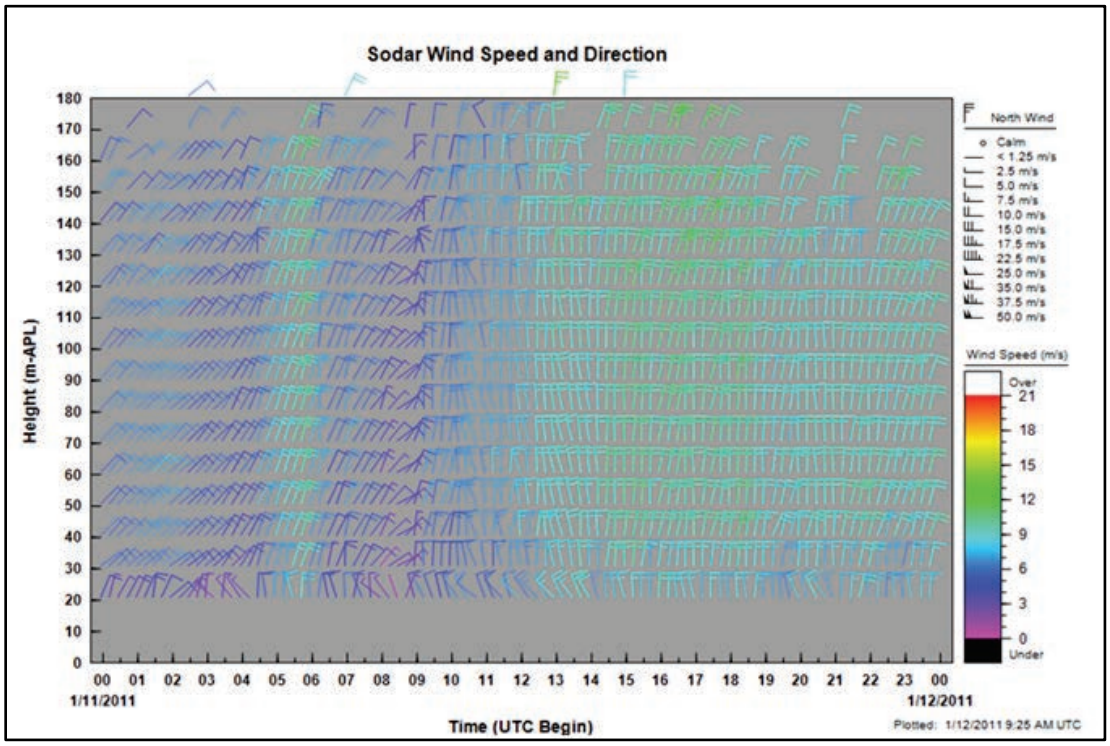


Figure 33. Mini-sodar wind data on January 11, 2011.

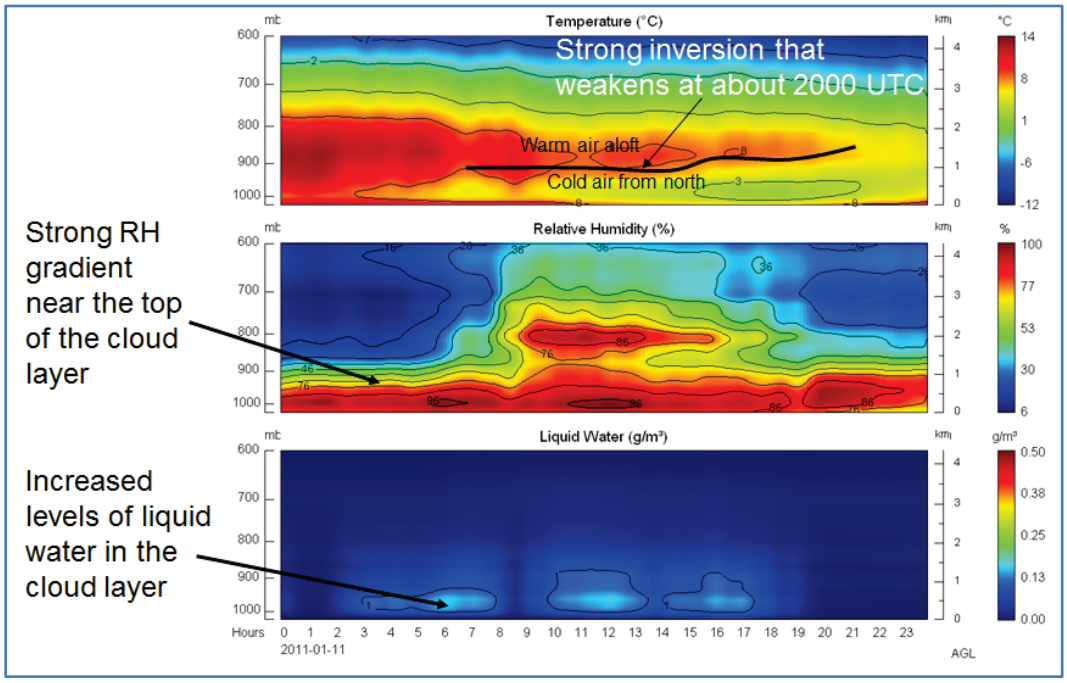


Figure 34. Microwave radiometer temperature, relative humidity, and liquid water data on January 11, 2011. Times are in UTC.

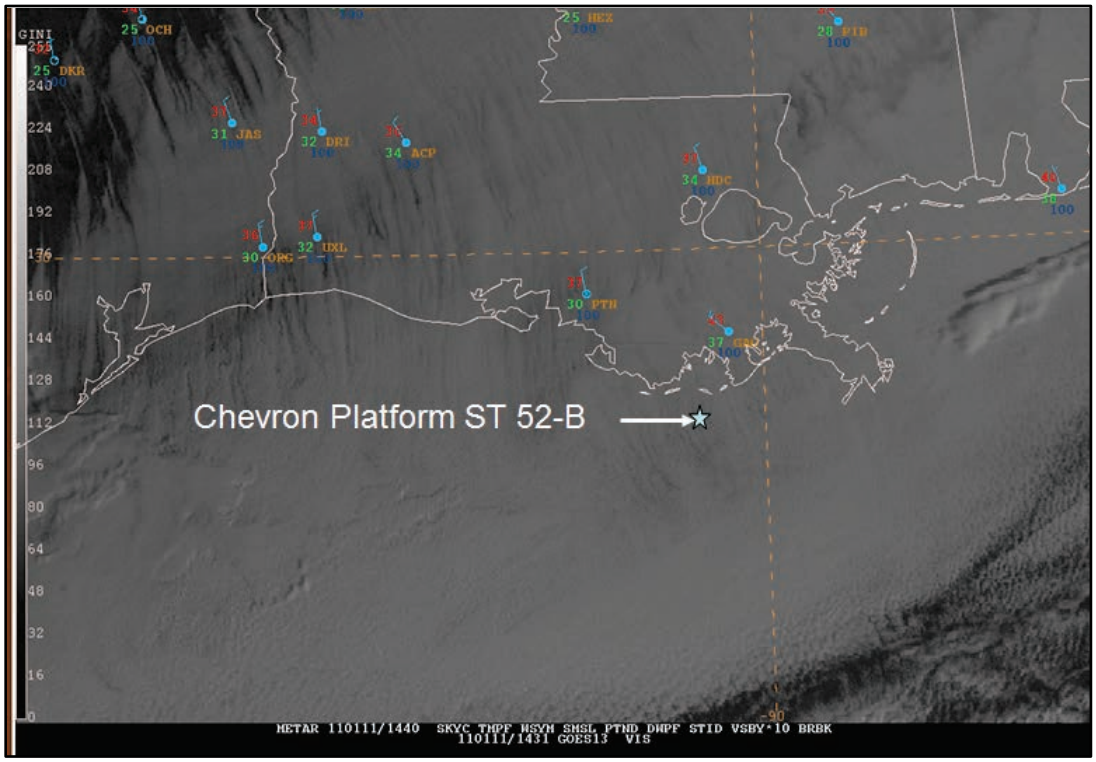


Figure 35. Visible satellite image taken at 1431 UTC on January 11, 2011.

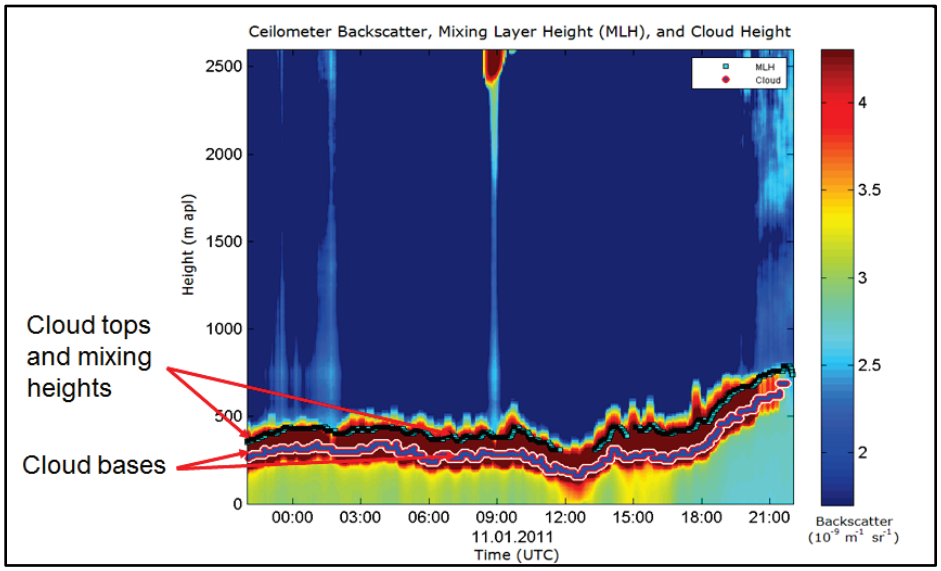


Figure 36. Ceilometer backscatter data, cloud base and top heights, and mixing heights on January 11, 2011.

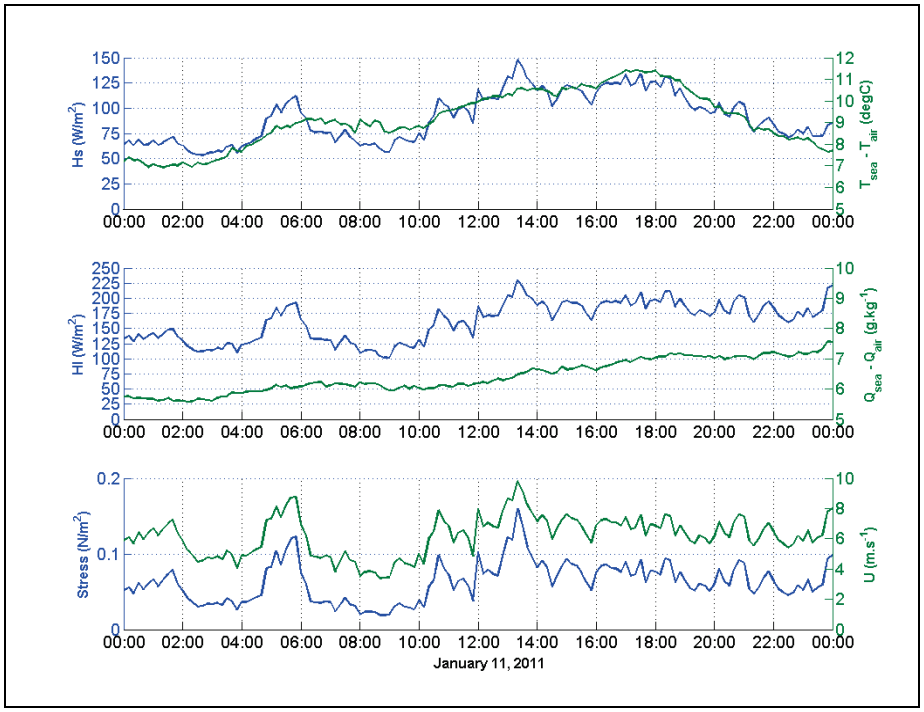


Figure 37. COARE-calculated sensible heat flux (Hs) and air-sea temperature (T) difference (top), and COARE-calculated latent heat (Hl) and air-sea specific humidity (Q) difference (middle), and COARE-calculated streamwise stress and wind speed (bottom). Times are in UTC. An additional explanation of the calculations and variables used is provided in Section 7.3.5.

7.2 MEASURED AND MODELED VERTICAL WIND PROFILES

This analysis illustrates how data collected from this study could be used to better understand the wind characteristics within the lowest 200 m over the Gulf of Mexico and how well models represent these characteristics. We calculated and compared seasonal scalar-average winds collected by the mini-sodar and platform "surface" winds to predictions provided by the North American Model for October 2, 2010, through September 30, 2011. The data processing consisted of the following elements:

- Sodar data were 15-minute averages.
- Near-platform deck level winds were hourly averages and were combined with the sodar winds to create a complete profile from ~45 to ~180 m asl.
- NAM model predictions were for 0000, 0600, 1200, and 1800 UTC. The 0000 and 1200 UTC predictions were model initializations, and the 0600 and 1800 UTC predictions were 6-hr forecasts.
- Logarithmic interpolation between vertical model data was applied (dashed lines in Figure 38).
- Inverse distance interpolation among horizontal grid squares was applied to estimate model winds at the platform location.

As shown in Figures 38 and 39, we can conclude the following:

- The surface and sodar measurements characterize the actual winds from 40 to ~200 m asl for an entire year over the Gulf. This provides unique information regarding winds in the Gulf.
- At 150 m asl, the average winds exceed 13 mph in all seasons except summer. This is higher than expected and is higher than predicted by NAM.
- There is diurnal variability in the observed winds; the stronger winds tend to occur in the afternoon and overnight hours.
- The average model winds do not represent actual conditions. For example, (1) the model winds are often slower than the observed, and (2) the model winds do not always capture the vertical structure. For example, in the winter, there is a wind speed jet between about 100 and 150 m, which is not captured by the model.

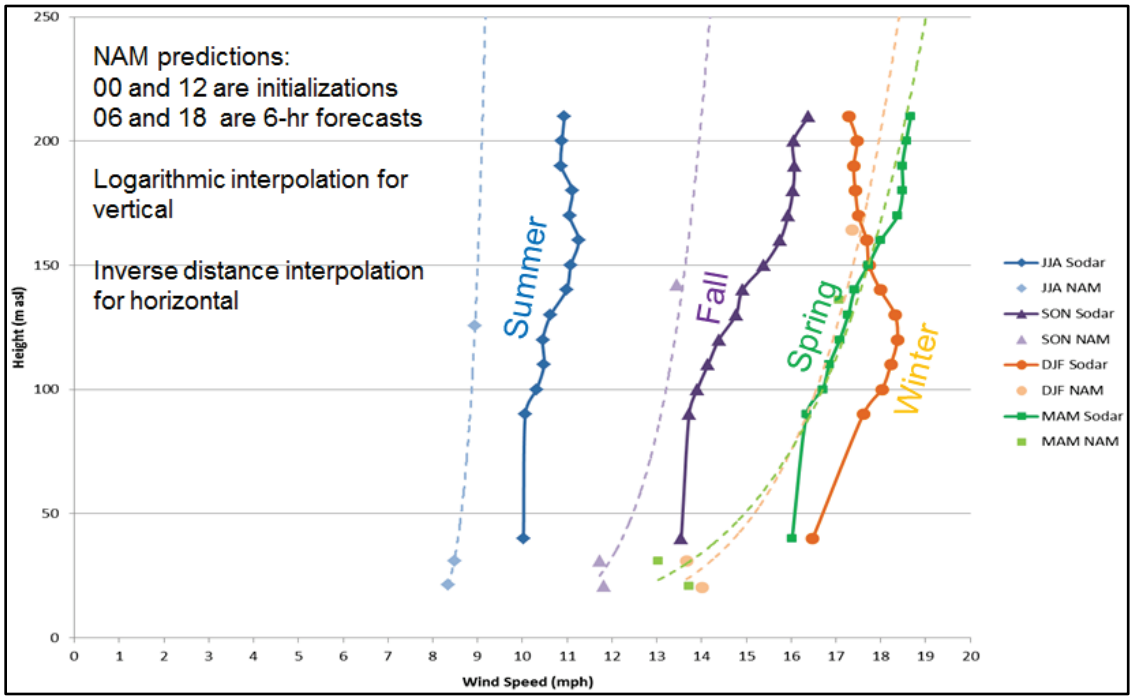


Figure 38.Seasonal averages of measured (sodar) versus model (NAM) winds.

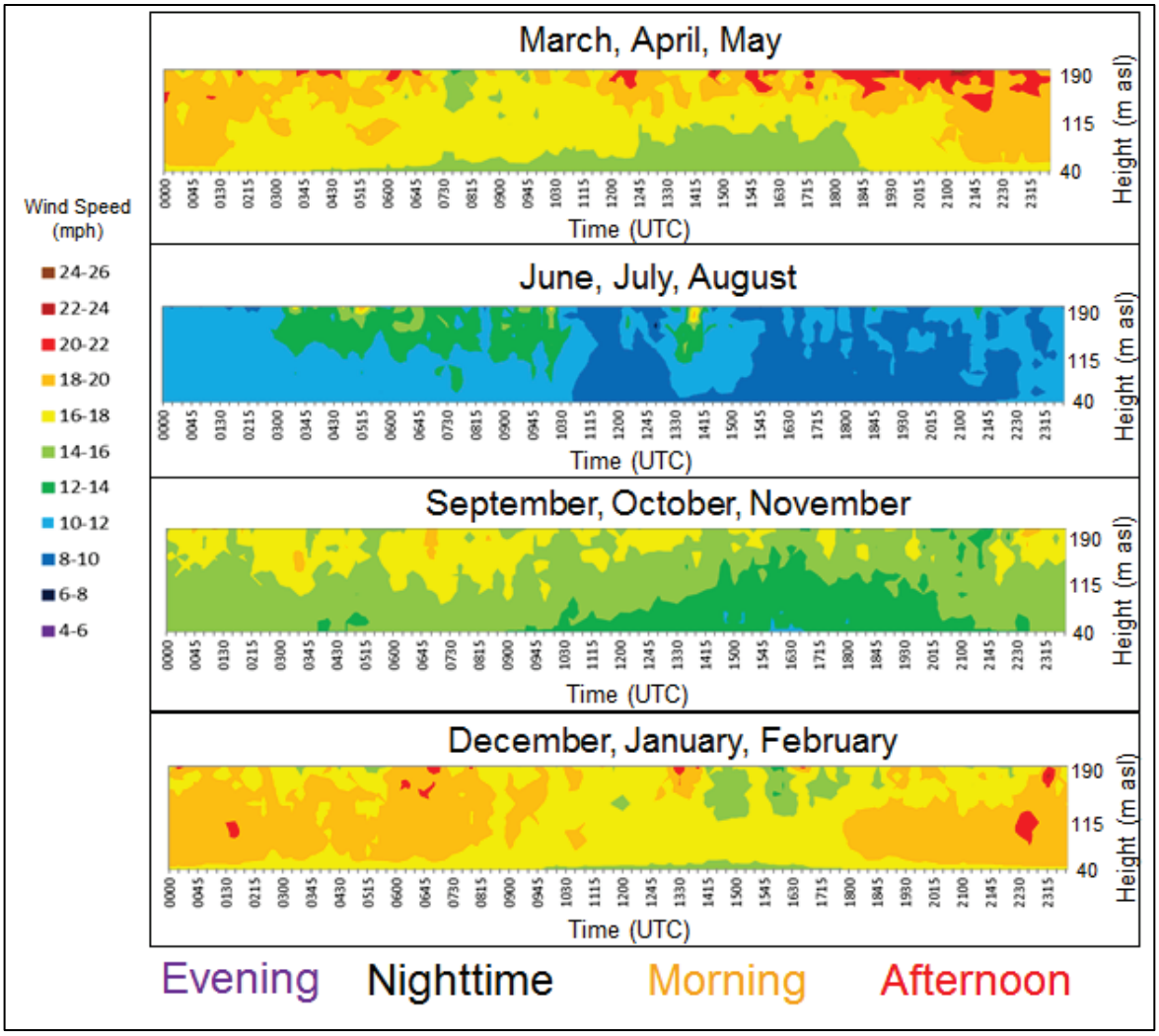


Figure 39. Seasonal average diurnal profile of boundary layer winds as measured by the mini-Sodar.

7.3 Observed and COARE-Calculated Fluxes

As part of this field effort with STI and LSU, the NOAA Earth System Research Laboratory (ESRL) Physical Sciences Division (PSD) Air-Sea Interaction Group and the University of Colorado provided a turbulent flux system composed of two sonic anemometers and two Li-Cor 7500 gas analyzers that were deployed on Chevron Platform ST-52B.

As part of this project, we conducted a preliminary analysis that compares the Coupled Ocean Atmosphere Response Experiment (COARE) algorithm calculations to the eddy-correlation flux measurements. The flux instruments used for this analysis are described in Section 7.3.1. Section 7.3.2 presents the methods used for the analysis. Results and discussion are provided in Sections 7.3.3 to 7.3.5. A COARE data analysis summary is given in Section7.3.6.

7.3.1 Flux System Description

The NOAA PSD turbulent flux system consists of two sets of each of the following components: a Gill WindMaster Pro sonic anemometer and a Li-Cor 7500 fast CO_2/H_2O analyzer. One flux "package" was located on the AB bridge of the platform and one was located on the AC bridge (see Figures 40 and 41). AB refers to the instruments on the AB bridge (i.e., AB sonic), and AC refers to the instruments on the AC bridge.

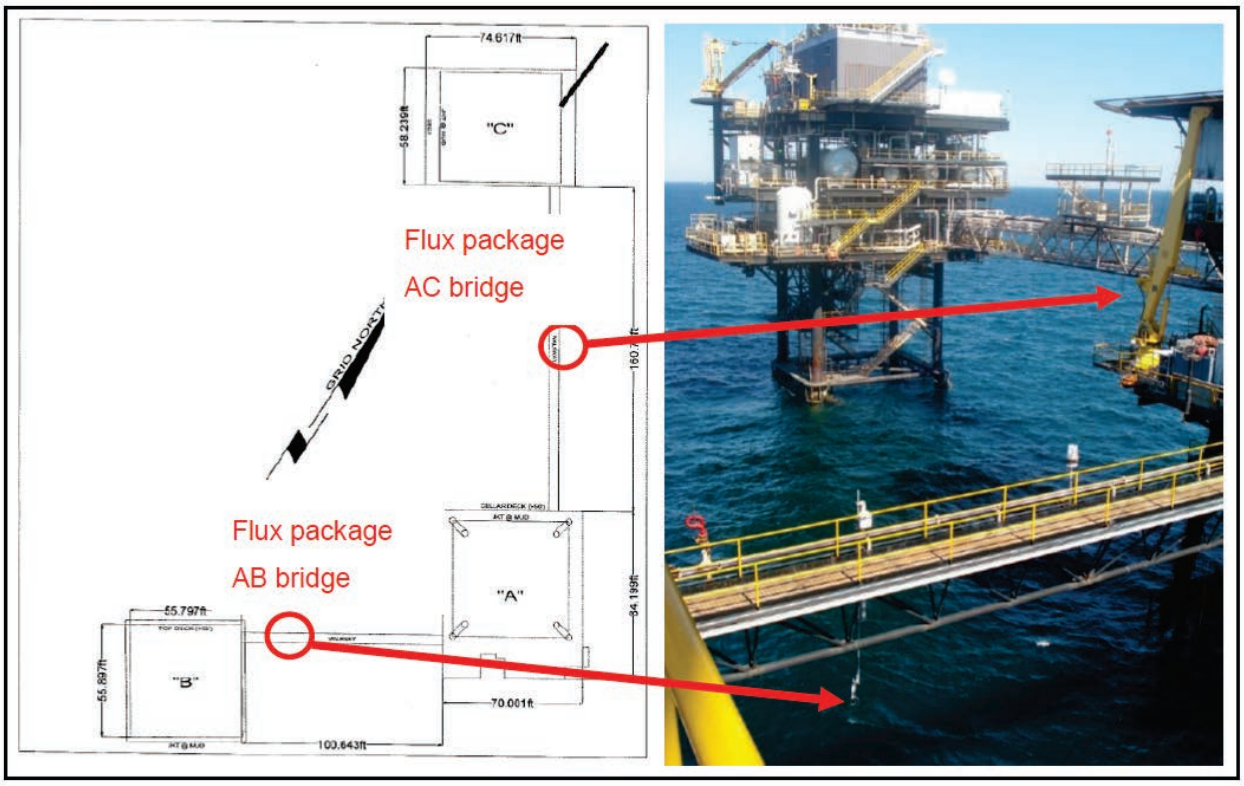


Figure 40. Location of the AB and AC flux packages on the platform.

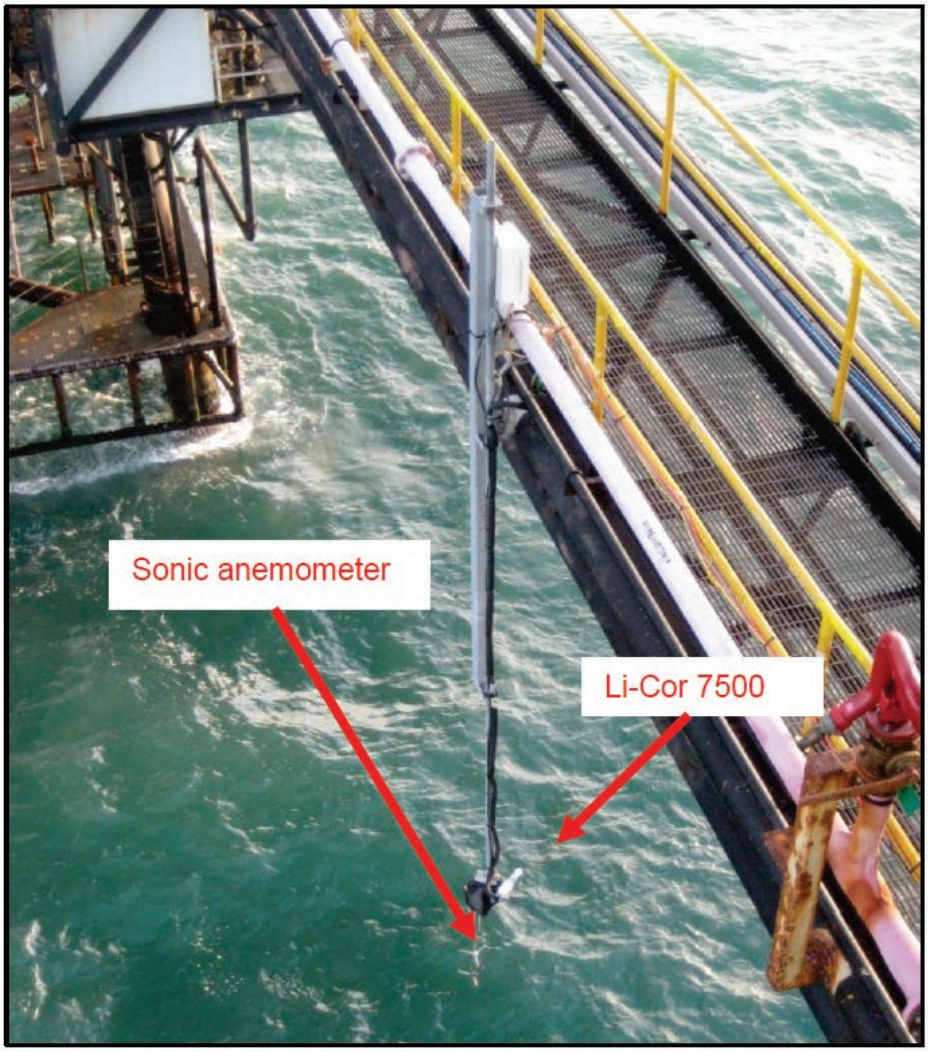


Figure 41.Close-up view of the AB flux package.

Table 11 shows sampling rates and deployment heights of the “flux” sensors.

Table 11.

Flux package sensor heights and sampling rates

Sensor	Sampling Rate (Hz)	Height (msl)
AB sonic	10	10.2
AB Li-Cor	10	10.8
AC sonic	10	11.6
AC Li-Cor	10	12.6

7.3.2 Method

The data used for the data analysis are from January 1, 2011, to December 31, 2011. Data from December 3, 2010, to December 31, 2010; and from January 1, 2012, to May 5, 2012, were also processed and delivered to BOEM, but were not used in this comparison. For illustration, the 10-minute average time series of wind speed, wind direction, air temperature, sea surface temperature, incident shortwave and longwave radiation, relative humidity, and atmospheric pressure are shown for 2011 and 2012 in Figures 42 and 43. Data gaps are due to instrument or acquisition system failures. About 90% of the meteorological data are available for 2011, and about 72–84% of the raw data are available for the flux packages (AC and AB, respectively).

For this analysis, the following data processing steps were taken:

- Covariance fluxes and mean meteorological states were calculated over a 10-minute time period. The sign convention for fluxes is positive upward (i.e. away from the surface).
- All meteorological data sources were compared and evaluated to select an ideal data set to compute fluxes from the COARE algorithm.
- Covariance fluxes were quality controlled (QC) via numerous filters (more details follow) and compared against BULK fluxes (Fairall et al. 1996).

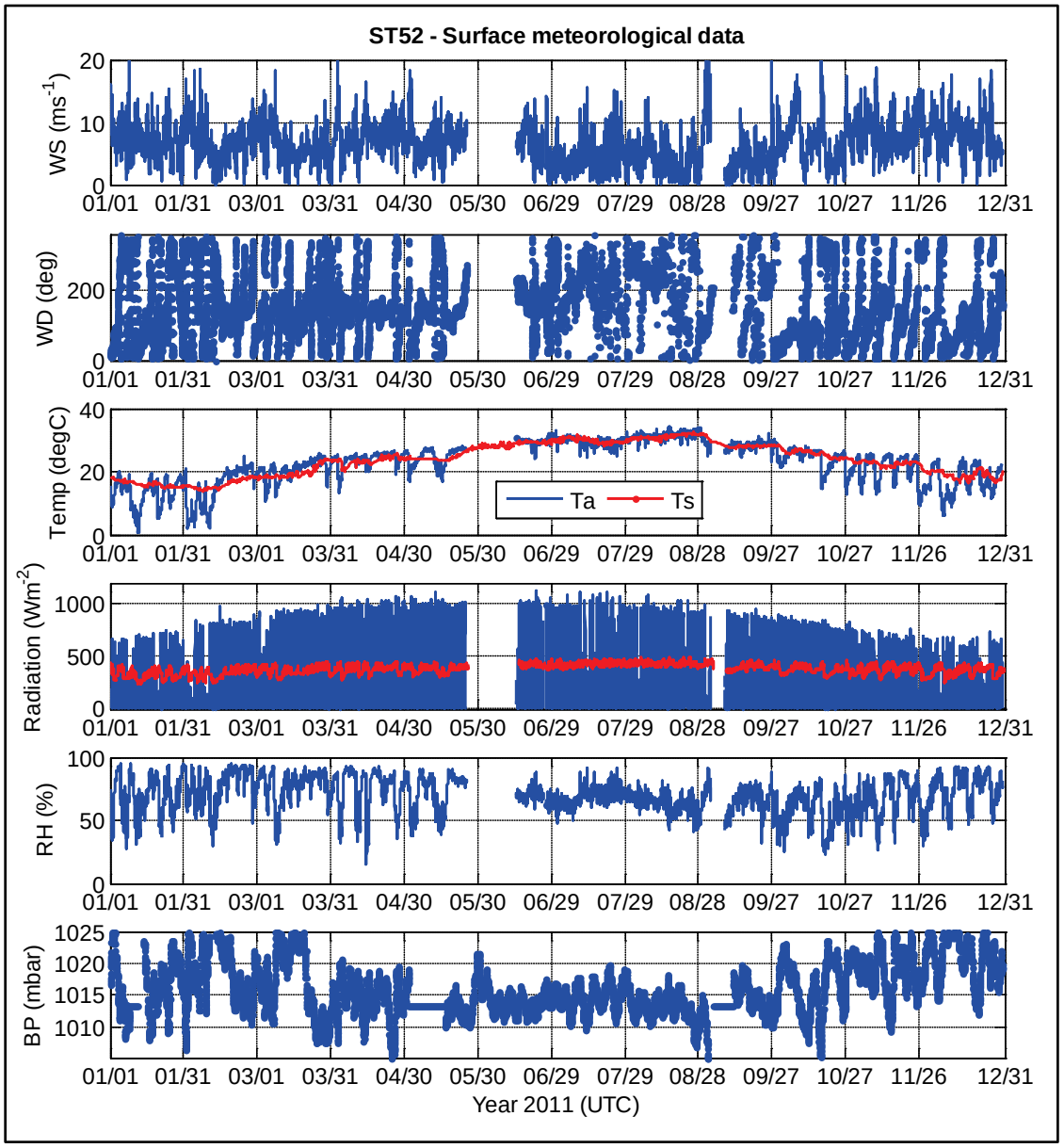


Figure 42. Meteorological conditions from the platform during 2011. From the top, panels show wind speed (ms^{-1}), wind direction in degrees relative to true north, air temperature (blue) and surface sea temperature (°C) (red), incident shortwave (blue) and longwave (red) radiations (Wm^{-2}), relative humidity (%), and barometric pressure (mb).

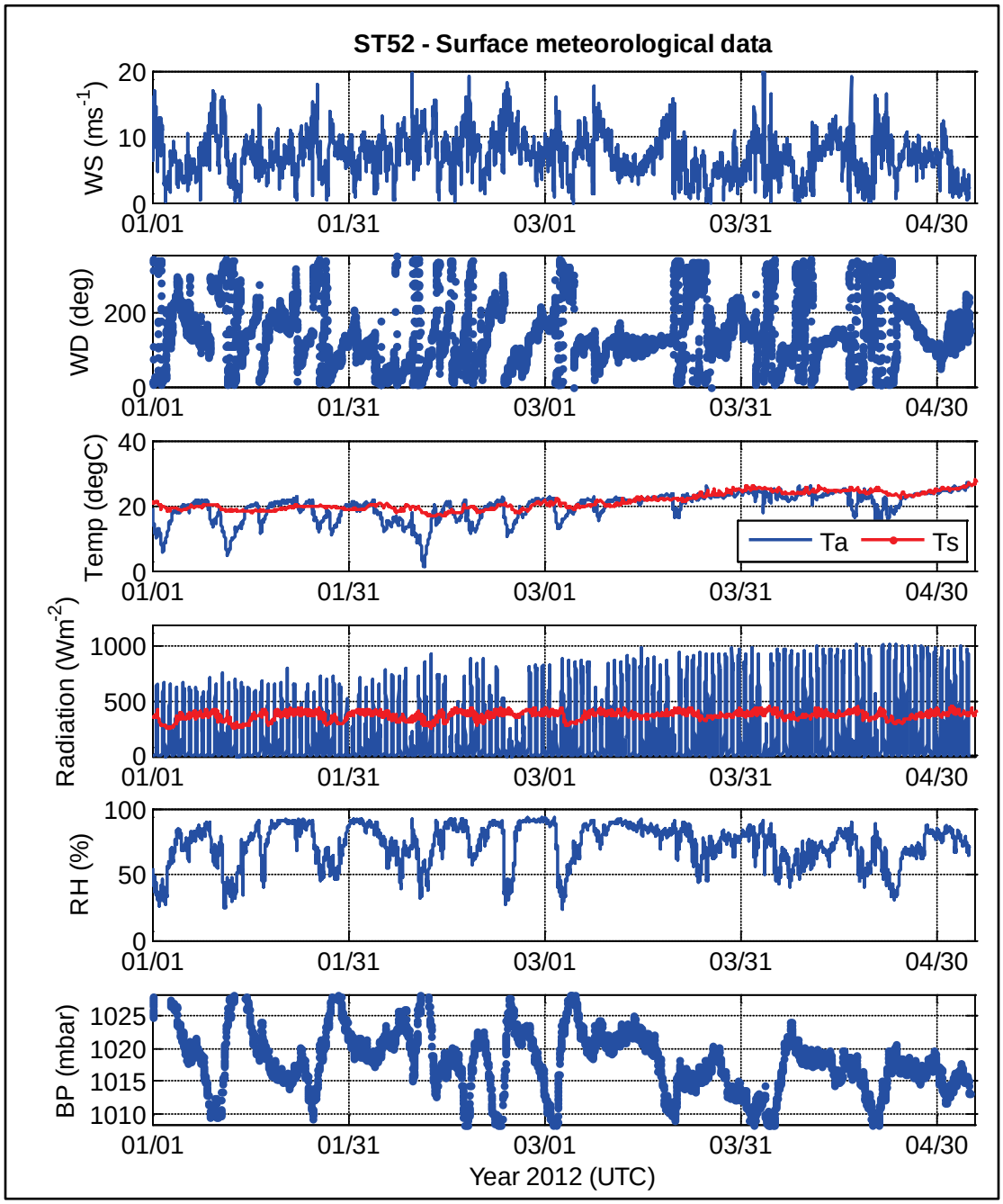


Figure 43. Meteorological conditions from the platform during 2012. From the top, panels show wind speed (ms^{-1}), wind direction in degrees relative to true north, air temperature (blue) and surface sea temperature (°C) (red), incident shortwave (blue) and longwave (red) radiations (Wm^{-2}), relative humidity (%), and the barometric pressure (mb).

7.3.3 Meteorological Data Evaluation

In this section, we briefly review the surface observations available and select the best data set for the COARE algorithm.

7.3.3.1 Air Temperature

Figure 44 shows a time series of air temperature measurements for 2011. As noted during deployment, the sonic anemometers were offset from one another by about 5°C. However, because fluxes are based on the variations instead of the means, this offset does not affect the turbulent fluxes. We also note that the LSU temperature measurement ran about 1°C lower than the STI unit in the first half of the year, but then measured about 2°C higher after replacement.

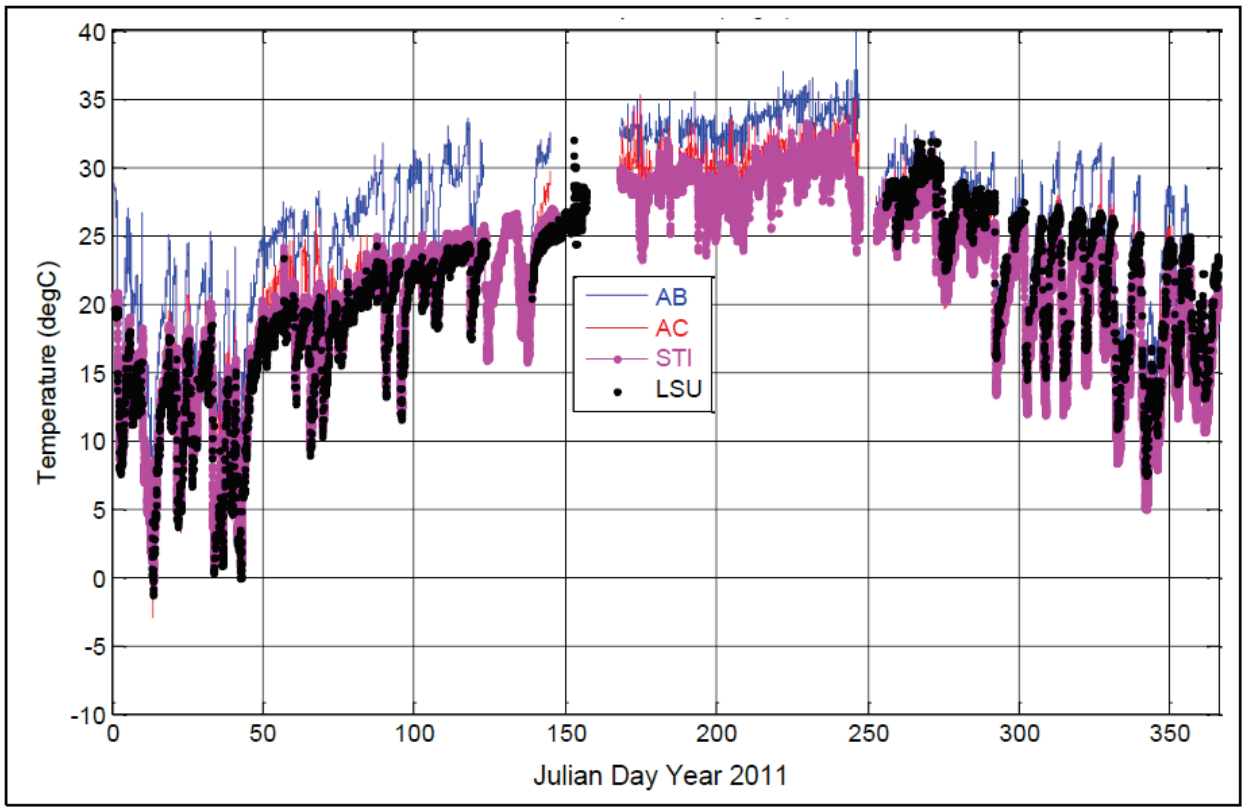


Figure 44. Time series of air temperatures for the two sonic anemometers (blue and red), and the temperature measurements from the roof of the B platform (magenta and black).

7.3.3.2 Relative Humidity

Figure 45 shows relative humidity measurements from the STI and LSU collocated instruments. Because the LSU instrument behaved abnormally several times before its replacement in fall 2011, we used the STI measurement for the COARE flux calculations.

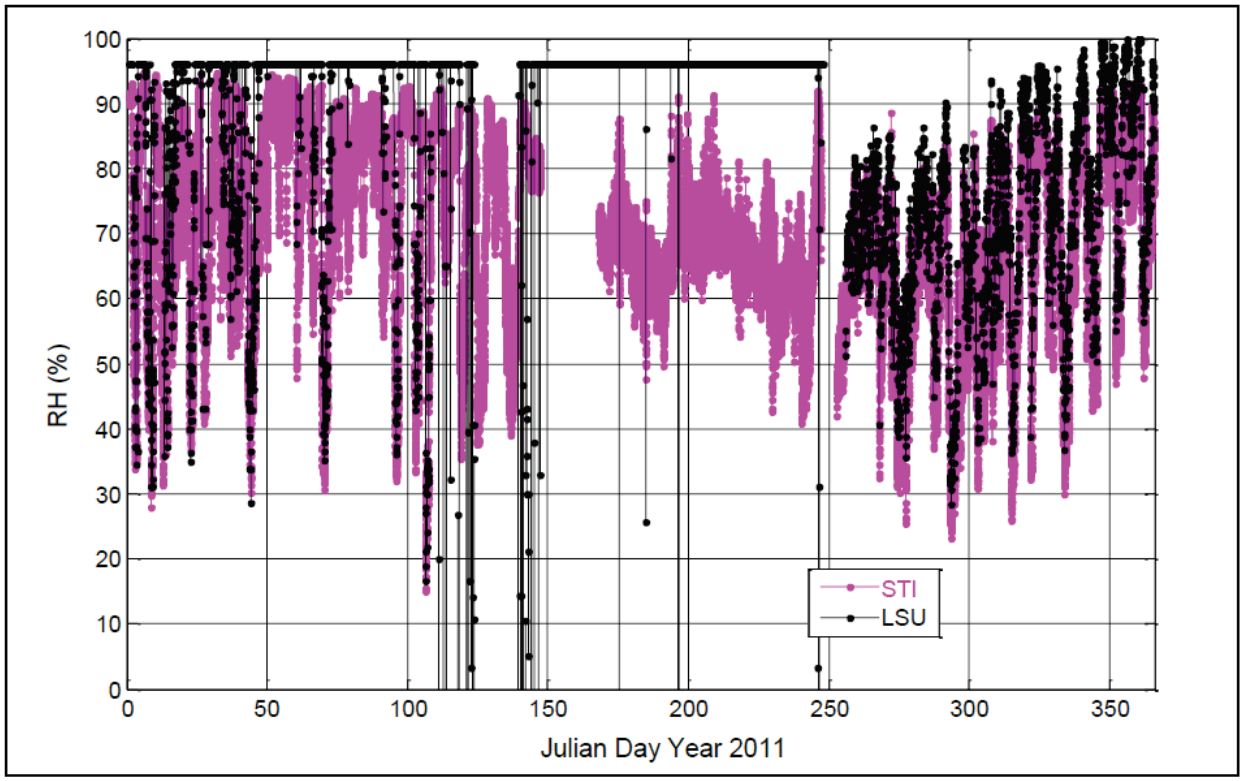


Figure 45. Relative humidity from STI (magenta) and LSU (black) instruments.

7.3.3.3 Sea Temperature

Figure 46 shows a time series of air and sea temperatures from an instrument at approximately 1 m below mean water level (LSU sensor) and from a floating thermistor (STI sensor) at a depth of approximately 20 cm deployed in July of 2011. Initially, the instruments were within 0.5°C of each other at night (no corrections applied), then drifted apart from each other as time passed (up to 1°C at night by the end of the year). For the BULK fluxes, we used the LSU instrument (1 m below mean water level) for the first half of the year, then the floating thermistor (~20 cm depth) for the second half of the year.

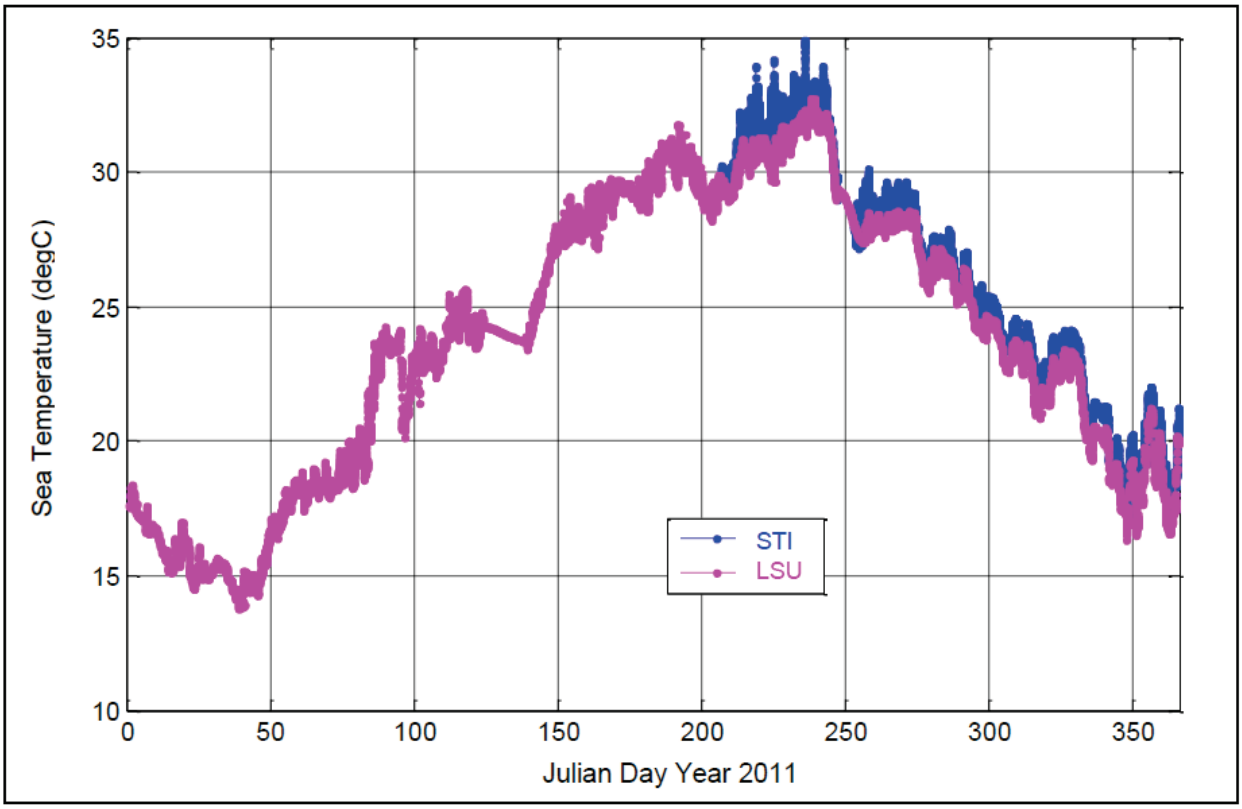


Figure 46. Time series of air and sea temperatures from STI (blue) and LSU (magenta) instruments.

7.3.3.4 Wind Speed and Direction

Figure 47 shows 10-m wind speed residuals (instrument to compare—for example, sonic wind speed—minus STI wind speed) as a function of true wind direction. Similarly, wind direction residuals as a function of true wind direction are plotted in Figure 48. Both STI and LSU wind speed measurements were within 0.5 m/s of each other and wind direction measurements were within 5 degrees. Therefore, we used the STI sensor for the COARE algorithm. We also note various flow distortion effects from the platform. Additional details are given in Section 7.3.4, Data Quality Control and Filtering.

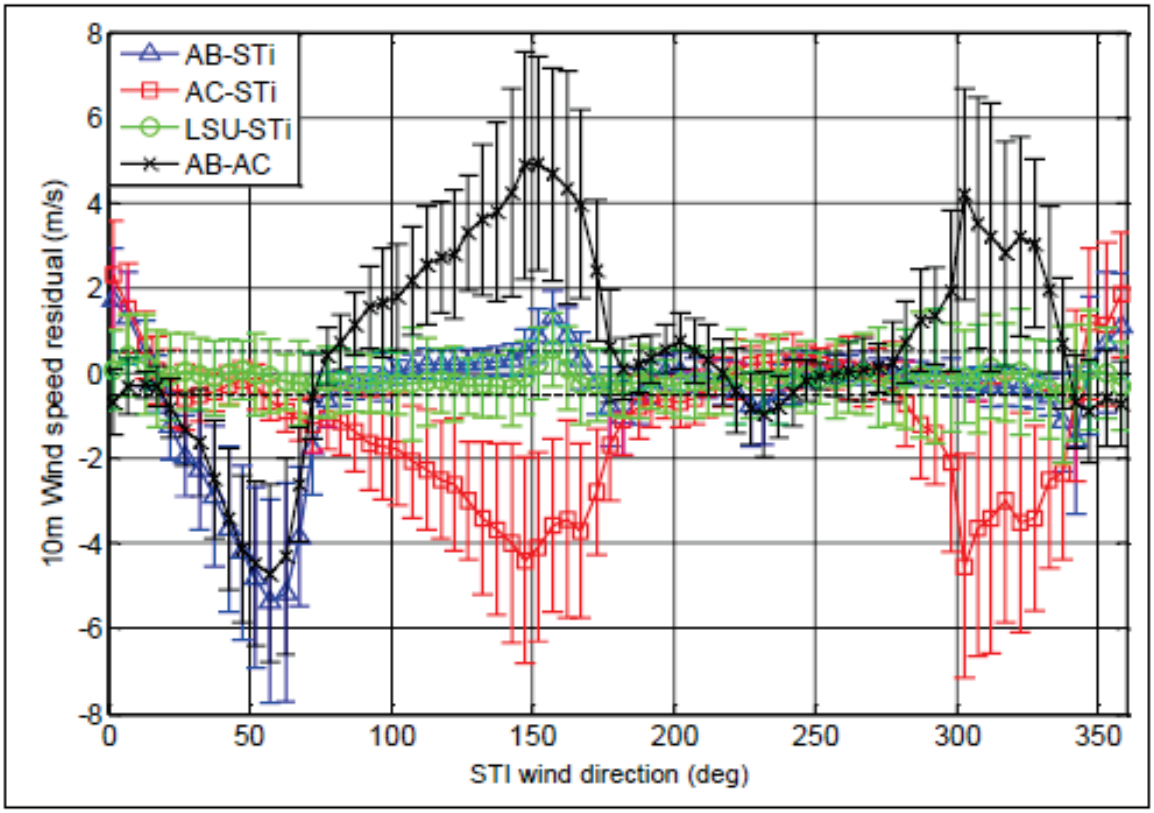


Figure 47. Wind speed residuals as a function of STI wind direction (1 m/s bins). Horizontal dash lines indicate ±0.5 m/s.

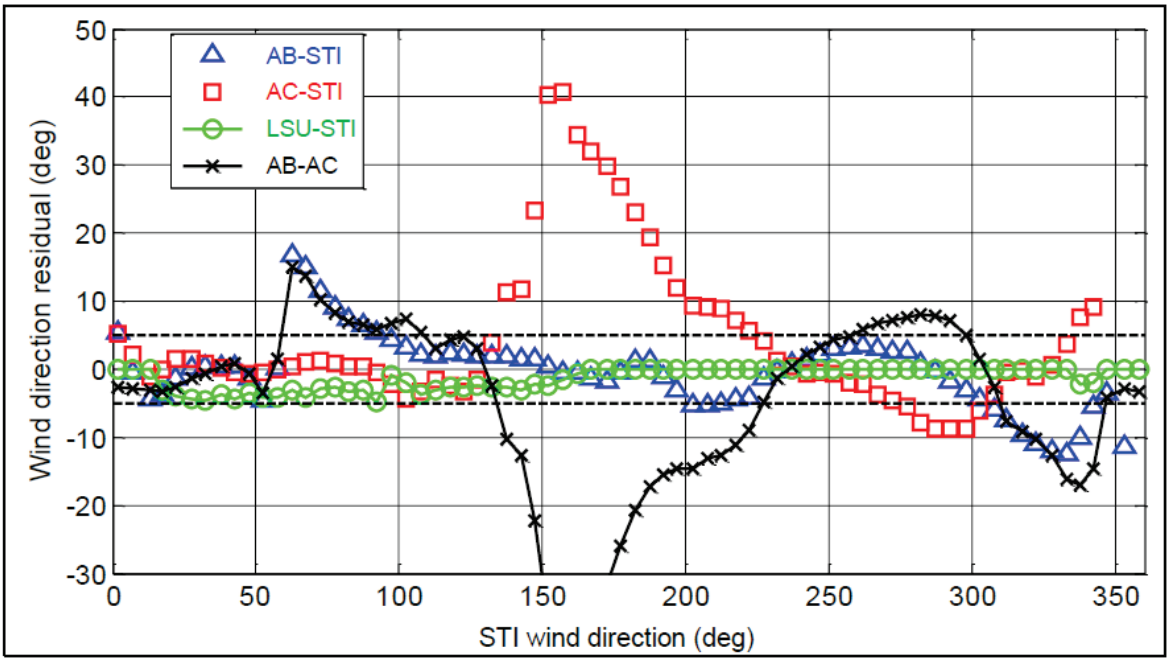


Figure 48. Wind direction residuals as a function of STI wind direction (5-degree bins). Horizontal dash lines indicate ± 0.5 degrees.

7.3.4 Data Quality Control and Filtering

In this section, we describe the main criteria used to quality control the flux data. We began with wind direction because it is one of the main factors affecting the flux observations due to distortion from the platform structure. At about 60 degrees, the wind blew straight into the AC flux package; however, at this angle, the A platform blocked the AB flux location. At 150 degrees, the wind blew straight into the AB location; the AC flux package was obstructed by the A platform (see Figure 49). This can be observed as deflections in wind directions (Figure 48) and decelerations in wind speeds (Figure 47).

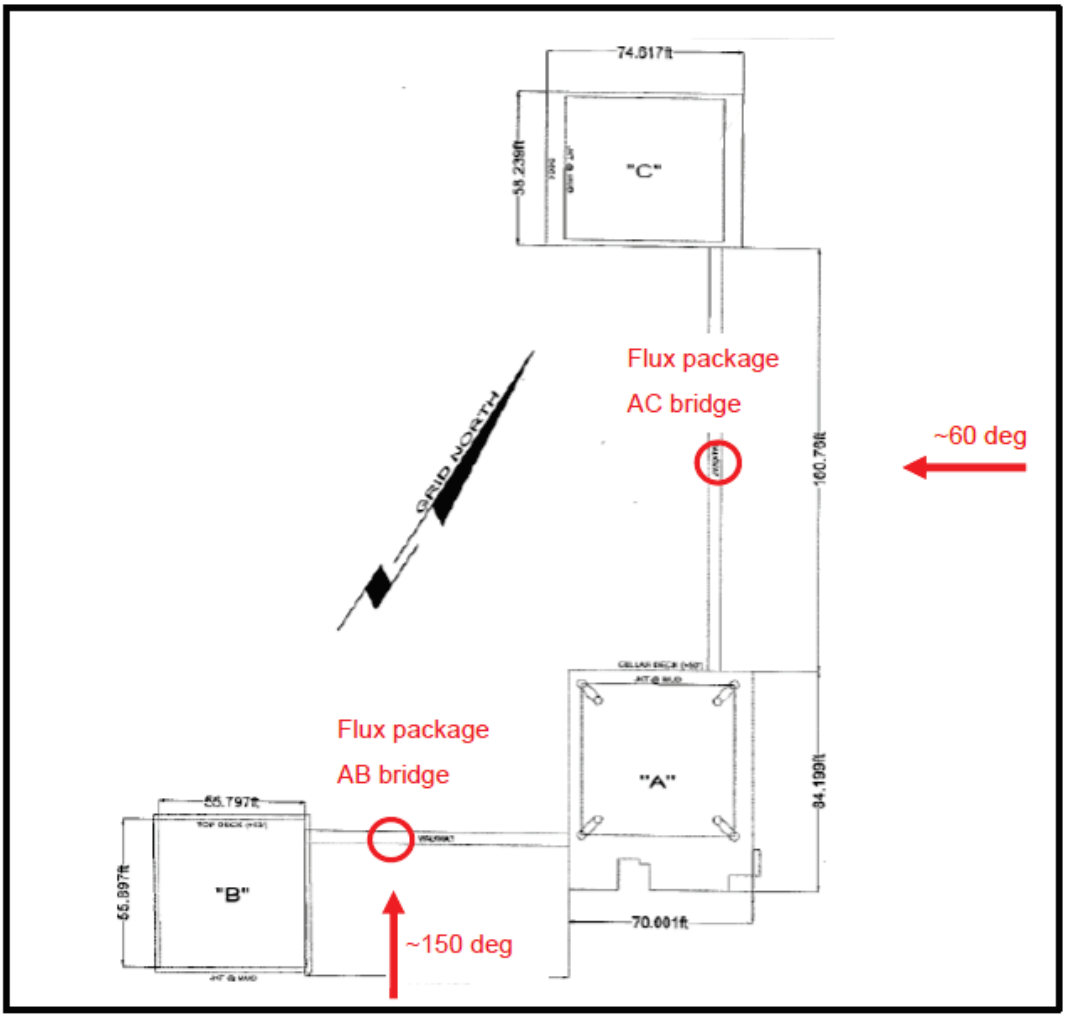


Figure 49. A, B, and C platform orientation relative to true north.

Using the information from Figures 47, 48, and 49, we selected the following wind sectors as good potential wind directions for flux observations: AB (80° to 170°), (240° to 310°); AC (10° to 80°), (220° to 280°). Using these "bins" results in about 60% of usable data for year 2011 (by combining AB and AC data).

Automatic screening criteria were applied to the flux data. Figure 50 shows examples of U and W spectra in good wind sectors for two different hours. The spectra fit well with the $f^{-2/3}$ inertial subrange line (blue and red solid lines) for a particular hour, then behaved strangely for a consecutive hour. This could be due to distortion effects or noise. To filter out suspect values, we used the inertial dissipation method and computed u*, T*, q*, and then used those variables as filters to constrain our direct covariance calculations.

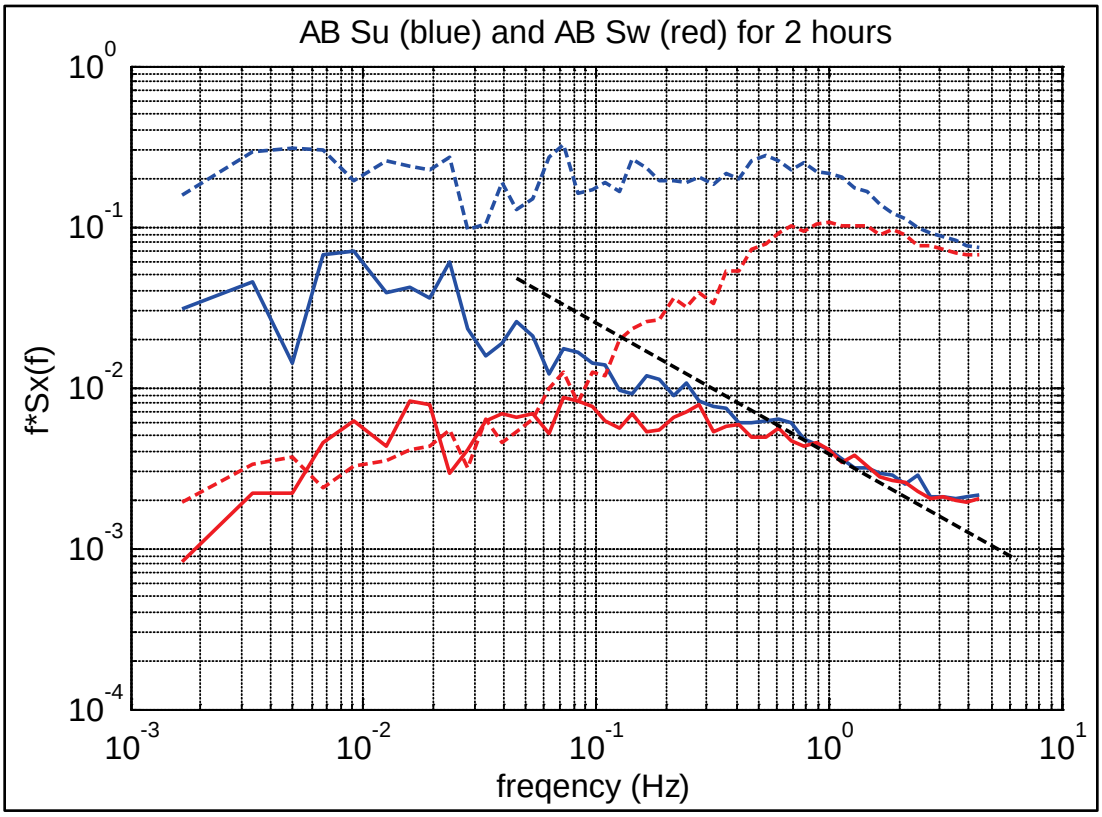


Figure 50. U (blue) and W (red) spectra from the AB flux package at 0 and 6 UTC on August 9, 2011. The black dashed line indicates a slope of -2/3.

The standard deviations of the 10 Hz data within the ten-minute averaging were also used to filter the data. As an example, the standard deviation of the Automatic Gain Control (AGC) of the Li-Cor 7500 was used in conjunction with other filters (such as the mean of the AGC and the standard deviation of the water vapor) to remove invalid data. Also, the timespans when the optics were routinely cleaned by the automated washing system (see Figure 51) were rejected. Li-Cor observations with an AGC standard deviation greater than four were rejected.

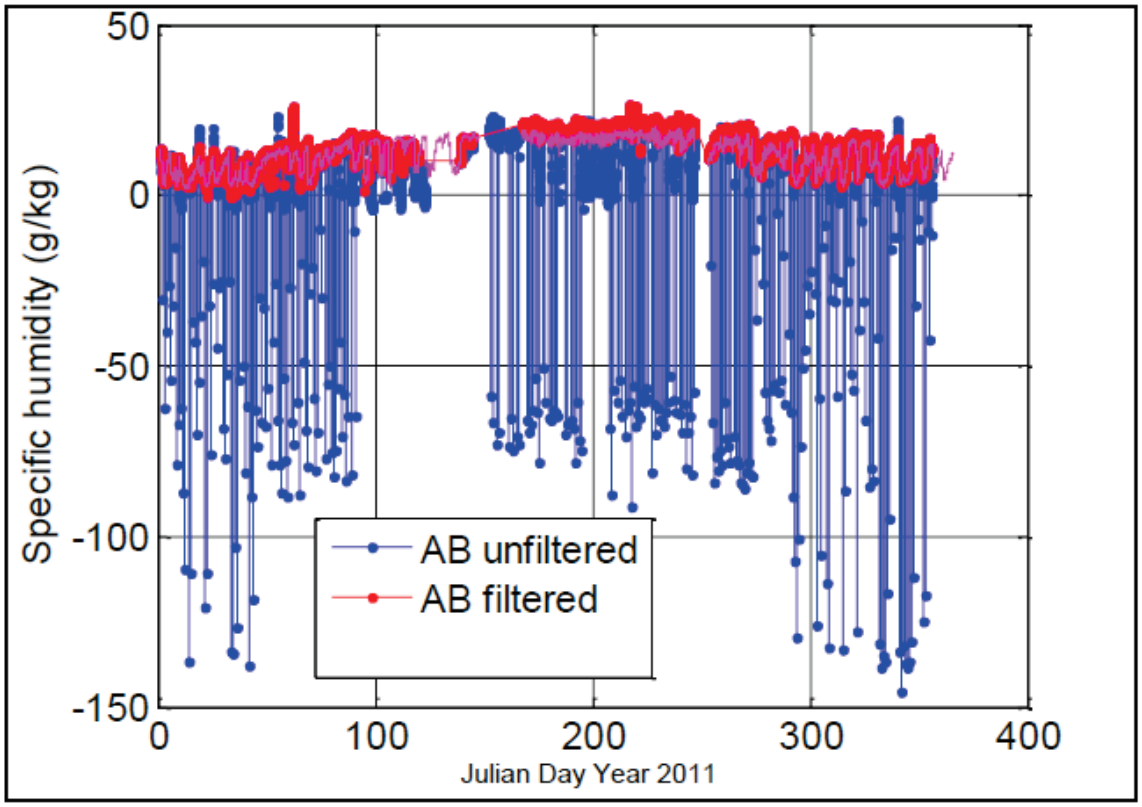


Figure 51. Illustration of unfiltered (blue) and filtered (red) specific humidity data from the AB Li-Cor 7500 sensor. The low values indicate the occurrence of washing or rain.

7.3.5 Comparison of Direct Covariance Flux to COARE-Calculated Flux

This section provides a summary of the analysis that compares observed and COARE-calculated sensible, latent, and momentum fluxes.

Bulk estimates of air-sea fluxes were computed using the COARE bulk algorithm, version 3.0 (Fairall et al. 2013). Cool-skin and warm-layer corrections were applied within the algorithm to correct the measured sea temperature to interfacial temperature. Direct wave measurements were not used in the code at this point in the analysis. Direct covariance latent heat fluxes were corrected for the density Webb effect. When computing the sensible heat flux, the humidity contribution to sonic temperature was removed using the bulk latent heat flux. No other corrections were applied for that comparison. After applying all corrections and filtering, about 50% (180 days) of the data for 2011 remained.

The scalar fluxes and stress components can be parameterized as

$$H_S = \rho_a \, c_p C_h \, U \, (T_S - T_a)$$
$$H_l = \rho_a \, L_v C_e \, U \, (q_S - q_a)$$
$$\tau_i = \rho_a \, C_d \, U \, (u_{si} - u_i)$$

where ρ_a is the air density, c_p is the specific heat of air at constant pressure, and L_v is the latent heat of vaporization. Cd, Ch, and Ce are the transfer coefficients for stress, sensible heat, and latent heat, respectively. U is the average value of the wind speed relative to the sea surface, T_a is the air temperature, q_a is the water vapor mixing ratio, and u_i is one of the horizontal wind components. The remaining parameters are the sea surface skin temperature T_S, the interfacial water vapor mixing ratio q_S, and the surface current u_{si}. Note that sea surface skin temperature T_S (Tsea in figures below) was estimated from the LSU temperature sensor (1 m below mean water level) before installation of the floating thermistor (~20 cm depth), and using the 20 cm thereafter (for additional information, see Section 7.3.3.3, Sea Temperature). The measured skin temperature was not used in this preliminary analysis. Qs (Qsea in the figures below) is the calculated interfacial water vapor mixing ratio and is computed from the saturation mixing ratio for pure water at the sea skin temperature:

$$q_s = 0.98 \, q_{sat} \, (T_s)$$

where the dimensionless constant, 0.98, accounts for the reduction in water vapor pressure caused by a typical salinity of 34 parts per thousand.

To compare the measured versus calculated fluxes, we have created two types of figures: one to show the flux as a function of its corresponding scalar differences (e.g., $T_S - T_a$ for sensible heat), and the other to separate the data from the AB and AC bridges. Plot details and findings for wind stress, sensible heat flux, and latent heat flux follow.

7.3.5.1 Wind Stress

We plotted the 10-minute average BULK (calculated) stress (Taub) and the measured streamwise stress (Tauc) as a function of 10-m neutral wind speed so that effects of stability are removed (Figure 52, lower panel). The data have been averaged in wind speed bins with 1 m/s bin widths. The streamwise measured stresses were averaged together when coincident wind sectors were found for both the AB and AC bridges. To determine whether the stress measured on one bridge was more biased than the stress measured on the other bridge compared to COARE-calculated stress, we have also plotted the scatter plots of calculated stress (Taub) versus measured streamwise stress (Tauc) for the AB and AC bridges (Figure 52, top panel).

Figure 52 shows that (1) measured stress is usually much less than calculated stress, and (2) both bridges appear to observe similar stress, so the discrepancy between measured and calculated stress is not because one measurement system is more biased than the other one.

7.3.5.2 Sensible Heat Flux

We plotted the BULK (calculated) sensible heat flux (Hsb) and the measured sensible heat flux (Hsc) as a function of the temperature difference ($T_S - T_a$) to look at possible temperature biases that could affect the measured flux. Hsc and Hsb were also normalized by wind speed to remove the wind speed dependency (Figure 53, lower panel). The data have been averaged in temperature bins with 0.5°C bin widths. Similarly, to determine whether flux from one bridge was more biased than the other compared to calculated flux, we also plotted the scatter plots of calculated sensible heat flux (Hsb) versus measured sensible heat (Hsc) for the AB and AC bridges (Figure 53, top panel).

Figure 53 shows that (1) measured sensible heat flux is usually much less than calculated sensible heat flux, and (2) besides some outliers, observations from both bridges appear similar.

7.3.5.3 Latent Heat Flux

We plotted the BULK (calculated) latent heat flux (Hlb) and the measured latent heat flux (Hsc) as a function of the specific humidity difference ($q_S - q_a$). The fluxes were also normalized by wind speed (Figure 54, lower panel). The data have been averaged in specific humidity bins with 0.5 g/kg bin widths. We also plotted the scatter plots of BULK latent heat flux (Hlb) versus measured latent heat (Hlc) for the AB and AC bridges (Figure 54, top panel).

Figure 54 shows that (1) measured latent heat flux is usually much less than calculated latent heat flux, and (2) the AC measured latent heat flux is noisier than the AB bridge latent heat flux, which might slightly affect the measured flux versus calculated flux comparison. However, it does not explain the large disagreement between the measured and calculated latent heat flux.

7.3.5.4 Discussion

Several possibilities have been investigated as to why the fluxes do not compare well, but no physical reasons have yet explained the differences. Additional analysis will be required to fully characterize the data. For example:

The BULK meteorological data inputs need to be further evaluated.

Regional wave and sea surface temperature effects (cool skin/warm layer) need to be researched to determine their influence on flux estimates in the Gulf of Mexico.

No obvious flow distortion effects were identified, but additional analysis and comparison to data from nearby sources will be required to evaluate flow tilt limits and the wind speed/direction data. However, this relates to mean state variables and the turbulence variables could behave differently. Flow distortion is more of a concern for stress rather than sensible and latent heat flux.

After further analysis, corrections may need to be applied to the latent heat flux (Li-Cor specific humidity). The Li-Cor 7500 signal has higher mean humidity (~10-15%) compared to the surface sensor measurements. Scaling the turbulent fluctuations based upon the mean ratio of

the Li-Cor humidity measurements and the surface humidity measurements may help reduce the discrepancies between the BULK and covariance latent heat fluxes.

The discrepancies between the BULK and covariance latent heat fluxes could also be real and show that the COARE algorithm needs to be refined for use in the Gulf of Mexico. Perhaps investigating offshore flow versus inland flow might help explain some of the differences. Additional analysis of inter-comparison of instruments used in this study might also be beneficial.

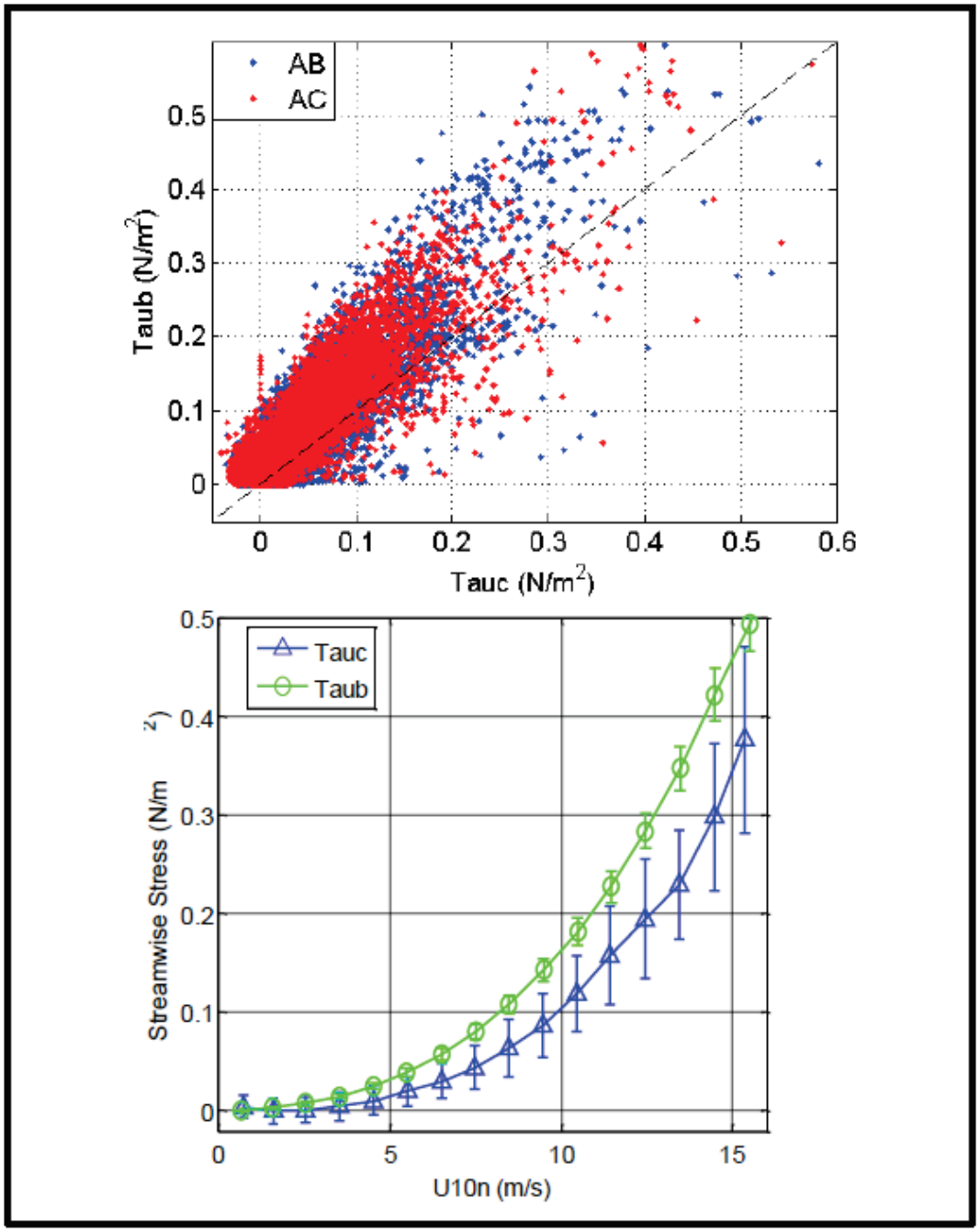


Figure 52. Top panel: BULK (calculated) stress (Taub) versus measured streamwise stress (Tauc) for the AB and AC bridges combined. Lower panel: Same flux, but bin-averaged and plotted as a function of 10-m neutral wind speed.

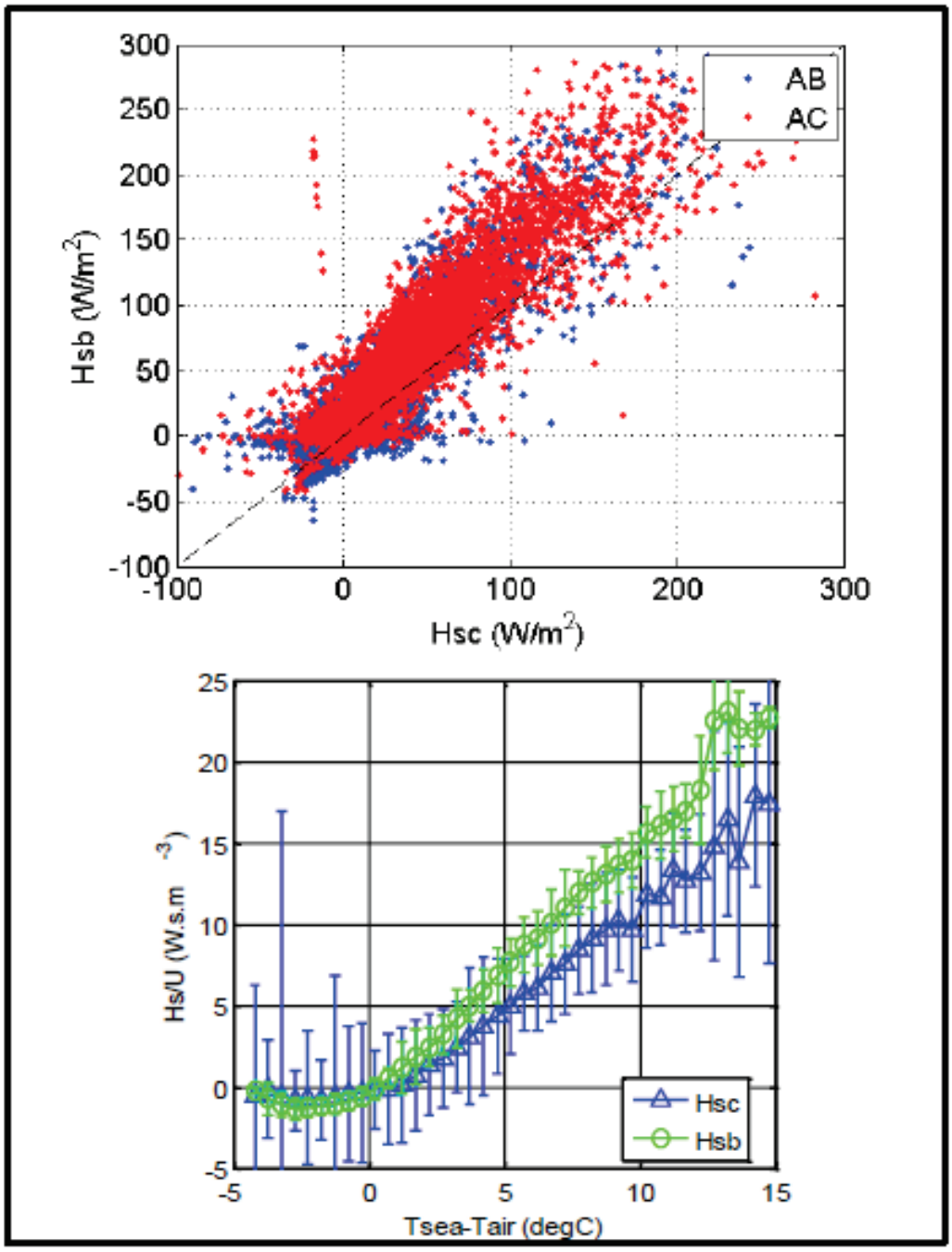


Figure 53. Top panel: BULK (calculated) sensible heat flux (Hsb) versus measured sensible heat flux (Hsc) for the AB and AC bridges. Lower panel: Same flux, but divided by wind speed and plotted as a function of sea-air temperature difference.

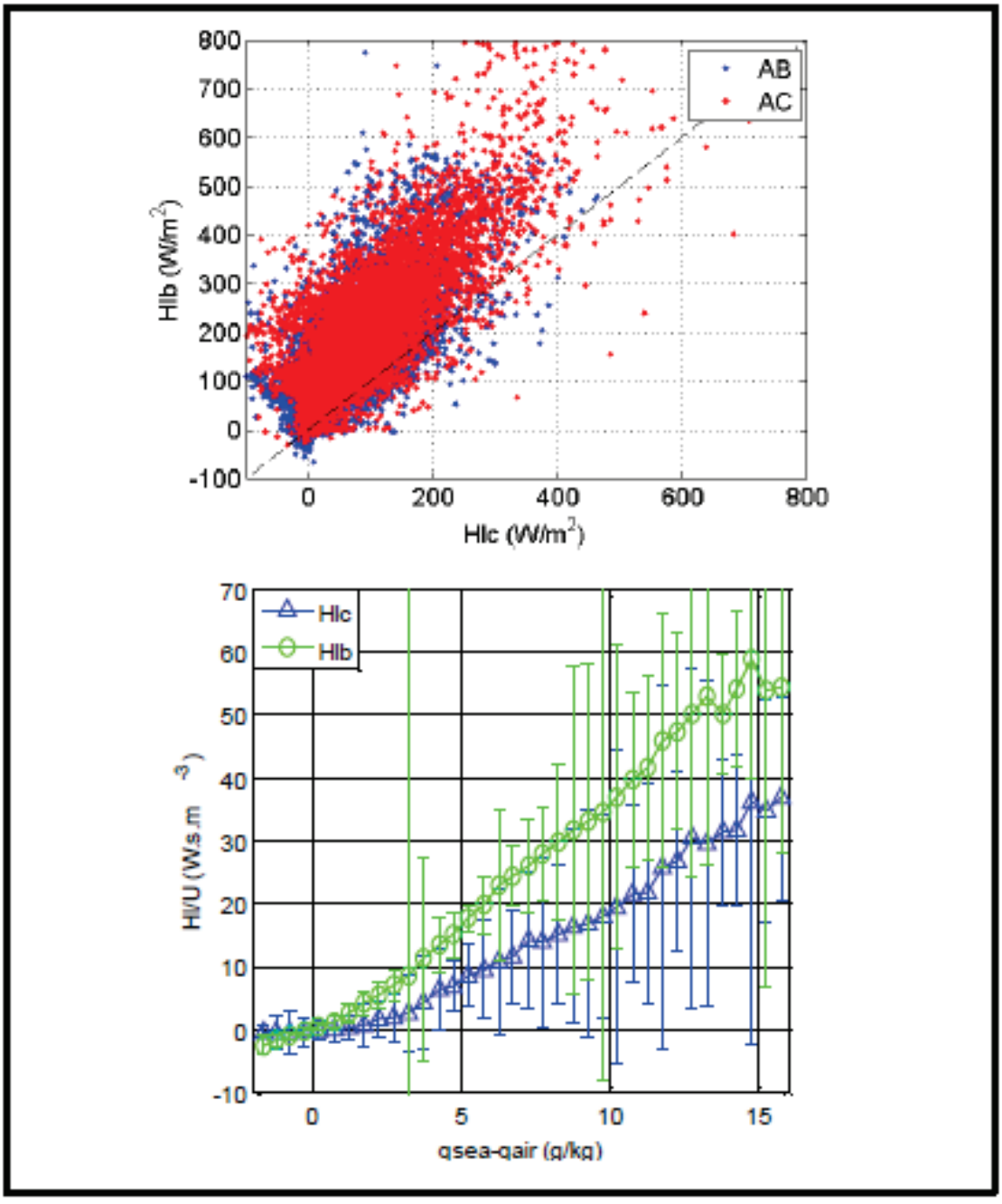


Figure 54. Top panel: BULK (calculated) latent heat flux (Hlb) versus measured latent heat flux (Hlc) for the AB and AC bridge. Lower panel: Same flux, but divided by wind speed and plotted as a function of sea-air specific humidity difference.

7.3.6 COARE Data Analysis Summary

A preliminary analysis comparing the COARE flux estimates with direct measurements was performed for data collected from the ST-52 platform. Preliminary results show discrepancies between the BULK and covariance fluxes that require extensive analysis to be fully understood. The differences may be due to the platform distortion effects or may be real. The COARE algorithm may need to be updated for the Gulf of Mexico region. Further study is needed to characterize offshore compared with inshore influences and to optimize the COARE algorithm for wave effects.

8. CONCLUSIONS AND RECOMMENDATIONS

The overall objective of this study was to collect meteorological and oceanographic data that will later be used to better characterize the atmospheric boundary layer over the Gulf of Mexico. This information will be used in future work to improve meteorological and air quality modeling along the Gulf Coast. This project was successful in yielding an unprecedented set of atmospheric boundary layer and oceanographic measurements covering about 18 months over the Gulf of Mexico, which represents a range of air-sea interactions and processes that occur over all seasons. All data have been quality-controlled, are ready for use in data analysis and modeling, and are available on DVD.

From this study we concluded that long-term, unmanned operations of highly sophisticated instruments on an active oil platform are feasible and can provide high quality data, provided that the following key elements are addressed:

1. Sodar instruments require both electronic and physical noise reduction systems to obtain high-quality measurements from lower-boundary-layer winds in the busy and noisy environment of an operating oil platform.
2. Fast-response specific humidity instruments require a daily lens cleaning to remove salt deposits.
3. Catwalks placed between platforms are useful for capturing near-surface flux measurements.
4. A mini-shelter cooled with only dilute anti-freeze can be used to house computers if an air-conditioned shelter is not available.
5. Constant-depth, near-surface ocean temperature measurements can be made without a buoy using a system mounted to a platform leg.
6. Two-way Internet is needed to monitor instruments and their data so that problems can be quickly identified and resolved.

In addition, preliminary analysis has shown that model predictions of boundary-layer processes do not always agree with the observations from this study; thus, these measurement data provide an excellent source of information to use for evaluating and improving meteorological models.

Based on lessons learned during the study, preliminary data analysis, and discussions with other experts in the field, we provide the recommendations outlined below.

8.1 MEASUREMENT-RELATED RECOMMENDATIONS

- Investigate the integration of robust boundary-layer offshore measurements into a long-term network for various applications.
- Extend this type of study to other locations in the Gulf (deep water) or other offshore locations. Because air-sea interactions can be highly dependent on wave conditions, the current data taken in shallow water may not be representative of conditions in deep water.

- Investigate critical heights for flux measurements, including measurement locations for mean state variables for the COARE model (e.g., surface-layer depth).
- Conduct measurements to better characterize the influence of the platform heating and cooling cycles on the on-deck measurements and how the cycles influence the bulk flux calculations.

8.2 DATA ANALYSIS-RELATED RECOMMENDATIONS

- Evaluate the spatial representativeness of the measurements by comparing routine measurements taken on the platform in this study to other nearby measurements, such as those collected at nearby buoys. This information will help guide the applicability of findings from future analyses to other areas in the Gulf.
- Characterize offshore atmospheric boundary layer conditions and processes; investigate the influence of large- and local-scale meteorology and ocean conditions on atmospheric boundary processes; and characterize air-sea processes under storm conditions. There is currently limited information on the above processes. The data collected in this study can help us better characterize and understand meteorological conditions and processes in the Gulf.
- Evaluate the NAM and other meteorological models' abilities to accurately represent the atmospheric and oceanographic conditions, including the various processes (e.g., warm-ocean, cool-skin, fluxes, wind profiles). Models are relied upon for a range of applications (e.g., emergency response, wind energy, forecasting, etc.); thus, accuracy is important. Preliminary analysis suggests that the NAM may not always represent boundary layer conditions over the Gulf, but more investigation is needed.
- Further compare COARE bulk flux estimates with measurements, including how each calculation in COARE influences the estimates. Preliminary analysis showed that the COARE bulk flux estimates and measurements do not always agree, but more analysis is required to determine when and why they do and do not agree.

LITERATURE CITED

Berman S., J.-Y. Ku, J. Zhang, and S.T. Rao. **1997**. Uncertainties in estimating the mixing depth--comparing three mixing-depth models with profiler measurements. Atmos. Environ., 31:3023-3039.

Crescenti G.G. **1997**. A look back on two decades of Doppler sodar comparison studies. Bulletin of the American Meteorological Society, 78:651-673.

Fairall C., E.F. Bradley, and D.P. Rogers. **2013**. COARE bulk air-sea flux algorithm. Website. http://coaps.fsu.edu/COARE/flux_algor/flux.html.

Fairall C.W., E.F. Bradley, D.P. Rogers, J.B. Edson, and G.S. Young. **1996**. Bulk parameterization of air-sea fluxes for Tropical Ocean-Global Atmosphere Coupled-Ocean Atmosphere Response Experiment. Journal of Geophysical Research, 101:3747-3764.

Fairall C.W., E.F. Bradley, J.E. Hare, A.A. Grachev, and J.B. Edson. **2003**. Bulk parameterization of air-sea fluxes: updates and verification for the COARE algorithm Journal of Climate, 16:571-591.

Gilroy M. **2008**. Use of the Vaisala ceilometer for boundary layer height detection. Presentation at the U.S. EPA's 2008 National Air Quality Conference, April 6-9, 2008, Portland, OR, by the Puget Sound Clean Air Agency, Seattle, WA. Available at http://www.epa.gov/airnow/2008conference/Forecasting/Tuesday/gilroy-forecasting_tuesday.ppt.

Hanna S.R., C.P. MacDonald, M. Lilly, C.A. Knoderer, and C.H. Huang. **2006**. Analysis of three years of boundary layer observations over the Gulf of Mexico and its shores. Estuarine, Coastal and Shelf Science, 70(4):541-550, (STI-3090).

Holzworth G. **1972**. Mixing heights, wind speeds, and potential for urban air pollution throughout the contiguous United States. Prepared by the Office of Air Programs, U.S. Environmental Protection Agency, Research Triangle Park, NC, Publication No. AP-101.

Knoderer C.A., C.P. MacDonald, M.R. Lilly, S. Hanna, and C. Huang. **2004**. Comparison of EDAS predictions and RWP data collected over the Western and Central Gulf of Mexico. Presented at The Seventh International Marine Environmental Modeling Seminar, Special Session: Modeling Coastal Meteorology, Washington, DC, October 19-21 by Sonoma Technology, Inc., Petaluma, CA (STI-2629).

MacDonald C.P., P.T. Roberts, C.A. Knoderer, D.S. Miller, M.R. Lilly, and S.R. Hanna. **2003**. Boundary layer study in the Western and Central Gulf of Mexico. Presentation at the final meeting of the Technical Review Group, Minerals Management Group, New Orleans, LA, STI-998555-2265, October.

MacDonald C.P., P.T. Roberts, M.R. Lilly, C.A. Knoderer, D.S. Miller, and S.R. Hanna. **2004**. Boundary layer study in the Western and Central Gulf of Mexico. Final report prepared for the Minerals Management Service, New Orleans, LA, by Sonoma Technology, Inc., Petaluma, CA, STI-998555-2266-FR3, September.

NIST and USNO. **2013**. The official U.S. time. A public service website provided by the National Institute of Standards and Technology (NIST) and the U. S. Naval Observatory (USNO). http://www.time.gov/.

Vaisala. **2004**. Ceilometer CL31 user's guide. M210482EN-B, October. Available at http://www.iag.co.at/uploads/tx_iagproducts/pdf_handbuch/CL31.de.pdf.

Vaisala Meteorological Systems, Inc. and Sonoma Technology, Inc. **2002**. Profilers and data collection for the MMS boundary layer study in the Western and Central Gulf of Mexico: final performance report. Prepared for the U.S. Department of the Interior, Minerals Management Service, Gulf of Mexico OCS Region, New Orleans, LA, OCS Study MMS 2002-028.

The Department of the Interior Mission

As the Nation's principal conservation agency, the Department of the Interior has responsibility for most of our nationally owned public lands and natural resources. This includes fostering the sound use of our land and water resources; protecting our fish, wildlife, and biological diversity; preserving the environmental and cultural values of our national parks and historical places; and providing for the enjoyment of life through outdoor recreation. The Department assesses our energy and mineral resources and works to ensure that their development is in the best interests of all our people by encouraging stewardship and citizen participation in their care. The Department also has a major responsibility for American Indian reservation communities and for people who live in island communities.

The Bureau of Ocean Energy Management Mission

The Bureau of Ocean Energy Management (BOEM) promotes energy independence, environmental protection, and economic development through responsible, science-based management of offshore conventional and renewable energy.